

1 **Thrombolysis by PLAT/tPA increases serum free IGF1 leading**
2 **to a decrease of deleterious autophagy following brain**
3 **ischemia**

4 **Running title: Inhibition of ischemia-induced autophagy by tissue-type plasminogen**
5 **activator through the regulation of IGF1-IGF1R receptor axis**

6 Audrey M Thiebaut¹, Izaskun Buendia¹, Vanessa Ginet^{2,3}, Eloise Lemarchand⁴, Mehdi
7 Boutagouga Boudjadja⁵, Yannick Hommet¹, Laurent Lebouvier¹, Charlotte Lechevallier¹, Mike
8 Maillason⁶, Elodie Hedou¹, Nicole Déglon⁷, Franck Oury⁸, Marina Rubio¹, Joan Montaner⁹,
9 Julien Puyal^{2,10}, Denis Vivien^{1,11}, Benoit D Roussel^{1*}.

10 1- Normandy University, UNICAEN, INSERM, UMR-S U1237, Physiopathology and Imaging of Neurological
11 Disorders (PHIND), Institute Blood and Brain @Caen-Normandie (BB@C), GIP Cyceron, Caen, FRANCE

12 2- Department of Fundamental Neurosciences, University of Lausanne, Lausanne, Switzerland

13 3- Clinic of Neonatology, Department of Women, Mother and Child, University Hospital Center of Vaud,
14 Lausanne, Switzerland

15 4- Division of Neuroscience and Experimental Psychology, School of Biological Sciences, Faculty of Biology,
16 Medicine and Health, University of Manchester, Manchester, UK

17 5- Metofico Scientific, Courbevoie, France

18 6- CRCINA-IMPACT core facility, INSERM, UMR-S U1232, NANTES University, Nantes, FRANCE

19 7- Department of Clinical Neurosciences, Laboratory of Neurotherapies and Neuromodulation, Lausanne
20 University Hospital (CHUV) and University of Lausanne (UNIL), 1011 Lausanne, Switzerland

21 8- INSERM U1151, Institut Necker Enfants-Malades (INEM), Team 14, Université Paris Descartes-Sorbonne-
22 Paris Cité, 75014 Paris, France

23 9- Department of Neurology, Hospital Universitario Virgen Macarena, Sevilla, Spain

24 10- CURML, University Center of Legal Medicine, Lausanne University Hospital, Lausanne, Switzerland

1 11- CHU Caen, Caen University Hospital, Department of clinical research, Caen, France

2 * Corresponding author: Dr Roussel Benoit: broussel@cyceron.fr; +33231470213

3 Key words: IGF1R, IGFBP3, LC3, MTORC1, SQSTM1/p62, stroke.

4

5

1 **Abstract**

2 Cerebral ischemia is a pathology involving a cascade of cellular mechanisms, leading to the
3 deregulation of proteostasis, including macroautophagy/autophagy, and finally to neuronal
4 death. If it is now accepted that cerebral ischemia induces autophagy, the effect of
5 thrombolysis/energy recovery on proteostasis remains unknown. Here, we investigated the
6 effect of thrombolysis by PLAT/tPA (plasminogen activator, tissue) on autophagy and neuronal
7 death. In two *in vitro* models of hypoxia reperfusion and an *in vivo* model of thromboembolic
8 stroke with thrombolysis by PLAT/tPA, we found that ischemia enhances neuronal deleterious
9 autophagy. Interestingly, PLAT/tPA decreases autophagy to mediate neuroprotection by
10 modulating the PI3K-AKT-MTOR pathways both *in vitro* and *in vivo*. We identified IGF1R
11 (insulin-like growth factor I receptor; a tyrosine kinase receptor) as the effective receptor and
12 showed *in vitro*, *in vivo* and in human stroke patients and that PLAT/tPA is able to degrade
13 IGFBP3 (insulin-like growth factor binding protein 3) to increase IGF1 (insulin-like growth
14 factor 1) bioavailability and thus IGF1R activation.

15

1 **Abbreviations**

2 AKT/protein kinase B: thymoma viral proto-oncogene 1; EGFR: epidermal growth factor
3 receptor; Hx: hypoxia; IGF1: insulin-like growth factor 1; IGF1R: insulin-like growth factor I
4 receptor; IGFBP3: insulin-like growth factor binding protein 3; Ka: Kainate; MAP1LC3/LC3:
5 microtubule-associated protein 1 light chain 3; MAPK/ERK: mitogen-activated protein kinase;
6 MTOR: mechanistic target of rapamycin kinase; MTORC1: MTOR complex 1; OGD: oxygen and
7 glucose deprivation; OGD_{reox} : oxygen and glucose deprivation + reoxygenation; PepA:
8 pepstatin A1; PI3K: phosphoinositide 3-kinase; PLAT/tPA: plasminogen activator, tissue; PPP:
9 picropodophyllin; SCH77: SCH772984; ULK1: unc-51 like kinase 1; Wort: wortmannin

10

1 INTRODUCTION

2 Stroke is the second leading cause of death and the most frequent cause of disability in adults
3 [1]. Acute treatments have been developed: the recent endovascular thrombectomy and
4 thrombolysis by PLAT/tPA (plasminogen activator, tissue) [2]. However, endovascular
5 thrombectomy is restricted to large vessels occlusion [3], while thrombolysis with PLAT/tPA
6 has a short therapeutic windows, a low recanalization rate, and a higher risk of haemorrhagic
7 transformation [2, 4]. Therefore, a better comprehension of ischemic stroke's
8 pathophysiology is required to improve prevention, therapy and reparation following the
9 disease.

10 Ischemic stroke is a complex disease involving a cascade of cellular mechanism, which
11 deregulates proteostasis and leads to cell death [5]. A key mechanism involved in proteostasis
12 regulation is autophagy [5], a protein degradation/recycling system highly conserved.
13 Macroautophagy (hereafter called autophagy) is characterized by the synthesis of a double-
14 layered membrane structure called an autophagosome, which contains cargos targeted for
15 degradation. Autophagosomes then fuse with lysosomes to form autolysosomes resulting in
16 the degradation of their contents. The main autophagy-regulating pathway involves MTOR
17 (mechanistic target of rapamycin kinase). Under physiological conditions, MTOR complex 1
18 (MTORC1) is phosphorylated and associated with ULK1 (unc-51 like kinase 1)-ULK2, allowing
19 the phosphorylation of ATG13 and ULK1-ULK2. This inhibits ULK1-ULK2 kinase activity, leading
20 to an inhibition of autophagy [6]. Under pathological conditions, such as starvation or
21 metabolic stress, MTORC1 is inactivated by dephosphorylation and the ULK1-ULK2 kinase
22 activity is restored.

1 Interestingly, PLAT/tPA is involved in proteostasis by decreasing ischemia-induced
2 endoplasmic reticulum stress [7]. Moreover, PLAT/tPA has been shown to increase neuronal
3 survival following dissociation and plating in a JAK (Janus kinases)-STAT (signal transducer and
4 activator of transcription)-MTOR dependent manner [8, 9] and is involved in the detection and
5 the adaption to metabolic stress [10]. However, the impact on neuronal autophagy and its
6 consequences during cerebral ischemia has never been explored.

7 Here, we first evidence that neuronal autophagy is an important deleterious pathway
8 activated by ischemia/reperfusion. We found that autophagy contributes to ischemia-induced
9 neuronal death both *in vitro* and *in vivo*. We then show that PLAT/tPA is able to decrease
10 ischemia-enhanced autophagy and mediates neuroprotection by modulating the
11 phosphoinositide 3-kinase (PI3K)-AKT/protein kinase B (thymoma viral proto-oncogene)-
12 MTORC1 pathway both *in vitro* and *in vivo*. We identified IGF1R (insulin-like growth factor I
13 receptor) as a new receptor implicated in autophagy modulation by PLAT/tPA. Finally, we
14 showed that during thrombolysis in human stroke patients, PLAT/tPA is able to degrade
15 IGFBP3 (insulin-like growth factor binding protein 3) to increase IGF1 (insulin-like growth
16 factor 1) bioavailability and thus IGF1R activation, opening new strategies for the detection
17 and the treatment of the disease.

18

1 RESULTS

2 *Autophagy pathways are increased by oxygen and glucose deprivation followed by* 3 *reoxygenation in cortical neurons.*

4 To determine the pathways affected by oxygen and glucose deprivation (OGD) and PLAT/tPA
5 treatments (300 nM), we performed a RNAseq followed by an enrichment pathways analysis.
6 In total 5383 transcripts are differentially expressed in the Ctrl Vs OGD_{reox} condition, 5126 in
7 the Ctrl Vs OGD_{reox}+ PLAT/tPA condition, and 229 in the OGD_{reox} Vs OGD_{reox}+ PLAT/tPA
8 condition (Fig. 1A). The enrichment pathway analysis shows 33 pathways differentially
9 expressed between Ctrl/OGD_{reox}/OGD_{reox}+ PLAT/tPA (Table 1). Among them, 5 are linked to
10 hypoxia/ischemia and 12 are linked to autophagy. Indeed, the most affected pathways are
11 MAPK (mitogen-activated protein kinase) (Fig. 1B), PI3K-AKT (Fig. 1C), MTOR (Fig. 1D) and the
12 autophagy (Fig. 1E) pathways. Focusing on these autophagic pathways, we found that 30
13 genes are significantly deregulated in the MAPK pathway under OGD_{reox} condition compared
14 to Ctrl (Fig. 1F), 28 genes in the PI3K-AKT pathway (Fig. 1G), 10 genes in the MTOR pathway
15 (Fig. 1H) and 14 genes in the autophagy pathway (Fig. 1I). Furthermore, the presence of
16 PLAT/tPA during OGD_{reox} modified the expression of 10 genes in the PI3K-AKT pathway
17 compared to OGD_{reox} condition (Fig. 1J), 15 in the MAPK pathway (Fig. 1K), 5 in the MTOR
18 pathway (Fig. 1L) and 7 in the autophagy pathway (Fig. 1M). Altogether, these results show
19 that autophagy and upstream pathways are strongly affected during OGD_{reox}, and that
20 PLAT/tPA seems to counteract these deregulations.

21 *PLAT/tPA decreases OGD-enhanced autophagy flux and cell death in primary cortical* 22 *neurons.*

1 To deepen the RNAseq, we evaluated the effect of OGD_{reox} on autophagy flux in mice primary
2 cortical neurons in the presence or not of PLAT/tPA (Fig. 2A). We investigated the flux by
3 measuring the levels of both MAP1LC3/LC3 (microtubule-associated protein 1 light chain 3)-II
4 (recruited to phagophore membranes, the precursor to autophagosomes) and SQSTM1/p62
5 (a selective autophagy receptor) [11]. As shown by western blots, the level of LC3-II increases
6 by 106.7% following OGD_{reox} (Fig. 2B and C), reflecting an increase of autophagosome
7 presence, while the level of SQSTM1/p62 decreases by 66.5% (Fig. 2B and D), suggesting that
8 OGD_{reox} enhances the autophagy flux. We next confirmed this observation by using lentivirus
9 transducing GFP-LC3 in neurons. Puncta of GFP-LC3, presumably autophagosomes, are
10 increased by 143.9% in OGD_{reox} conditions (Fig. S1A and S1B).

11 OGD_{reox} induces neuronal death by several mechanisms, including excitotoxicity, apoptosis, ER
12 stress and autophagy [5, 7, 9, 12]. To assess the role of enhanced autophagy observed in
13 OGD_{reox} conditions, we pre-treated neurons with a combination of the lysosomal enzyme
14 inhibitors E64d (10 µg/ml) and pepstatin A1 (PepA) (10 µg/ml) to block the flux and we
15 measured the neuronal death. In neurons subjected to OGD_{reox}, E64d-PepA blocks autophagy
16 as demonstrated by the greater accumulation of LC3-II (+69.1%; Fig. 2F and G), and by the
17 accumulation of SQSTM1/p62 (+41.4%, Fig. 2F and H) compared to OGD_{reox} alone. E64d-PepA
18 has no effects on neurons in control conditions; but decreases neuronal death under OGD_{reox}
19 (Fig. 2E). Chloroquine, an inhibitor of the maturation step of autophagy by preventing the
20 fusion between autophagosomes and lysosomes, also protects neurons from OGD_{reox}-induced
21 cell death in a dose-dependent manner (Fig. S1C). Taken together, autophagy is deleterious in
22 our model of neuronal OGD_{reox}, and its blocking offers neuroprotection.

1 Interestingly, PLAT/tPA (300 nM) also protects neurons from death at the same level than
2 E64d-PepA (38.6% protection, Fig. 2E). As suggested by the RNAseq analysis, the presence of
3 PLAT/tPA within the media decreases OGD_{reox}-induced autophagy as demonstrated by the
4 drop of LC3-II accumulation (-42.4%, Fig. 2B and C) together with an increase of SQSTM1/p62
5 (+85.44%, Fig. 2B and D). Of note, we do not observe an effect of PLAT/tPA on autophagic flux
6 in normoxic conditions (Fig. S1D-F). The decrease of OGD_{reox}-induced autophagy flux is
7 confirmed by the use of GFP-LC3 lentivirus, showing a decrease of GFP-LC3-positive puncta
8 following PLAT/tPA treatment (-40.1%, Fig. S1A and B). Additionally, several doses of PLAT/tPA
9 have been tested (from 0.3 to 300 nM): only the high dose of PLAT/tPA is able to inhibit both
10 autophagosome formation and SQSTM1/p62 degradation induced by OGD_{reox} (Fig. S1G-H).
11 However, the lowest dose of PLAT/tPA decreases autophagosome formation as suggested by
12 LC3-II western blot, without affecting SQSTM1/p62 levels (Fig. S1G-I).

13 Altogether, PLAT/tPA is able to decrease OGD_{reox}-enhanced autophagy leading to
14 neuroprotection in an *in vitro* model of ischemia.

15 ***PLAT/tPA prevents hypoxic/excitotoxic-enhanced autophagy and neuronal death.***

16 In another model, we previously shown that the combination of kainate (Ka, 30 μ M) and
17 hypoxia (Hx, 6% oxygen) for 30 min in primary cortical neuron cultures enhanced autophagy
18 and that both pharmacological (3-methyladenine or E64d-pepA) and genetic (downregulation
19 of Beclin1 and ATG7) inhibition of autophagy reduced neuronal death[12]. In this KaHx model,
20 the presence of PLAT/tPA (300 nM) is strongly neuroprotective as shown by both a reduction
21 of LDH release in the medium (-60%, Fig. 3A) and a reduction of the number of PI-positive
22 nuclei (-80%, Fig. 3B and C) 6h after the stimulus. Moreover, the KaHx-induced increase in LC3-
23 II levels (Fig. 3D and E) and SQSTM1/p62 degradation (Fig. 3D and F) was nearly fully prevented

1 by PLAT/tPA treatment suggesting that autophagy was almost completely blocked. To confirm
2 this result, primary cortical neurons were transfected with a tandem mRFP-GFP-LC3 plasmid
3 that allows to simultaneously monitor autophagy induction and degradation efficiency. Based
4 on the pH sensitivity of GFP signal, autophagosome presence is reflected by the number of
5 RFP+/GFP+ dots and active autolysosome/amphisome are revealed by the number of
6 RFP+/GFP- dots. As shown in Fig. 3G-J, in the presence of PLAT/tPA KaHx has no effect on the
7 number of both types of dots demonstrating that PLAT/tPA treatment completely prevented
8 the KaHx-induced autophagy flux.

9 ***OGD-enhanced autophagy is dependent on MTOR pathway.***

10 The next step was then to investigate by which mechanism PLAT/tPA could modulate OGD-
11 enhanced autophagy and neuronal death. The main signaling pathway leading to autophagy
12 initiation is the MTOR pathway [6]. MTOR is a large multidomain protein that exists in two
13 multiprotein complexes: MTOR complex 1 (MTORC1) associated with RPTOR/Raptor, and
14 MTOR complex 2 (MTORC2) associated with RICTOR [13]. When MTORC1 is phosphorylated,
15 it blocks the initiation of autophagy by phosphorylating ULK1-ULK2 on the Ser757, resulting in
16 the inhibition of ULK1-ULK2 complex kinase activity needed in the early steps of
17 autophagosome biogenesis [6]. On the contrary, when MTORC1 activity is low, ULK1-ULK2
18 Ser757 is dephosphorylated and the complex kinase activity is restored, leading to autophagy
19 activation [6, 14]. Therefore, we measured the levels of phosphorylated MTORC1 (Ser2448; p-
20 MTORC1) following OGD_{reox} (Fig. 4A). We found that p-MTORC1 is reduced under OGD_{reox} (-
21 62.4%, Fig. 4A and B) suggesting an increase of autophagy. Accordingly, we also observed that
22 OGD_{reox} leads to a decrease of p-ULK1-ULK2 (Ser757) (-57.8%, Fig. 4A and D). Lastly, we found
23 that PLAT/tPA prevents the decrease of p-MTORC1 (Fig. 4A and B) and p-ULK1-ULK2 (Fig. 4A

1 and D) during OGD_{reox}. Similarly, KaHx-induced neuronal death involves a strong decrease in
2 MTORC1 (Ser2448) phosphorylation that was completely prevented by PLAT/tPA treatment
3 (Fig. S2) reinforcing the fact that PLAT/tPA prevents OGD-induced MTOR-dependent
4 autophagy.

5 We also observed that OGD_{reox} also induces a drop in the phosphorylation of MTORC2 (-67.7%,
6 Fig. 4A and C). However, the effect of PLAT/tPA on p-MTORC2 is much weaker than the one
7 observed on p-MTORC1 as PLAT/tPA partially prevents the drop of phosphorylation (Fig. 4A
8 and C).

9 ***PLAT/tPA decreases OGD-enhanced autophagy through PI3K-AKT pathway.***

10 MTORC1 is controlled by 2 main upstream pathways: MAPK/ERK and PI3K-AKT [15, 16]. We
11 confirmed that OGD_{reox} leads to a decrease of both p-MAPK/ERK (-71.2%) and p-AKT (-64%,
12 Fig5A-C), in line with our previous observations showing that OGD_{reox} leads to the inhibition
13 of MTORC1 (Fig. 4). Interestingly, when PLAT/tPA is present in the media, the decrease of p-
14 MAPK/ERK and p-AKT are partially reversed (Fig. 5A-C).

15 To test whether PLAT/tPA modulates autophagy *via* MAPK/ERK or PI3K-AKT pathways, we
16 used pharmacological inhibitors of each pathway: SCH772984 (SCH77) [17] and A6730 [18]
17 respectively. In the presence of PLAT/tPA, SCH77 does not reverse the drop of LC3-II (Fig5D
18 and E), nor the increase of SQSTM1/p62 (Fig5D and F). However, A6730 reverses the decrease
19 of LC3-II (Fig5G and H) and the increase of SQSTM1/p62 induced by PLAT/tPA during OGD_{reox}
20 (Fig5G and I). It suggests that OGD_{reox} decreases p-MAPK/ERK and p-AKT, leading to p-MTORC1
21 inhibition and autophagy activation during OGD_{reox}. Also, PLAT/tPA decreases autophagy
22 through MTORC1 activation by its ability to prevent the drop of p-AKT.

1 It is also supported by the use of Wortmannin (Wort, 250 nM) a broad PI3K and class III
2 phosphatidylinositol 3-kinase (PtdIns3K) inhibitor. Our results demonstrate that Wort by itself
3 does not modify OGD_{reox}-induced autophagy flux (Fig5J-L). In the presence of PLAT/tPA, Wort
4 almost reverses the decrease of LC3-II ($p=0.051$, Fig5J and K) and restores the degradation of
5 SQSTM1/p62 ($p=0.055$, Fig5J and L); thus reinforcing the implication of the PI3K-AKT pathway
6 in the effect of PLAT/tPA on MTORC1 and autophagy.

7 ***PLAT/tPA decreases OGD-enhanced PI3K-AKT signaling through IGF1R receptor.***

8 We and others have already shown that PLAT/tPA can induce PI3K-AKT signaling through
9 various receptors [19-21]. For instance, PLAT/tPA is able to activate EGFR (epidermal growth
10 factor receptor), a tyrosine kinase receptor promoting PI3K-AKT signaling, to mediate
11 neuroprotection [22-24]. Therefore, we tested the ability of AG1478 (a specific EGFR inhibitor)
12 to prevent the effects of PLAT/tPA on neuronal autophagy during OGD_{reox}. When EGFR activity
13 is blocked, PLAT/tPA still decreases LC3-II accumulation (Fig. 6A and B) and increases
14 SQSTM1/p62 level (Fig. 6A and C). Surprisingly enough, we observed that AG1478 alone can
15 reverse LC3-II conversion induced by OGD_{reox} (-43.5%, Fig. 6A and B), but has no effect on
16 SQSTM1/p62 level (Fig. 6A and C) indicating that AG1478 has probably no effect on OGD-
17 enhanced autophagy.

18 We next tested picropodophyllin (PPP), a selective inhibitor of the tyrosine kinase receptor
19 IGF1R [25]. In neurons subjected to OGD_{reox} conditions, PPP (100 nM) slightly exacerbates the
20 decrease of p-AKT (-32.3%, Fig. 6D and E). However, PPP has no effects by itself neither on
21 MTORC1 (Fig. 6D and F) nor on autophagy flux (Fig. 6G-I). Interestingly, when PPP is added in
22 the presence of PLAT/tPA, LC3-II accumulation is no more reversed (-34.2%, Fig. 6G and H)
23 and SQSTM1/p62 degradation is restored (+34.4%, Fig. 6G and I). PPP also prevents the

1 inhibition of autophagy pathways by PLAT/tPA by decreasing PLAT/tPA -induced MTORC1
2 phosphorylation (-31.1%, Fig. 6D and F). In the presence of PPP, PLAT/tPA does not longer
3 induce AKT signaling under OGD_{reox} conditions (-55.2%, Fig. 6D and E).

4 We also activated the IGF1R by adding IGF1 (250 nM) to the culture media during OGD_{reox} (Fig.
5 6J-L). Contrary to the inhibition of IGF1R by PPP, its activation leads to a decrease of autophagy
6 flux as shown by the decrease of LC3-II (-47.6%, Fig. 6J and K) and the increase of SQSTM1/p62
7 (+77.3%, Fig. 6J and L). Altogether, these results indicate that PLAT/tPA decreases autophagy
8 by influencing IGF1R activation.

9 ***Proteolytically active PLAT/tPA protects neurons from cell death by decreasing autophagy***
10 ***through IGFR/PI3k-AKT/MTORC1.***

11 As we showed in Fig5, PLAT/tPA decreased-autophagy is independent of p-MAPK/ERK. As
12 expected, MAPK/ERK inhibition by SCH77 does not reverse the neuroprotection induced by
13 PLAT/tPA (Fig. 7A). On the contrary, Wortmannin reverses the protective effect of PLAT/tPA
14 on neuronal death (Fig. 7B). AKT inhibition with A6730 also prevents PLAT/tPA -mediated
15 neuroprotection (Fig. 7C). These results support the notion that PLAT/tPA protects neurons
16 by decreasing autophagy through the PI3K-AKT pathway. Importantly, PPP reverses the
17 neuroprotection mediated by PLAT/tPA (Fig. 7D).

18 Interestingly, we investigated the ability of an inactive form of PLAT/tPA (d-GGACK-tPA) to
19 mediate its effect in our OGD_{reox} model *in vitro*. Our results show that inactive PLAT/tPA does
20 not protect neurons from death (Fig. 7E). In addition, PLAT/tPA effect is independent from its
21 capacity to activate plasminogen into active plasmin, as the use of Aprotinin, an antifibrinolytic
22 molecule, does not reverse its neuroprotection (Fig. 7F). Altogether, these results show that

1 PLAT/tPA needs to be active to mediate both neuroprotection and a decrease in OGD-
2 enhanced autophagy through the IGFR/PI3K-AKT/MTORC1 pathway.

3 ***PLAT/tPA decreases autophagy and ischemic lesion in a mouse model of cerebral ischemia.***

4 We then moved to an *in vivo* model of cerebral ischemia consisting in the injection of thrombin
5 directly into the middle cerebral artery to form a clot [26, 27] (Fig. 8A). Twenty-four h after,
6 the lesion volume is assessed by MRI, motor deficits are assessed by grip test, and brains are
7 harvested for further analysis. In this model, we perform thrombolysis by PLAT/tPA like in
8 clinic (i.e. 10% bolus, 90% infusion), resulting in a decrease of the infarct size 24 h after
9 ischemia (-10.11 mm³, Fig. 8B). In addition, thrombolysed animals present a higher total force
10 at the grip test (Fig. 8C). Interestingly, the force deficit observed in non-thrombolysed animals
11 only comes from the left paw (Fig. 8E), which is in agreement with the ischemia performed on
12 the right middle cerebral artery. In this model, stroke leads to the cerebral activation of
13 autophagy, as demonstrated by the increase of LC3-II (Fig. 8F and G) together with a drop of
14 SQSTM1/p62 (Fig. 8F and H). Importantly, we found that autophagy decreases in PLAT/tPA -
15 thrombolysed animals (Fig. 8I). Indeed, we showed that MTORC1 phosphorylation is increased
16 (Fig. 8J), and that LC3-II (Fig. 8K), ATG5 (Fig. 8M), and ATG7 (Fig. 8N) are decreased in PLAT/tPA
17 treated animals. However, we did not observe any difference in SQSTM1/p62 protein levels
18 (Fig. 8L).

19 Altogether, our results show the neuroprotective effect of PLAT/tPA on neuronal death in
20 different *in vitro* models and in a thromboembolic mouse model of cerebral ischemia,
21 associated to a decrease of autophagy.

22 ***PLAT/tPA cleaves IGFBP3 and increases the bioavailability of IGF1 in vitro and in vivo in mice.***

1 Our results show that PLAT/tPA decreases autophagy and cell death through IGF1R. Therefore,
2 we tested the ability of PLAT/tPA to directly bind to and activate IGF1R. For this purpose, we
3 measured Actilyse (the recombinant form of PLAT/tPA), Wt- PLAT/tPA (a recombinant
4 PLAT/tPA produced in the lab) and Δ EGF- PLAT/tPA (a PLAT/tPA lacking its EGF-like domain,
5 produced in the same conditions than WT PLAT/tPA; Fig. S3A) binding capacity to IGF1R. All
6 tested PLAT/tPAs are able to bind to IGF1R in a dose dependent manner (Fig. S3B), however
7 KDs are too high to mediate a biological effect (from 1.71 to 7.78 μ M; Fig. S3C). We then
8 hypothesized a role of PLAT/tPA on the bioavailability of IGF1, the natural ligand of the
9 receptor. IGF1 is normally bound to IGFBPs (insulin like growth factor binding protein) and
10 cannot activate its receptor [28]. Interestingly, IGFBP3 cerebral levels are upregulated
11 following hypoxia [29, 30]. Moreover, IGFBP3 is sensitive to protease degradation [31].
12 Therefore, we incubated recombinant IGFBP3 with PLAT/tPA (equimolar) from 15 to 280 min.
13 After 15 min of incubation, PLAT/tPA promotes the cleavage of IGFBP3, and becomes total at
14 60 min (Fig. 9A). We analyzed by ELISA the levels of IGFBP3 in our neurons supernatants from
15 OGD_{reox}^{+/-} PLAT/tPA, and found that PLAT/tPA leads to a decrease of IGFBP3 in the media (-
16 266.6 μ g/ml, Fig. 9B). In addition, we also measured the levels of IGFBP3 in the serum of mice
17 subjected to the thromboembolic model +/- thrombolysis by PLAT/tPA at 1 and 24 h following
18 thrombolysis. We observed that without thrombolysis, the serum level of IGFBP3 stays
19 identical at 1 h and 24 h (Fig. 9C). Interestingly, like *in vitro*, PLAT/tPA induces the cleavage of
20 IGFBP3 in the serum of stroke mice at 1 and 24h following thrombolysis (Fig. 9C).
21 As PLAT/tPA mediates proteolysis of IGFBP3, we investigated the amount of IGF1 in serum of
22 ischemic mice with or without PLAT/tPA treatment (Fig. 9D-F). As expected, thrombolysis
23 increases free IGF1 at both 1 h (+4.13ng/ml, Fig. 9E) and 24 h (+7.01ng/ml, Fig. 7E) compared

1 to non-thrombolysed animals at the same time points. Surprisingly, thrombolysis by PLAT/tPA
2 increases also the concentration of the serum total IGF1 (Fig. 9D). However, after analyzing
3 the ratio between total and free IGF1, this increase in free IGF1 over time in PLAT/tPA -treated
4 mice was no more significant, whereas we confirmed that thrombolysis increases the
5 bioavailability of IGF1 in mice serum at both 1 and 24 h (Fig. 9F).

6 ***PLAT/tPA cleaves IGFBP3 in humans following cerebral ischemia.***

7 With a translational prospective, we decided to investigate in clinic the effect of thrombolysis
8 on serum levels of IGFBP3. In 5 acute stroke patients eligible for intravenous thrombolysis
9 (Table 2 for the clinical parameters), we measured baseline levels of serum IGFBP3 at 1, 2, and
10 24 h following PLAT/tPA injection (0.9 mg/kg). We found that IGFBP3 is decreased at 1 h and
11 recover with time (Fig. 9G); confirming that thrombolysis by PLAT/tPA is also responsible for
12 IGFBP3 cleavage in human.

13

1 **DISCUSSION**

2 Our study gives new important insight into the neuroprotective mechanisms of PLAT/tPA in
3 cerebral ischemia. We showed first that autophagy and its upstream pathways are strongly
4 activated in neurons *in vitro* during ischemia and *in vivo* after thromboembolic stroke and that
5 PLAT/tPA treatment is associated with a reduction in autophagy in ischemic conditions.
6 Second, we demonstrated that PLAT/tPA decreases autophagy through IGF1R activation and
7 MTORC1 phosphorylation, a key inhibitor of autophagy. Finally, we showed that, to mediate
8 its effects on IGF1R, PLAT/tPA degrades IGFBP3, the main inhibitor of IGF1, thus increasing its
9 bioavailability. This is particularly true with thrombolysis by PLAT/tPA in stroke patients,
10 where we show a drop of IGFBP3, opening new therapeutic approaches for the disease.

11 Using RNA sequencing in hypoxic neurons, we found a strong modulation of the major genes
12 controlling autophagy and its upstream and downstream pathways. We validated this *in vitro*
13 by using different pharmacological approaches. We found that OGD_{reox}-induced autophagy is
14 due to a drop of both MAPK/ERK and AKT signaling, and a decrease of phospho-MTORC1.
15 OGD_{reox} also decreases the phosphorylation of MTORC2, a complex between MTOR and Rictor
16 that activates and phosphorylates AKT at Ser⁴⁷³ to promote cell survival [32, 33]. MTORC2
17 could then indirectly activate MTORC1 through AKT.

18 Autophagy has often been associated with cell death during cerebral ischemia [5, 34-37]. We
19 have previously clearly demonstrated the role of enhanced autophagy in KaHx-induced
20 neuronal death [12] (Sup Fig. 3). In the present study, the protective effect of E64d-PepA (Fig.
21 2G) and chloroquine (Sup Fig. 1) also demonstrates a direct implication of autophagy in
22 neuronal death. The presence of PLAT/tPA is neuroprotective and alleviates the deregulation
23 of the autophagic pathways during OGD_{reox} (Fig. 1 and 2) and in KaHx (Sup Fig. 3). We found

1 that PLAT/tPA is able to decrease autophagy by increasing the phosphorylation of MTORC1,
2 through the activation of the PI3K-AKT pathway.

3 It has been suggested that some PLAT/tPA neuroprotection could be dependent on MTOR. In
4 non-stressed postnatal neurons, PLAT/tPA has been shown to promote survival mainly by
5 activating the MTOR cascade as its effect was reversed by rapamycin, an MTOR inhibitor [8].
6 Similarly, Wu and collaborators have shown, in an OGD model, that PLAT/tPA can decrease
7 neuronal cell death by mediating MTOR-dependent glucose recapture through SLC2A3/GLUT3
8 [9]. However, these studies did not investigate autophagy. Here, we report that PLAT/tPA can
9 directly activate MTORC1 phosphorylation and decrease autophagosome formation and
10 autophagy degradation.

11 It is well known that IGF1R can regulate autophagy through the PI3K-AKT/MTOR pathway [38-
12 40]. Here we show that the serine protease PLAT/tPA is able to mediate the activation of
13 IGF1R/PI3K-AKT/MTOR. We identified IGF1R as the receptor responsible for the PLAT/tPA -
14 dependent decrease of autophagy activation and subsequent neuronal death *in vitro* in OGD,
15 and *in vivo* in a mouse model of stroke. The natural ligand of IGF1R is IGF1, that has been
16 shown to be neuroprotective in many models of stroke [41]. Similarly, injections of circulating
17 IGF1 are able to mediate neuroprotection in a rat stroke model, validating IGF1R as a
18 promising target [42].

19 Six IGFBNs are known to inhibit the activity of IGF1, and almost 99% of the circulating IGF1 is
20 complexed with IGFBNs, and more particularly to IGFBN3 [43]. After cerebral ischemia, the
21 serum level of IGF1 and IGFBN3 is decreased [44], probably because their secretion is
22 regulated by growth hormones[45]. At the cellular level, IGFBN3 controls the bioavailability
23 and the half-life of IGF1, by preventing its binding to IGF1R [46-48]. IGFBN3 can be cleaved by

1 many proteases such as plasmin, thrombin and MMPs [49, 50]. Interestingly it has already
2 been suggested that PLAT/tPA, as well as uPA, are capable to cleave circulating IGFBP3 during
3 pregnancy [51]. In our study, we demonstrate that PLAT/tPA can directly cleave IGFBP3 *in vitro*
4 and *in vivo* during ischemia, resulting in an increase of free circulating IGF1. Through the
5 cleavage of IGFBP3, PLAT/tPA can modulate IGF1R signaling. This is the first time that a direct
6 link between PLAT/tPA and IGF1R is described. Interestingly both are expressed in the brain
7 parenchyma and are involved in many responses including brain development [52, 53],
8 neuronal survival following hypoxia [7, 54], inflammation [55-57], tissue remodeling after an
9 ischemic lesion [42, 58] and BBB integrity [59-61].

10 Overall, we show here that the thrombolytic drug PLAT/tPA degrades IGFBP3 in the blood of
11 mice and human stroke patients, leading to an increase of free IGF1 and the activation of IGFR.
12 This activates the PI3K-AKT signaling and MTOR phosphorylation to decrease the
13 enhancement of autophagic flux and its toxic effects. Our study demonstrate a new function
14 of the serine protease PLAT/tPA and highlight the IGFR/PI3K/MTOR pathway as a potential
15 therapeutic pathway to decrease deleterious enhanced autophagy following cerebral
16 ischemia.

1 MATERIALS AND METHODS

2 *Reagents.*

3 Dulbecco's modified eagle's medium (DMEM; D0819), poly-D-lysine (P7280), cytosine β -d-
4 arabinoside (C1768), fetal bovine serum (H7524), horse serum (H1270), D-glucose (G8644),
5 Tween 20 (P9416), phosphatase inhibitor cocktail (P2850), protease inhibitor cocktail (P2714),
6 Triton X-100 (T8787) paraformaldehyde, picropodophyllotoxin (T9576), wortmannin (W1628),
7 AKT1/AKT2 kinase inhibitor (A6730), isopropyl b-D-1-thiogalactopyranoside (IPTG; 16768),
8 E64d (E8640), aprotinin (A6130), human recombinant IGFBP3 (I5278) and TRI reagent (93289)
9 were from Sigma-Aldrich. Glutamine (25030123), laminin (23017015), glucose-free DMEM
10 (A1443001) and Pierce ECL Plus (32209) were purchased from Thermo Fisher. AG1478 (N-(3-
11 chlorophenyl)-6,7-dimethoxy-4-quinazolinane hydrochloride; 1276) and chloroquine (4109)
12 were from Tocris; Bicinchoninic acid assay (BCA Protein Assay kit; 23225) was from Pierce;
13 human recombinant PLAT/tPA (actilyse[®]) was from Boehringer Ingelheim; and MAPK1/ERK2-
14 MAPK3/ERK1 inhibitor (SCH772984) was from Selleckchem. Human recombinant IGF1R (291-
15 G1) was purchased from Bio-Techne. Pepstatin A (ALX-260-085) was purchased from Enzo Life
16 Sciences.

17 *Primary neuronal cell culture for Oxygen and glucose deprivation model.*

18 Primary cultures of cortical neurons were prepared from fetal mice (embryonic day 14) as
19 previously described [62]. Briefly, cells were cultured on individual glass bottom Petri dishes
20 (MatTek Corporation, P35G) or 24-well plates, previously coated with poly-d-lysine
21 (0.1 mg/ml) and laminin (0.02 mg/ml), in DMEM supplemented with 5% fetal bovine serum,
22 5% horse serum and 1 mM glutamine. Cultures were maintained at 37°C in a humidified 5%

1 CO₂ atmosphere. Cytosine β-D-arabinoside (10 μM) was added after 3 days in vitro (DIV) to
2 inhibit glial proliferation in the 24-well plates.

3 ***Oxygen and glucose deprivation (OGD).***

4 Neuronal cultures (12 DIV) were subjected for 1 h to OGD in a hypoxic chamber (AWEL
5 International, Ruskinn InvivO₂ 500) programmed at 0.2% O₂, 5% CO₂ and 37°C in
6 glucose/serum-free deoxygenated DMEM. Cortical neurons are treated with PLAT/tPA and/or
7 inhibitors in the hypoxic chamber, at the beginning of OGD. For reoxygenation, D-glucose
8 (4.5 mg/l) is added in cell media under normoxic conditions. Controls were subjected to sham
9 washes.

10 ***Primary neuronal cell culture for kainate/hypoxia model.***

11 Primary cultures of cortical neurons were prepared from 2-day-old Sprague-Dawley rat pups
12 (from Janvier) in accordance with the Swiss Laws for the protection of animals as previously
13 described [63] and the procedures were approved by the Vaud Cantonal Veterinary Office.
14 Dissociated neurons were plated on poly-D-lysine pre-coated 6 wells or 12 wells in neurobasal
15 medium supplemented with 2% B27, 0.5 mM L-glutamine and 100 μg/ml penicillin-
16 streptomycin. For PI staining, neurons were plated on poly-D-lysine pre-coated 12-mm glass
17 coverslips (Electron microscopy Sciences, 72294-02). Primary neuronal cultures were
18 maintained at 37°C with a humidified 5% CO₂-containing atmosphere and experiments were
19 performed after 11–13 DIV. These cultures contain around 15% of non-neuronal cells (MAP2
20 or RBFOX3/NeuN-negative).

21 ***Kainate/hypoxia model (KaHx).***

1 Primary cortical neurons were subjected to a hypoxic/excitotoxic stimulus by combining
2 kainate treatment (Ka, 30 μ M) with hypoxia performed in a sealed modular incubator chamber
3 (Billups-Rothenberg, MIC-101) that had been flushed for 5 min with a gas mixture at 6%
4 oxygen, as previously described [12]. KaHx stimulation was performed for 30 min in
5 bicarbonate-buffered saline (BBS) solution (116 mM NaCl, 5.4 mM KCl, 0.8 mM MgSO₄, 1 mM
6 NaH₂PO₄, 26.2 mM NaHCO₃, 0.01 mM glycine, 1.8 mM CaCl₂, pH 7.4) containing 4.5 mg/mL
7 glucose and previously deoxygenated for 1 h in the hypoxic chamber. At the end of KaHx
8 stimulation, BBS was replaced with the reserved neurobasal medium. For control stimulation,
9 primary cortical neurons were subjected to 30 min in normoxic BBS.

10 ***RNA sequencing.***

11 Three RNA-seq libraries per population (three biological replicates) were prepared using the
12 TruSeq Stranded mRNA sample Prep kit (Illumina) and sequenced on an Illumina GAIIx
13 sequencer as 75 bp paired reads by Hybrigenics-Helixio (Clermont-Ferrand, France). Samples
14 were quantified with Qubit 2.0 Fluorometer (Thermo Fischer) and checked with Nanodrop ND-
15 1000 (Thermo Fisher). Libraries were prepared with three kits: NEBNext Ultra II Directional
16 Library prep Kit (New England Biolabs, E7760), NEBNext Poly(A) mRNA Isolation Module (New
17 England Biolabs, E7490) and NEBNext Multiplex Oligos (New England Biolabs, E7140).
18 Sequencing was done with NextSeq 500 (Illumina). Data were processed with Bcl2fastq
19 (Illumina). Raw data were checked with FastQC (Babraham Institute). Reads were mapped on
20 reference genome (GRCm38, release 91) with TopHat (<https://ccb.jhu.edu/software/tophat>)
21 and differential expression analysis is done with Cuffdiff (Cufflinks suite,
22 <https://github.com/cole-trapnell-lab/cufflinks>). IT performs tests between supplied
23 conditions. FPKM values were calculated for each transcript in each sample (geometric library

1 normalization, pooled dispersion method). IT uses the reference annotation GTF file (GRCm38,
2 release 91) and quantitates the expression values and differential regulation across BAM files.
3 CummeRbund (<https://bioconductor.org/packages/release/bioc/html/cummeRbund.html>) R
4 package is designed to process global statistics and quality control. Pie charts and heatmaps
5 were generated using MATLAB 2020.

6 ***Neuronal death.***

7 Neuronal death was quantified 4 h after reoxygenation by measuring the LDH (lactate
8 dehydrogenase) activity released from damaged cells into the bathing medium with a
9 cytotoxicity detection kit (Roche Diagnostics, 91963). For KaHx experiments, neuronal death
10 was measured by both LDH assay using the Cytotox 96 nonradioactive cytotoxicity assay kit
11 (Promega, G1780) and quantification of the number of propidium iodide (PI)-positive nuclei
12 as previously described [12]. For PI-staining, cortical neurons on coverslips were washed and
13 incubated for 5 min in 5 µg/ml PI (Sigma-Aldrich, P4170) diluted in PBS (Sigma, 14190144)
14 containing 1 mM MgCl₂. After PBS washes neurons were fixed in 4% paraformaldehyde in 0.1
15 M PBS (pH 7.4) for 15 min. After a Hoechst staining, coverslips were mounted with FluorSave
16 (Calbiochem, 345-789-20) and images were taken using a Zeiss Axioplan 2 imaging
17 microscope.

18 ***Construction and production of recombinant PLAT/tPA***

19 WT PLAT/tPA and ΔEGF PLAT/tPA, rat PLAT/tPA sequence signal (aa 1–32) were amplified from
20 the full-length *Rattus norvegicus* PLAT/tPA cDNA (Swiss-prot accession P19637) using the
21 upstream primer 5'-CGGCTAGCATGAAGGGAGAGCTGTTG-3' and the downstream primer 5'-
22 GCGGATCC-GTGATGGTGAT-GGTGATGCCGA-GCTCCTCTTCT-3', thus including the NheI and

1 BamHI restriction sites, respectively, and a 6xHis tag just before the BamHI site. PCR products
2 were digested and inserted into the eukaryotic expression system pcDNA5/FRT. Coding
3 sequence for mature rat WT PLAT/tPA and Δ EGF PLAT/tPA proteins were amplified from the
4 same PLAT/tPA cDNA sequence by using the appropriate primers. Deletion of the EGF domain
5 was obtained by fusing the PCR product corresponding to the finger and K1 domains of
6 PLAT/tPA with the PCR product corresponding to the protease domain of PLAT/tPA. PCR
7 products were inserted into pcDNA5/FRT plasmid between the BamHI and XhoI restriction
8 sites. The various plasmids obtained were systematically checked by automated sequencing
9 (GATC-Biotech, Ebersberg). 293 HEK FlpIn Cells (Invitrogen, R75007) were then transfected
10 using Lipofectamine 2000 and positive clones were isolated using a 300 μ g/ml hygromycin B
11 (Sigma-Aldrich, H3274) selection. Supernatants containing PLAT/tPA -related mutants were
12 harvested and the proteins of interest purified on a nickel affinity matrix (Qiagen, 30210) as
13 described by the manufacturer. Elimination of imidazole was performed by overnight dialysis
14 against 0.5 M ammonium bicarbonate buffer. After concentration using Amicon Ultra (cutoff,
15 10 kD; Millipore, UFC5010), recombinant proteins were subjected to zymography to assess
16 their enzymatic activity and confirm their molecular mass.

17 ***Immunoblotting.***

18 Cells and tissues were dissociated in ice-cold TNT buffer (50 mM Tris-HCl, pH 7.4, 150 mM
19 NaCl, 0.5% Triton X-100, phosphatase and protease inhibitors cocktails) and centrifuged
20 (12,000 g, 4°C, 15 min). Protein concentration was measured by BCA Protein Assay method,
21 before migration on an SDS-PAGE gel (Bio-Rad) and a transfer onto a polyvinylidene difluoride
22 membrane. Membranes were blocked with PBS+0.1% Tween 20, 5% milk and incubated
23 overnight at 4°C in blocking buffer containing primary antibodies. The following primary

1 antibodies and dilutions were used: rabbit anti-MTOR (1:1000; Cell Signaling Technology,
2 2983), rabbit anti-phospho-MTOR Ser2448 (1:1000; Cell Signaling Technology, 2971), rabbit
3 anti-phospho-MTOR Ser2481 (1:1000; Cell Signaling Technology, 2974), rabbit anti-AKT
4 (1:1000; Cell Signaling Technology, 9272), rabbit anti-phospho/AKT Ser473 (1:1000; Cell
5 Signaling Technology, 9271), rabbit anti-ULK1-ULK2 (1:1000; Cell Signaling Technology, 8054),
6 rabbit anti-phospho-ULK1-ULK2 Ser757 (1:1000; Cell Signaling Technology, 6888), rabbit anti-
7 MAPK/ERK p44/42 (1:1000; Cell Signaling Technology, 9102), rabbit anti-phospho-MAPK/ERK
8 p44/42 (Thr202/Tyr204, 1:1000; Cell Signaling Technology, 9101), mouse anti-SQSTM1/p62
9 (1:1000; Abcam, ab56416), goat anti-IGFBRP3 (1:1000; Abcam, ab77635), rabbit anti-LC3B
10 (1:1000; Sigma-Aldrich, L7543), mouse anti-ATG5 (1:1000; Santa Cruz Biotechnology, sc-
11 133158), mouse anti-ATG7 (1:1000, Santa Cruz Biotechnology, sc-376212). Membranes were
12 then incubated with the corresponding peroxidase-conjugated secondary antibodies
13 (1:25000-50000; Sigma-Aldrich, A0545 and A9917) in blocking buffer, and visualized with an
14 enhanced chemiluminescence Pierce ECL Plus kit.

15 For KaHx experiments, primary cortical neurons were collected in lysis buffer (20 mM HEPES,
16 pH 7.4, 10 mM NaCl, 3 mM MgCl₂, 2.5 mM EGTA, 0.1 mM dithiothreitol, 50 mM NaF, 1 mM
17 Na₃VO₄, 1% Triton X-100) (reagents from Sigma-Aldrich), and a protease inhibitor cocktail
18 (Roche, 11873580001). After a brief sonication, protein concentration was measured by a
19 Bradford assay and proteins were separated by SDS PAGE, transferred on nitrocellulose
20 membrane and analysed by fluorescent immunoblotting. Primary antibodies were diluted in
21 blocking buffer solution (0.1% casein [Sigma-Aldrich, C8654], 0.2% PBS, dH₂O, 0.02% sodium
22 azide). The following primary antibodies were used: mouse anti-ACTB (1:2000; Invitrogen,
23 MAS-11869), rabbit anti-LC3 (1:1000; Abcam, ab48394) and rabbit anti-SQSTM1/p62 (1:2000;
24 Sigma, P0067). Membranes were then incubated with the corresponding Dy light-conjugated

1 secondary antibodies (1:10000; Cell Signaling Technology, 7074-7076). The Odyssey Infrared
2 Imaging System (LI-COR) was used to analyze protein bands using Odyssey v1.2 software (LI-
3 COR).

4 ***mRFP-GFP-LC3 plasmid transfection and quantification.***

5 Rat primary cortical neuronal cultures on 12-mm coverslips were transfected using
6 Lipofectamine 2000 (Invitrogen, 11668-019) as described previously [64]. Two-thirds of the
7 medium was removed and replaced for 5h by freshly prepared Neurobasal medium (Life
8 Technologies, 21103-049) plus transfection mix (3 µg of DNA for 6 µl of Lipofectamine) with
9 the tandem mRFP-GFP-LC3-expressing plasmid ptf LC3 (Addgene, 21074; deposited by
10 Tamotsu Yoshimori), allowing the distinction between acidic (GFP⁻ RFP⁺) and nonacidic (GFP⁺
11 RFP⁺) LC3-positive structures. One day after transfection, cortical neurons were subjected to
12 KaHx in the presence of absence of PLAT/tPA (300 nM), then washed in PBS MgCl₂, fixed for
13 15 min in 4% paraformaldehyde in PBS and finally stained with Hoechst (2 µg/ml for 5 min).
14 Coverslips were then mounted in FluorSave (Calbiochem, 345-789-20). Confocal images were
15 acquired using a Zeiss LSM 780 Meta confocal laser scanning microscope (Carl Zeiss). Signals
16 were sequentially visualized in the same section with acquisition performed in separated
17 mode. Images were processed with Zen software (Carl Zeiss) and mounted using Adobe
18 Photoshop 10.0 (Adobe Systems). Total LC3-positive dots (GFP⁺ RFP⁺ and GFP⁻ RFP⁺ dots), early
19 autophagosomes (GFP⁺ RFP⁺ dots) and autolysosomes (GFP⁻ RFP⁺ dots) were analyzed using
20 ImageJ software and expressed as a number of positive dots per neuron per µm².

21 ***Construction and production of lentivirus.***

1 The pGFP-LC3 (Addgene, 21074; deposited by Tamotsu Yoshimori) [65] was cloned in the
2 pENTR4 entry vector (Invitrogen, K253520). The GFP-LC3 was then transferred with the LR
3 clonase recombination system in the SIN-cPPT-PGK-gateway vector-WPRE [66] to generate
4 the SIN-cPPT-PGK-GFP-LC3-WPRE plasmid. The lentiviral vector was produced in 293T cells
5 with a four-plasmid system, concentrated by ultracentrifugation and resuspended in PBS
6 containing 1% bovine serum albumin (BSA; A9418) as previously reported [67]. Primary
7 cortical neurons were infected at DIV2 and OGD is performed at DIV12 as described below.

8 ***Immunocytochemistry.***

9 After a brief wash in PBS, neuronal cultures grown on glass bottom Petri dishes were fixed
10 during 5 min in 0.1 M PBS containing 4% paraformaldehyde and 5% sucrose. After PBS washes,
11 cells were blocked for 1 h in PBS-Tween 20 0.1% containing 2% BSA and then incubated
12 overnight at 4 °C in blocking buffer containing primary antibodies (chicken anti-GFP, 1:1000;
13 Abcam, ab13970; and mouse anti-RBFOX3/NeuN, 1:800, Millipore, MAB377). Primary
14 antibodies were revealed using FITC or Alexa Fluor 647-coupled secondary F(ab')₂ (1:800;
15 Jackson ImmunoResearch, 715-606-150). Confocal laser-scanning microscopy was performed
16 using a Leica SP5 confocal microscope (Leica Microsystems SAS).

17 ***Surface Plasmon Resonance.***

18 All SPR binding experiments were performed on BIACORE T200 instrument (GE Healthcare) at
19 25°C. Human recombinant IGF1R at 20 µg/mL in 5 mM maleate buffer pH 5, was immobilized
20 at 1000 RU by THIOL coupling procedure (according to recommendations and kits from GE
21 Healthcare, BR-1005-57). PLAT/tPA actilyse, WT PLAT/tPA and ΔEGF PLAT/tPA were injected
22 at 10, 5, 2.5, 1.25 and 0.625 µM in a kinetic titration series (Single Cycle Kinetics) at a flow rate

1 of 30 $\mu\text{L}/\text{min}$ for a contact time of 120 s, followed by a dissociation time of 10 min. The
2 regeneration between each SCK cycle has been realized by a 30-s injection of 1 M
3 ethanolamine pH 8. All SPR data processing and analyses were performed using BiaEvaluation
4 software 4.1 (GE Healthcare). The SPR response as a function of time, namely the sensorgram,
5 was then fitted globally or at the steady state by using a 1:1 binding model.

6 **IGFBP3 cleavage.**

7 Human recombinant IGFBP3 (300 nM) was incubated in the presence or not of equimolar
8 human recombinant PLAT/tPA (300 nM). The reaction was carried out at 37°C in PBS + 1% BSA.
9 After 15 min, 1 h, 2 h or 4 h of incubation. Samples were then analyzed to SDS/PAGE and
10 western blotting probed with anti-IGFBP3 antibody.

11 ***IGFBP3 dosage.***

12 Enzyme-linked immunosorbent assay (ELISA) was used to measure cell culture media
13 concentrations of mouse IGFBP3 (Bio-Techne, MGB300). Assays were performed according to
14 the manufacturers' instructions. Each sample was analyzed in duplicate and the mean of the
15 two values was used.

16 ***Animals.***

17 All the experiments were approved by the French ministry of education and research
18 (agreement numbers: #18344). The animal investigations were performed under the current
19 European directive (2010/63/EU) as incorporated in national legislation (Decree 87/848) and
20 in authorized laboratories (GIP Cyceron; approval n° E14118001). Experiments were

1 performed on groups of male mice (urss) weighing 25-40g aged of 8-12 weeks. All animals
2 were housed under standard conditions with a 12 h light/dark cycle.

3 ***Middle Cerebral Artery occlusion (MCAo) and PLAT/tPA (actilyse) treatment.***

4 Mice were separated in two groups: vehicle group (n=10) and PLAT/tPA group (n=9). Animals
5 were anesthetized with isoflurane 5% and maintained with 2% isoflurane in a 70%-30%
6 mixture of N₂O/O₂. Rectal temperature was controlled and maintained at 37 +/- 0.5°C
7 throughout the surgical procedure using a heating pad. Once placed in the stereotactic frame,
8 a catheter was placed in the tail vein of mice, to allow intravenous injection. Then, the skin
9 between the right eye and ear was incised, the middle cerebral artery (MCA) was exposed
10 through a small craniotomy and the dura was excised. A micropipette filled with purified
11 murine alpha-thrombin (0.05 mg; Stago BNL) was introduced into the MCA lumen, and 1 µL of
12 thrombin (1UI) was injected to induce in situ clot formation. The pipette was removed 10 min
13 post occlusion (time required for clot stabilization). The fibrinolytic (Actilyse® 10 mg/kg 10%
14 bolus, 90% perfusion for 40 min) or the control vehicle (saline) was injected 20 min after MCAo
15 in the tail vein. Physiological parameters were recorded by the MouseOxPlus® system (Starr
16 Life Sciences) and blood pressure values were assessed by the tail-cuff system BP-2000 Bioseb
17 system® (Visitech Systems). Surgeries and treatments were randomized and performed blind.
18 A sample of blood for serum purification was collected 1 h and 24 h after the end of PLAT/tPA
19 or vehicle injection.

20 ***Serum assays.***

21 After blood collection, tubes are put 1 h at room temperature to promote coagulation. Then,
22 serum is separated by two centrifugations at 1500g for 15 min at room temperature, and

1 stored at 80°C until total IGFBP3, IGF1 and free IGF1 were measured. ELISAs were used to
2 measure serum concentrations of mouse IGFBP3 (Bio-Techne, MGB300), mouse total IGF-I
3 and mouse free IGF-I (Biosynex, AL136-AL137). Assays were performed according to the
4 manufacturers' instructions.

5 ***Perfusion.***

6 Animals were deeply anesthetized with isoflurane 5%, and thereafter maintained with 2.5%
7 isoflurane in a 70%-30% mixture of N₂O/O₂. A transcatheter perfusion was performed with ice
8 cold 0.9% NaCl heparinized. Brains were removed and ipsilateral cortex are collected and
9 stored at –80°C immediately until processing.

10 ***Magnetic resonance imaging.***

11 Experiments were carried out on a Pharmascan 7 T/12 cm system using surface coils (Bruker).
12 T2-weighted images were acquired 24 h after cerebral ischemia using a multislice multiecho
13 sequence: TE/TR 33 ms/2500 ms. Lesion sizes were quantified on these images using ImageJ
14 software. T2*-weighted sequences were used to control if animals underwent hemorrhages
15 events. Two-dimensional time-of-flight angiographies (TE/TR 12 ms/7 ms) were acquired and
16 analyses of the MCA angiogram were performed to control the spontaneous recanalization of
17 the arteries of the mice.

18 ***Functional recovery assessment.***

19 Functional recovery was assessed using the grip strength test (BIOSEB). Mice, holding by the
20 tail, were dropped on a T-like-bar and gently removed by the experimenter. In this context of
21 unilateral (right) ischemic lesion due to stroke, the individual strength of each forepaw was

1 assessed with a wrench connected to the device, while a fake wrench (unconnected to the
2 electronic device) was placed on the other side. To obtain the mean strength, 5 assays per
3 mouse were performed to reduce variabilities with 1 min of rest between each assay. Data
4 were assessed in grams. Measurements were picked up the day before MCAo surgery
5 (baseline acquisition) and 24 h after MCAo surgery, ratio between the two values is calculated
6 in order to normalize each mouse with its own baseline values.

7 ***Human patient study.***

8 Human study protocol (PR[AG]154/2004 and PR[AG]157/2011) was approved by the local
9 ethics committee at Hospital Universitari Vall d'Hebron, and all patients or relatives gave
10 written informed consent. The study was performed in accordance with the ethical standards
11 as laid down in the 1964 Declaration of Helsinki and its later amendments. The study included
12 5 patients with an acute ischemic stroke and a proximal occlusion of the middle cerebral artery
13 occlusion documented by transcranial Doppler (TCD) admitted to the Emergency Department
14 who received PLAT/tPA in a standard 0.9-mg/kg dose (10% bolus, 90% continuous infusion for
15 1 h) within 3 h of symptom onset.

16 A clinical examination was performed on admission, after PLAT/tPA infusion and at 24 h from
17 symptom onset and at discharge. Stroke severity and neurological outcome were assessed
18 using the National Institutes of Health Stroke Scale (NIHSS). TCD assessments were performed
19 by an experienced neurologist using a Multi-Dop® X4 (DWL Elektronische Systeme GmbH,
20 Sipplingen) device as previously described 29, to assess recanalization.

21 Serial extractions were performed to test the effect of treatment on IGFBP3, peripheral blood
22 samples were drawn in all five patients at study entry (prior to t-PA administration) at 1 h and

1 2 h after PLAT/tPA infusion and at 24 h after stroke onset to obtain a temporal profile after
2 therapy. SST tubes were used to collect the blood, and serum was immediately separated by
3 centrifugation at 1500g for 15 min at 4°C, and stored at 80°C until IGFBP-3 was measured.

4 IGFBP-3 was measured using two ELISAs (RayBiotech, ELH-IGFBP3-1). Serum samples were
5 diluted at 1:300, and the assay was performed according to manufacturer's instructions. Each
6 sample was analyzed in duplicate and the mean of the two values was used. The mean intra-
7 assay coefficient of variation was <15% in all cases. And inter-assay variation was determined
8 testing two times in each plate a sample from one patient, and it was <15%.

9 ***Statistics.***

10 Statistical analyses were performed using GraphPad Prism 8.0.2 software. Results are
11 represented as mean \pm S.E.M. The distribution was assessed by the D'agostino Pearson
12 normality test. When data were normally distributed, Student's t-tests were used to compare
13 two conditions. When analysis of the data sets via parametric approaches turned out to be
14 inappropriate due to violation of residual normality, non-parametric approaches were used
15 (Mann-Whitney's U-tests for independent samples). An alpha level of $p < 0.05$ was used for
16 determination of significance in all statistical tests; all tests are two tailed.

17 For KaHx experiments if the data were normally distributed, one-way ANOVA was done
18 followed by a Tukey's multiple comparison test. If values were not normally distributed, the
19 non-parametric equivalent Kruskal-Wallis test was used followed by a Dunn's multiple
20 comparison test.

1 **ACKNOWLEDGEMENTS**

2 This work was supported by the INSERM (French National Institute for Health and Medical
3 Research), the French Ministry for Research and upper Education, the Caen-Normandy
4 University, the RHU project Marvelous (16-RHUS-0009), the ENTRAIN Marie Sklodowska-Curie
5 Innovative Training Network, Fonds Européens de Développement Economique et Régional
6 (FEDER) Normandie and AIRC IG n. 15572 to PC. J.P. is supported by grants from the Swiss
7 National Science Foundation (310030-163064 and 310030-182332).

8

1 **DISCLOSURE STATEMENT**

2 The authors declare no competing interests.

3

1 REFERENCES

- 2 1. Global, regional, and national burden of neurological disorders, 1990-2016: a
3 systematic analysis for the Global Burden of Disease Study 2016. *Lancet neurology* 2019;
4 18:459-80.
- 5 2. Thiebaut AM, Gauberti M, Ali C, et al. The role of plasminogen activators in stroke
6 treatment: fibrinolysis and beyond. *Lancet neurology* 2018; 17:1121-32.
- 7 3. Berkhemer OA, Fransen PS, Beumer D, et al. A randomized trial of intraarterial
8 treatment for acute ischemic stroke. *The New England journal of medicine* 2015; 372:11-20.
- 9 4. Tissue plasminogen activator for acute ischemic stroke. The National Institute of
10 Neurological Disorders and Stroke rt-PA Stroke Study Group. *The New England journal of*
11 *medicine* 1995; 333:1581-7.
- 12 5. Thiebaut AM, Hedou E, Marciniak SJ, et al. Proteostasis During Cerebral Ischemia.
13 *Frontiers in neuroscience* 2019; 13:637.
- 14 6. Jung CH, Jun CB, Ro SH, et al. ULK-Atg13-FIP200 complexes mediate mTOR signaling to
15 the autophagy machinery. *Mol Biol Cell* 2009; 20:1992-2003.
- 16 7. Louessard M, Bardou I, Lemarchand E, et al. Activation of cell surface GRP78 decreases
17 endoplasmic reticulum stress and neuronal death. *Cell Death Differ* 2017; 24:1518-29.
- 18 8. Grummisch JA, Jadavji NM, Smith PD. tPA promotes cortical neuron survival via mTOR-
19 dependent mechanisms. *Molecular and cellular neurosciences* 2016.
- 20 9. Wu F, Wu J, Nicholson AD, et al. Tissue-type plasminogen activator regulates the
21 neuronal uptake of glucose in the ischemic brain. *J Neurosci* 2012; 32:9848-58.
- 22 10. Wu F, Echeverry R, Wu J, et al. Tissue-type plasminogen activator protects neurons
23 from excitotoxin-induced cell death via activation of the ERK1/2-CREB-ATF3 signaling
24 pathway. *Molecular and cellular neurosciences* 2013; 52:9-19.
- 25 11. Klionsky DJ, Abdel-Aziz AK, Abdelfatah S, et al. Guidelines for the use and interpretation
26 of assays for monitoring autophagy (4th edition). *Autophagy* 2021:1-382.
- 27 12. Ginet V, Spiehlmann A, Rummel C, et al. Involvement of autophagy in hypoxic-
28 excitotoxic neuronal death. *Autophagy* 2014; 10:846-60.
- 29 13. Bhaskar PT, Hay N. The two TORCs and Akt. *Dev Cell* 2007; 12:487-502.
- 30 14. Kim J, Kundu M, Viollet B, et al. AMPK and mTOR regulate autophagy through direct
31 phosphorylation of Ulk1. *Nat Cell Biol* 2011; 13:132-41.
- 32 15. Huang J, Manning BD. A complex interplay between Akt, TSC2 and the two mTOR
33 complexes. *Biochemical Society transactions* 2009; 37:217-22.
- 34 16. Carriere A, Cargnello M, Julien LA, et al. Oncogenic MAPK signaling stimulates mTORC1
35 activity by promoting RSK-mediated raptor phosphorylation. *Current biology : CB* 2008;
36 18:1269-77.
- 37 17. Morris EJ, Jha S, Restaino CR, et al. Discovery of a novel ERK inhibitor with activity in
38 models of acquired resistance to BRAF and MEK inhibitors. *Cancer discovery* 2013; 3:742-50.
- 39 18. Zheng Y, Gu S, Li X, et al. Berbamine postconditioning protects the heart from
40 ischemia/reperfusion injury through modulation of autophagy. *Cell death & disease* 2017;
41 8:e2577.
- 42 19. Echeverry R, Wu J, Haile WB, et al. Tissue-type plasminogen activator is a
43 neuroprotectant in the mouse hippocampus. *The Journal of clinical investigation* 2010;
44 120:2194-205.

- 1 20. An J, Zhang C, Polavarapu R, et al. Tissue-type plasminogen activator and the low-
2 density lipoprotein receptor-related protein induce Akt phosphorylation in the ischemic brain.
3 *Blood* 2008; 112:2787-94.
- 4 21. Liot G, Roussel BD, Lebeurrier N, et al. Tissue-type plasminogen activator rescues
5 neurones from serum deprivation-induced apoptosis through a mechanism independent of its
6 proteolytic activity. *J Neurochem* 2006; 98:1458-64.
- 7 22. Bertrand T, Lesept F, Chevilly A, et al. Conformations of tissue plasminogen activator
8 (tPA) orchestrate neuronal survival by a crosstalk between EGFR and NMDAR. *Cell death &*
9 *disease* 2015; 6:e1924.
- 10 23. Lemarchand E, Maubert E, Haelewyn B, et al. Stressed neurons protect themselves by
11 a tissue-type plasminogen activator-mediated EGFR-dependent mechanism. *Cell Death Differ*
12 2015.
- 13 24. Parcq J, Bertrand T, Montagne A, et al. Unveiling an exceptional zymogen: the single-
14 chain form of tPA is a selective activator of NMDA receptor-dependent signaling and
15 neurotoxicity. *Cell Death Differ* 2012; 19:1983-91.
- 16 25. Duan Z, Choy E, Harmon D, et al. Insulin-like growth factor-I receptor tyrosine kinase
17 inhibitor cyclolignan picropodophyllin inhibits proliferation and induces apoptosis in
18 multidrug resistant osteosarcoma cell lines. *Molecular cancer therapeutics* 2009; 8:2122-30.
- 19 26. Orset C, Haelewyn B, Allan SM, et al. Efficacy of Alteplase in a Mouse Model of Acute
20 Ischemic Stroke: A Retrospective Pooled Analysis. *Stroke* 2016; 47:1312-8.
- 21 27. Orset C, Macrez R, Young AR, et al. Mouse model of in situ thromboembolic stroke and
22 reperfusion. *Stroke* 2007; 38:2771-8.
- 23 28. Ballard FJ, Knowles SE, Walton PE, et al. Plasma clearance and tissue distribution of
24 labelled insulin-like growth factor-I (IGF-I), IGF-II and des(1-3)IGF-I in rats. *The Journal of*
25 *endocrinology* 1991; 128:197-204.
- 26 29. Forbes K, Souquet B, Garside R, et al. Transforming growth factor- β (TGF β)
27 receptors I/II differentially regulate TGF β 1 and IGF-binding protein-3 mitogenic effects in
28 the human placenta. *Endocrinology* 2010; 151:1723-31.
- 29 30. Gluckman P, Klempt N, Guan J, et al. A role for IGF-1 in the rescue of CNS neurons
30 following hypoxic-ischemic injury. *Biochem Biophys Res Commun* 1992; 182:593-9.
- 31 31. Xu S, Savage P, Burton JL, et al. Proteolysis of insulin-like growth factor-binding protein-
32 3 by human skin keratinocytes in culture in comparison to that in skin interstitial fluid: the role
33 and regulation of components of the plasmin system. *The Journal of clinical endocrinology*
34 *and metabolism* 1997; 82:1863-8.
- 35 32. Guertin DA, Stevens DM, Thoreen CC, et al. Ablation in mice of the mTORC components
36 raptor, rictor, or mLST8 reveals that mTORC2 is required for signaling to Akt-FOXO and
37 PKC α , but not S6K1. *Dev Cell* 2006; 11:859-71.
- 38 33. Jacinto E, Facchinetti V, Liu D, et al. SIN1/MIP1 maintains rictor-mTOR complex
39 integrity and regulates Akt phosphorylation and substrate specificity. *Cell* 2006; 127:125-37.
- 40 34. Wen YD, Sheng R, Zhang LS, et al. Neuronal injury in rat model of permanent focal
41 cerebral ischemia is associated with activation of autophagic and lysosomal pathways.
42 *Autophagy* 2008; 4:762-9.
- 43 35. Wang N, Yang L, Zhang H, et al. MicroRNA-9a-5p Alleviates Ischemia Injury After Focal
44 Cerebral Ischemia of the Rat by Targeting ATG5-Mediated Autophagy. *Cellular physiology and*
45 *biochemistry : international journal of experimental cellular physiology, biochemistry, and*
46 *pharmacology* 2018; 45:78-87.

- 1 36. Puyal J, Vaslin A, Mottier V, et al. Postischemic treatment of neonatal cerebral ischemia
2 should target autophagy. *Annals of neurology* 2009; 66:378-89.
- 3 37. Xie C, Ginet V, Sun Y, et al. Neuroprotection by selective neuronal deletion of Atg7 in
4 neonatal brain injury. *Autophagy* 2016; 12:410-23.
- 5 38. Troncoso R, Vicencio JM, Parra V, et al. Energy-preserving effects of IGF-1 antagonize
6 starvation-induced cardiac autophagy. *Cardiovascular research* 2012; 93:320-9.
- 7 39. Lin Y, Deng W, Pang J, et al. The microRNA-99 family modulates hepatitis B virus
8 replication by promoting IGF-1R/PI3K/Akt/mTOR/ULK1 signaling-induced autophagy. *Cellular*
9 *microbiology* 2017; 19.
- 10 40. Wang S, Gu K. Insulin-like growth factor 1 inhibits autophagy of human colorectal
11 carcinoma drug-resistant cells via the protein kinase B/mammalian target of rapamycin
12 signaling pathway. *Molecular medicine reports* 2018; 17:2952-6.
- 13 41. Kooijman R, Sarre S, Michotte Y, et al. Insulin-like growth factor I: a potential
14 neuroprotective compound for the treatment of acute ischemic stroke? *Stroke* 2009; 40:e83-
15 8.
- 16 42. De Geyter D, De Smedt A, Stoop W, et al. Central IGF-I Receptors in the Brain are
17 Instrumental to Neuroprotection by Systemically Injected IGF-I in a Rat Model for Ischemic
18 Stroke. *CNS neuroscience & therapeutics* 2016; 22:611-6.
- 19 43. Kelley KM, Oh Y, Gargosky SE, et al. Insulin-like growth factor-binding proteins (IGFBPs)
20 and their regulatory dynamics. *Int J Biochem Cell Biol* 1996; 28:619-37.
- 21 44. Schwab S, Spranger M, Krempien S, et al. Plasma insulin-like growth factor I and IGF
22 binding protein 3 levels in patients with acute cerebral ischemic injury. *Stroke* 1997; 28:1744-
23 8.
- 24 45. Blum WF, Albertsson-Wikland K, Rosberg S, et al. Serum levels of insulin-like growth
25 factor I (IGF-I) and IGF binding protein 3 reflect spontaneous growth hormone secretion. *The*
26 *Journal of clinical endocrinology and metabolism* 1993; 76:1610-6.
- 27 46. Blat C, Villaudy J, Binoux M. In vivo proteolysis of serum insulin-like growth factor (IGF)
28 binding protein-3 results in increased availability of IGF to target cells. *The Journal of clinical*
29 *investigation* 1994; 93:2286-90.
- 30 47. Imai Y, Moralez A, Andag U, et al. Substitutions for hydrophobic amino acids in the N-
31 terminal domains of IGFBP-3 and -5 markedly reduce IGF-I binding and alter their biologic
32 actions. *J Biol Chem* 2000; 275:18188-94.
- 33 48. Jogie-Brahim S, Feldman D, Oh Y. Unraveling insulin-like growth factor binding protein-
34 3 actions in human disease. *Endocrine reviews* 2009; 30:417-37.
- 35 49. Booth BA, Boes M, Bar RS. IGFBP-3 proteolysis by plasmin, thrombin, serum: heparin
36 binding, IGF binding, and structure of fragments. *The American journal of physiology* 1996;
37 271:E465-70.
- 38 50. Fowlkes JL, Enghild JJ, Suzuki K, et al. Matrix metalloproteinases degrade insulin-like
39 growth factor-binding protein-3 in dermal fibroblast cultures. *J Biol Chem* 1994; 269:25742-6.
- 40 51. Bang P, Fielder PJ. Human pregnancy serum contains at least two distinct proteolytic
41 activities with the ability to degrade insulin-like growth factor binding protein-3.
42 *Endocrinology* 1997; 138:3912-7.
- 43 52. Pasquet N, Douceau S, Naveau M, et al. Tissue-Type Plasminogen Activator Controlled
44 Corticogenesis Through a Mechanism Dependent of NMDA Receptors Expressed on Radial
45 Glial Cells. *Cereb Cortex* 2018.

- 1 53. Nieto-Estevez V, Defterali C, Vicario-Abejon C. IGF-I: A Key Growth Factor that
2 Regulates Neurogenesis and Synaptogenesis from Embryonic to Adult Stages of the Brain.
3 *Frontiers in neuroscience* 2016; 10:52.
- 4 54. Liu W, D'Ercole JA, Ye P. Blunting type 1 insulin-like growth factor receptor expression
5 exacerbates neuronal apoptosis following hypoxic/ischemic injury. *BMC neuroscience* 2011;
6 12:64.
- 7 55. Bake S, Selvamani A, Cherry J, et al. Blood brain barrier and neuroinflammation are
8 critical targets of IGF-1-mediated neuroprotection in stroke for middle-aged female rats. *PLoS*
9 *One* 2014; 9:e91427.
- 10 56. Siao CJ, Fernandez SR, Tsirka SE. Cell type-specific roles for tissue plasminogen
11 activator released by neurons or microglia after excitotoxic injury. *J Neurosci* 2003; 23:3234-
12 42.
- 13 57. Flavin MP, Zhao G, Ho LT. Microglial tissue plasminogen activator (tPA) triggers
14 neuronal apoptosis in vitro. *Glia* 2000; 29:347-54.
- 15 58. Pu H, Shi Y, Zhang L, et al. Protease-independent action of tissue plasminogen activator
16 in brain plasticity and neurological recovery after ischemic stroke. *Proc Natl Acad Sci U S A*
17 2019; 116:9115-24.
- 18 59. Benchenane K, Berezowski V, Ali C, et al. Tissue-type plasminogen activator crosses the
19 intact blood-brain barrier by low-density lipoprotein receptor-related protein-mediated
20 transcytosis. *Circulation* 2005; 111:2241-9.
- 21 60. Liang M, Woodard LE, Liang A, et al. Protective role of insulin-like growth factor-1
22 receptor in endothelial cells against unilateral ureteral obstruction-induced renal fibrosis. *Am*
23 *J Pathol* 2015; 185:1234-50.
- 24 61. Polavarapu R, Gongora MC, Yi H, et al. Tissue-type plasminogen activator-mediated
25 shedding of astrocytic low-density lipoprotein receptor-related protein increases the
26 permeability of the neurovascular unit. *Blood* 2007; 109:3270-8.
- 27 62. Roussel BD, Mysiorek C, Rouhiainen A, et al. HMGB-1 promotes fibrinolysis and
28 reduces neurotoxicity mediated by tissue plasminogen activator. *Journal of cell science* 2011;
29 124:2070-6.
- 30 63. Grishchuk Y, Ginet V, Truttmann AC, et al. Beclin 1-independent autophagy contributes
31 to apoptosis in cortical neurons. *Autophagy* 2011; 7:1115-31.
- 32 64. Vaslin A, Puyal J, Borsello T, et al. Excitotoxicity-related endocytosis in cortical neurons.
33 *J Neurochem* 2007; 102:789-800.
- 34 65. Kabeya Y, Mizushima N, Ueno T, et al. LC3, a mammalian homologue of yeast Apg8p,
35 is localized in autophagosomal membranes after processing. *EMBO J* 2000; 19:5720-8.
- 36 66. Drouet V, Perrin V, Hassig R, et al. Sustained effects of nonallele-specific Huntingtin
37 silencing. *Annals of neurology* 2009; 65:276-85.
- 38 67. Hottinger AF, Azzouz M, Deglon N, et al. Complete and long-term rescue of lesioned
39 adult motoneurons by lentiviral-mediated expression of glial cell line-derived neurotrophic
40 factor in the facial nucleus. *J Neurosci* 2000; 20:5587-93.

41

42

1 **Table 1.** RNAseq pathway analysis of neurons subjected or not to OGDreox +/- 300 nM PLAT/tPA

AMPK signaling pathway	Apoptosis
Autophagy animal	Autophagy other
Calcium signaling pathway	cAMP signaling pathway
Cell cycle	EGFR tyrosine kinase inhibitor resistance
Endocytosis	ERBB signalling pathway
Focal adhesion	FOXO signaling pathway
GABAergic synapse	Glutamatergic synapse
HIF1 signaling pathway	JAK-STAT signaling pathway
Long-term potentiation	Lysosome
MAPK signaling pathway	MTOR signaling pathway
Neuroactive ligand-receptor interaction	Neurotrophin signaling pathway
NFKB signaling pathway	TP53 signaling pathway
Phagosome	Phosphatidylinositol signaling pathway
PLD (phospholipase D) signaling pathway	PI3K-AKT signaling pathway
Protein processing in endoplasmic reticulum	RAP1 signaling pathway
Regulation of actin cytoskeleton	TGFB/TGF- β signaling pathway
TLR (toll-like receptor) signaling pathway	

- 2 Pathways were analysed following the Kyoto Encyclopedia of Genes and Genomes (KEGG pathway).
- 3 Pathways linked to OGDreox or ischemia/hypoxia are highlighted in red; pathways linked to autophagy
- 4 are highlighted in green.

1

2 **Table 2.** Clinical parameters of the five acute stroke patients eligible for intravenous thrombolysis.

Patients	A	B	C	D	E	Median
Age	71	97	72	68	69	71
Gender	2	1	2	1	2	2
Smoking	1	0	DM	1	0	2
Hypertension	0	0	1	0	1	2
Diabetis	1	0	0	0	0	1
Atrial fibrillation	0	1	1	0	0	2
Myocardial ischemia	0	0	0	0	0	0
Hypercholesterolemia	0	0	0	0	1	1
Antiplatelet	0	0	DM	0	0	0
Statins	0	0	1	0	1	2
Diabetis treatment	0	0	1	0	1	0
Occlusion site	MCA	MCA	MCA	Basilar	MCA	/
Initial NIHSS score	21	23	9	16	17	17

Woman: 1 Man: 2 No: 0 Yes: 1 MD: Missing data

3

4 **LEGENDS**

5 **Figure 1.** Autophagy pathways are increased by oxygen and glucose deprivation in cortical
6 neurons. **(A)** Pie charts representing significantly ($p < 0.05$) up- and downregulated transcripts
7 in Ctrl Vs OGD_{reox}, Ctrl Vs OGD_{reox} + PLAT/tPA and OGD_{reox} Vs OGD_{reox} + PLAT/tPA conditions.
8 Heatmaps of genes significantly affected ($p < 0.05$) in both OGD_{reox} and OGD_{reox} + PLAT/tPA
9 conditions Vs Ctrl condition for **(B)** MAPK signaling pathway, **(C)** PI3K-AKT signaling pathway,
10 **(D)** MTOR signaling pathway, and **(E)** autophagy pathway. Heatmaps of genes significantly
11 affected ($p < 0.05$) between Ctrl and OGD_{reox} conditions for **(F)** MAPK signaling pathway, **(G)**
12 PI3K-AKT signaling pathway, **(H)** MTOR signaling pathway, and **(I)** autophagy pathway.
13 Heatmaps of genes significantly affected ($p < 0.05$) between Ctrl and OGD_{reox} + PLAT/tPA
14 conditions for **(J)** MAPK signaling pathway, **(K)** PI3K-AKT signaling pathway, **(L)** MTOR signaling
15 pathway, and **(M)** autophagy pathway.

1 **Figure 2.** PLAT/tPA decreases OGD-induced autophagy and cell death in cortical neurons. **(A)**
2 Schematic representation of *in vitro* ischemic model consisting in 1h of OGD followed by 3h of
3 reoxygenation (OGD_{reox}), on 12 days old murine primary cortical neurons in the presence or
4 not of treatments. **(B)** Representative western blots of LC3-II, SQSTM1/p62 and ACTB in
5 neurons subjected or not to OGD_{reox} with and without PLAT/tPA (300 nM). Densitometric
6 quantification of LC3-II **(C)** and SQSTM1/p62 **(D)** normalized to ACTB (mean±S.E.M. n=5 and 6
7 independent experiments for LC3 and SQSTM1/p62 respectively; ##: p<0.01 and #: p<0.05
8 compared to Ctrl; **: p<0.01 and *: p<0.05 compared between OGD_{reox} conditions; Mann–
9 Whitney test). **(E)** Neuronal death of pure cortical neurons assessed by LDH release after
10 OGD_{reox} in the presence or not of 10 µg/ml of E64d and 10 µg/ml pepstatin A (mean±S.E.M.
11 n=12 for Ctrl, n=16 for Ctrl+E64d-PepA, n=31 for OGD_{reox}, n=33 for OGD_{reox}+E64d-PepA, n=28
12 for OGD_{reox}+ PLAT/tPA from 4 independent experiments; ###: p<0.001 compared to Ctrl; ***:
13 p<0.001 compared between OGD_{reox}; Mann–Whitney test). **(F)** Representative western blots
14 of LC3-II, SQSTM1/p62 and ACTB in neurons subjected or not to OGD_{reox} in the presence or
15 not of 10 µg/ml of E64d and 10 µg/ml Pepstadin A. Densitometric quantification of LC3-II **(G)**
16 and SQSTM1/p62 **(H)** normalized to ACTB (mean±S.E.M. n=8 independent experiments; ##:
17 p<0.01 and ###: p<0.001 compared to Ctrl; ***: p<0.001 compared between OGD_{reox}; Mann–
18 Whitney test.

19 **Figure 3.** PLAT/tPA prevents hypoxic/excitotoxic-induced autophagy and neuronal death. **(A-**
20 **C)** PLAT/tPA (300 nM) affords strong neuroprotection against cell death induced by the
21 combination of kainate (Ka, 30 µM) and hypoxia (Hx, 6% oxygen) for 30 min in primary cortical
22 neuron cultures as shown by a reduction in both **(A)** the release of lactate dehydrogenase
23 (LDH) and **(B-C)** propidium iodide (PI)-staining 6h after KaHx treatment. **(A)** Quantification of
24 released LDH expressed as a percentage of the KaHx value (data are represented as

1 mean±S.E.M. n=8 from 3 independent experiments; ###: p<0.001 compared to Ctrl; ***:
2 p<0.001 compared between KaHx; Tukey's multiple comparisons tests) **(B)** Quantification of
3 the PI-positive nuclei expressed as a percentage of the number of KaHx PI-positive nuclei (data
4 are represented as mean±S.E.M. n=24 from 3 independent experiments; ###: p<0.001
5 compared to Ctrl; ***: p<0.001 and **: p<0.01 compared between KaHx; Tukey's multiple
6 comparisons tests) **(C)** Representative images of PI- (magenta) and Hoechst- (cyan) stained
7 nuclei. Bars = 100 μm. **(D-F)** PLAT/tPA treatment prevents KaHx-induced autophagy as
8 indicated by a suppression of both KaHx-induced **(E)** increase in LC3-II level and **(F)** degradation
9 of SQSTM1/p62. **(D)** Representative western blots of LC3-II and SQSTM1/p62 in neurons
10 subjected or not to KaHx in the presence of PLAT/tPA 0 to 300 nM. ACTB was used as loading
11 control. **(E)** Densitometric quantification of LC3-II normalized to ACTB. Levels expressed as a
12 percentage of KaHx value (data are represented as mean±S.E.M. n=8 independent
13 experiments; ##: p<0.01 compared to Ctrl; **: p<0.01 compared between KaHx; Tukey's
14 multiple comparisons tests). **(F)** Densitometric quantification of SQSTM1/p62 normalized to
15 ACTB. Levels expressed as a percentage of KaHx value (data are represented as mean±S.E.M.
16 n=8 independent experiments; ###: p<0.001 and ##: p<0.01 compared to Ctrl; ***: p<0.001
17 compared between KaHx; Tukey's multiple comparisons tests). **(G)** Representative confocal
18 images of transfected cortical neurons with a tandem mRFP-GFP-LC3-expressing plasmid in
19 control (Ct) or kainate/hypoxia (KaHx) condition with or without PLAT/tPA (300 nM)
20 treatment. **(H-I)** Corresponding quantifications of the number of dots per μm² of **(H)** GFP⁺
21 (yellow) /RFP⁺ (magenta) (early autophagosomes) **(I)** GFP⁻/RFP⁺ (mature
22 autophagosomes/autolysosomes) and **(J)** the total of the two types (total dots). PLAT/tPA
23 treatment prevents the increase in the autophagy flux (both autophagosome formation and
24 autophagosome/lysosome fusion) induced after 3h of KaHx stimulation. Data are represented

1 as mean±S.E.M. n=20; ###: p<0.001 compared to Ctrl; ***: p<0.001 compared with KaHx;
2 Tukey's multiple comparisons tests).

3 **Figure 4.** OGD-enhanced autophagy is dependent on MTOR pathway. **(A)** Representative
4 western blots of p-MTORC1 (Ser2448), p-MTORC2 (Ser2481), MTOR total, p-ULK1-ULK2
5 (Ser757) and ACTB in neurons subjected or not to OGD_{reox} with and without PLAT/tPA (300
6 nM). Densitometric quantification of p-MTORC1 (Ser2448) normalized to MTOR total **(B)**, of
7 p-MTORC2 (Ser2481) normalized to MTOR total **(C)**, of p-ULK1-ULK2 (Ser757) normalized to
8 ACTB **(D)** (mean±S.E.M. n=4 to 6 independent experiments; ##: p<0.01 and #: p<0.05
9 compared to Ctrl; **: p<0.01 and *: p<0.05 compared to OGD_{reox}; Mann–Whitney test).

10 **Figure 5.** PLAT/tPA decreases OGD-induced autophagy through the PI3K-AKT pathway. **(A)**
11 Representative western blots of p-MAPK/ERK1/2 (Thr202, Tyr204), MAPK/ERK1/2 total, p-AKT
12 (Ser473) and AKT total in neurons subjected or not to OGD_{reox} with and without PLAT/tPA (300
13 nM). Densitometric quantification of p-MAPK/ERK1/2 (Thr202, Tyr204) normalized to
14 MAPK/ERK1/2 total **(B)** and of p-AKT (Ser473) normalized to AKT total **(C)** (mean±S.E.M. n=5
15 independent experiments; ##: p<0.01 compared to Ctrl; **: p<0.01 and p<0.05 compared
16 between OGD_{reox} conditions; Mann–Whitney test). **(D)** Representative western blots of LC3-II,
17 SQSTM1/p62 and ACTB in neurons subjected or not to OGD_{reox} with and without PLAT/tPA
18 (300 nM) in the presence or not of 5 μM SCH772984 (SCH77; MAPK/ERK1/2 inhibitor).
19 Densitometric quantification of LC3-II **(E)** and SQSTM1/p62 **(F)** normalized to ACTB
20 (mean±S.E.M. n=6 independent experiments; #: p<0.05 compared to Ctrl; **: p<0.01 and *:
21 p<0.05 compared between OGD_{reox} conditions; Mann–Whitney test). **(G)** Representative
22 western blots of LC3-II, SQSTM1/p62 and ACTB in neurons subjected or not to OGD_{reox} with
23 and without PLAT/tPA (300 nM) in the presence or not of 10 μM A6730 (AKT inhibitor).

1 Densitometric quantification of LC3-II (**H**) and SQSTM1/p62 (**I**) normalized to ACTB
2 (mean±S.E.M. n=5 and 6 independent experiments for LC3 and SQSTM1/p62 respectively; ##:
3 p<0.01 and #: p<0.05 compared to Ctrl; **: p<0.01 and *: p<0.05 compared between OGD_{reox}
4 conditions; Mann–Whitney test). (**J**) Representative western blots of LC3-II, SQSTM1/p62 and
5 ACTB in neurons subjected or not to OGD_{reox} with and without PLAT/tPA (300 nM) in the
6 presence or not of 250 nM wortmannin (Wort; PI3K inhibitor). Densitometric quantification
7 of LC3-II (**K**) and SQSTM1/p62 (**L**) normalized to ACTB (as mean±S.E.M. n=5 independent
8 experiments; ##: p<0.01 and #: p<0.05 compared to Ctrl; *: p<0.05 compared between OGD_{reox}
9 conditions; Mann–Whitney test).

10 **Figure 6.** PLAT/tPA decreases OGD-induced PI3K-AKT signaling through IGF1R receptor. (**A**)
11 Representative western blots of LC3-II, SQSTM1/p62 and ACTB in neurons subjected or not to
12 OGD_{reox} with and without PLAT/tPA (300 nM) in the presence or not of 5 μM AG1478 (EGFR
13 inhibitor). Densitometric quantification of LC3-II (**B**) and SQSTM1/p62 (**C**) normalized to ACTB
14 (mean±S.E.M. n=4 and 5 independent experiments for LC3 and SQSTM1/p62 respectively; ##:
15 p<0.01 and #: p<0.05 compared to Ctrl; **: p<0.01 and*: p<0.05 compared between OGD_{reox}
16 conditions; Mann–Whitney test). (**D**) Representative western blots of p-AKT (Ser473), AKT
17 total, p-MTORC1 (Ser2448) and MTOR total in neurons subjected or not to OGD_{reox} with and
18 without PLAT/tPA (300 nM) in the presence or not of 100 nM Picropodophyllotoxin.
19 Densitometric quantification of p-AKT (Ser473) normalized to AKT total (**E**) and of MTORC1
20 (Ser2448) normalized to MTOR total (**F**) (mean±S.E.M. n=4 independent experiments; #:
21 p<0.05 compared to Ctrl; *: p<0.05 compared between OGD_{reox} conditions; Mann–Whitney
22 test). (**G**) Representative western blots of LC3-II, SQSTM1/p62 and ACTB in neurons subjected
23 or not to OGD_{reox} with and without PLAT/tPA (300 nM) in the presence or not of 100 nM
24 Picropodophyllotoxin (PPP; IGF1R inhibitor). Densitometric quantification of LC3-II (**H**) and of

1 SQSTM1/p62 (I) normalized to ACTB (mean±S.E.M. n=5 independent experiments; ##: p<0.01
2 compared to Ctrl; **: p<0.01 compared between OGD_{reox}; Mann–Whitney test). (J)
3 Representative western blots of LC3-II, SQSTM1/p62 and ACTB in neurons subjected or not to
4 OGD_{reox} with and without IGF1 (250 nM). Densitometric quantification of LC3-II (K) and
5 SQSTM1/p62 (L) normalized to ACTB (mean±S.E.M. n=6 and 7 independent experiments for
6 LC3 and SQSTM1/p62 respectively; ###: p<0.005 and ##: p<0.01 compared to Ctrl; **: p<0.01
7 compared between OGD_{reox} conditions; Mann–Whitney test).

8 **Figure 7.** Active PLAT/tPA protects neurons from cell death by decreasing autophagy through
9 IGF1R/PI3k-AKT/MTORC1. Neuronal death of pure cortical neurons assessed by LDH release
10 after OGD_{reox} in the presence or not of PLAT/tPA and 5 μM SCH772984 (SCH77; MAPK/ERK1/2
11 inhibitor) (A), 250 nM Wortmannin (Wort; PI3K inhibitor) (B), 10 μM A6730 (AKT inhibitor) (C),
12 100 nM Picropodophyllotoxin (PPP; IGF1R inhibitor) (D), 300 nM d-GGACK- PLAT/tPA (inactive
13 PLAT/tPA) (E) or 1 μM Aprotinin (plasmin inhibitor) (F) (mean±S.E.M. n=14 to 30 from 6
14 independent experiments; ###: p<0.001 compared to Ctrl; ***: p<0.001, **: p<0.01 and *:
15 p<0.05 compared between OGD_{reox}; Mann–Whitney test).

16 **Figure 8.** PLAT/tPA decreases autophagy and ischemic lesion in a mouse model of cerebral
17 ischemia. (A) Schematic representation of Middle Cerebral Artery occlusion (MCAo) based on
18 thrombin injection in the MCA. (B) Representative MRI images and infarct volumes (mm³) 24
19 h after MCAo in mice treated with vehicle or PLAT/tPA. (mean±S.E.M; n=10 for Vehicle; n=9
20 for PLAT/tPA; *: p<0.05; t test). Grip strength of both forepaws (C), right forepaw (D), or left
21 forepaw (E) in mice treated with vehicle or PLAT/tPA after MCAo. Measurements were picked
22 up the day before MCAo surgery (baseline acquisition) and 24 h after MCAo surgery, ratio
23 between the two values is calculated in order to normalize each mouse with its own baseline

1 values (mean±S.E.M; n=10 for Vehicle; n=9 for PLAT/tPA; ***: p<0.001, *: p<0.05; t test) **(F)**
2 Representative western blots of LC3-II, SQSTM1/p62 and ACTB in ipsilateral cortex of mice
3 after MCAo. Densitometric quantification of LC3-II **(G)** or SQSTM1/p62 **(H)** normalized to ACTB
4 (mean±S.E.M. n=4 independent experiments; *: p<0.05; Mann–Whitney test). **(I)**
5 Representative western blots of p-MTOR (Ser2448), MTOR tot, LC3-II, SQSTM1/p62, ATG5,
6 ATG7 and ACTB in cortex treated with vehicle or PLAT/tPA after MCAo. Densitometric
7 quantification of p-MTORC1 (Ser2448) normalized to MTOR total **(J)**, of LC3-II normalized to
8 ACTB **(K)**, of SQSTM1/p62 normalized to ACTB **(L)**, of ATG5 normalized to ACTB **(M)**, of ATG7
9 normalized to ACTB **(N)** (mean±S.E.M. n=8 to 10; *: p<0.05; Mann–Whitney test).

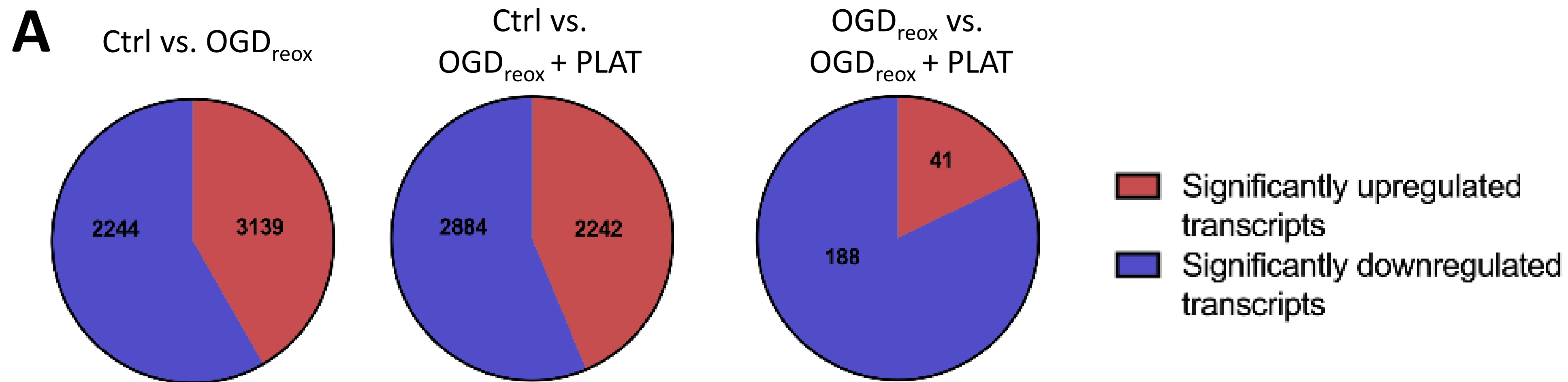
10 **Figure 9.** PLAT/tPA cleaves IGFBP3 and increases the bioavailability of IGF1 in vitro, in vivo in
11 mice and in humans. **(A)** Human recombinant IGFBP3 was incubated or not with PLAT/tPA
12 during 15 min, 1 h, 2 h or 4 h. Samples were then analyzed to SDS/PAGE and western blotting
13 probed with anti-IGFBP3 antibody. **(B)** Concentration of IGFBP3 (ng/ml) measured by ELISA in
14 cell culture medium of cortical neurons subjected or not to OGD_{reox} with or without PLAT/tPA
15 (300 nM) (mean±S.E.M. n=8 independent experiments; ***: p<0.001; t test). **(C)**
16 Concentration of IGFBP3 (ng/ml) measured by ELISA in serum of mice treated with vehicle or
17 PLAT/tPA after MCAo. Serum was collected 1 h and 24 h after treatment (mean±S.E.M; n=8
18 for vehicle 1h; n=9 for PLAT/tPA 1h; n=8 for vehicle 24h; n=7 for PLAT/tPA 1h; ###: p<0.01
19 vehicle 1h compared to PLAT/tPA 1h; \$: p<0.05 vehicle 24h compared to PLAT/tPA 24h; Mann-
20 Whitney test). Total IGF1 (ng/ml) **(D)**, Free IGF1 (ng/ml) **(E)**, and ratio between free and total
21 IGF1 **(F)** measured by ELISA in serum of mice treated with vehicle or PLAT/tPA after MCAo.
22 Serum was collected 1 h and 24 h after treatment (mean±S.E.M; n=8 for vehicle 1h; n=9 for
23 PLAT/tPA 1h; n=8 for vehicle 24h; n=7 for PLAT/tPA 1h; ###: p<0.001, #: p<0.01 vehicle 1h
24 compared to PLAT/tPA 1h; \$\$\$: p<0.001, \$\$: p<0.01 vehicle 24h compared to PLAT/tPA 24h;

1 ***: $p < 0.001$, *: $p < 0.05$ PLAT/tPA 1h compared to PLAT/tPA 24h; Mann-Whitney test). (G)
2 Concentration of IGFBP3 (ng/ml) was measured by ELISA in serum of stroke patients before
3 PLAT/tPA injection (baseline) and 1 h, 2 h and 24 h after t PLAT/tPA injection (mean \pm S.E.M;
4 n=5 patients; *: $p < 0.05$; Paired t test).

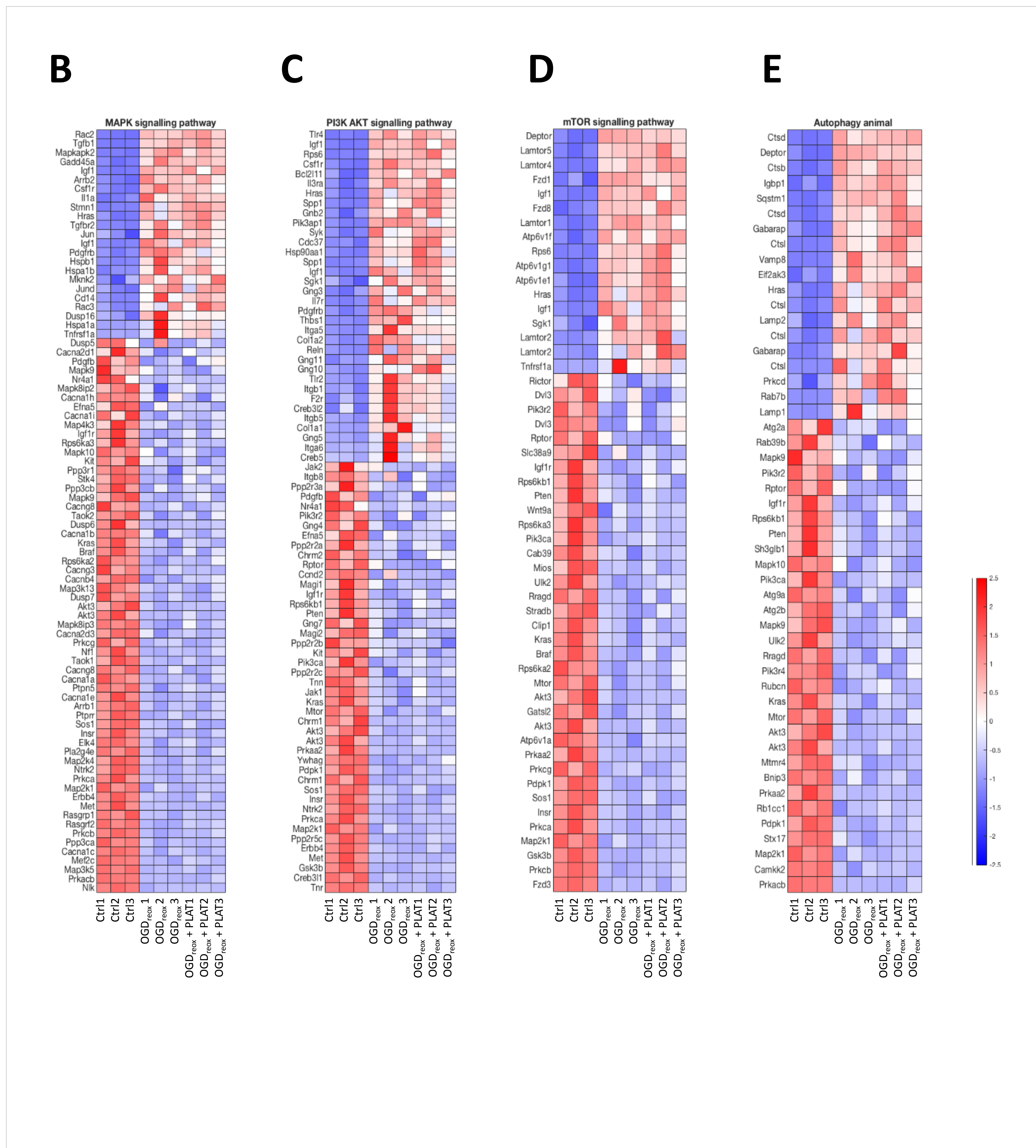
5

6

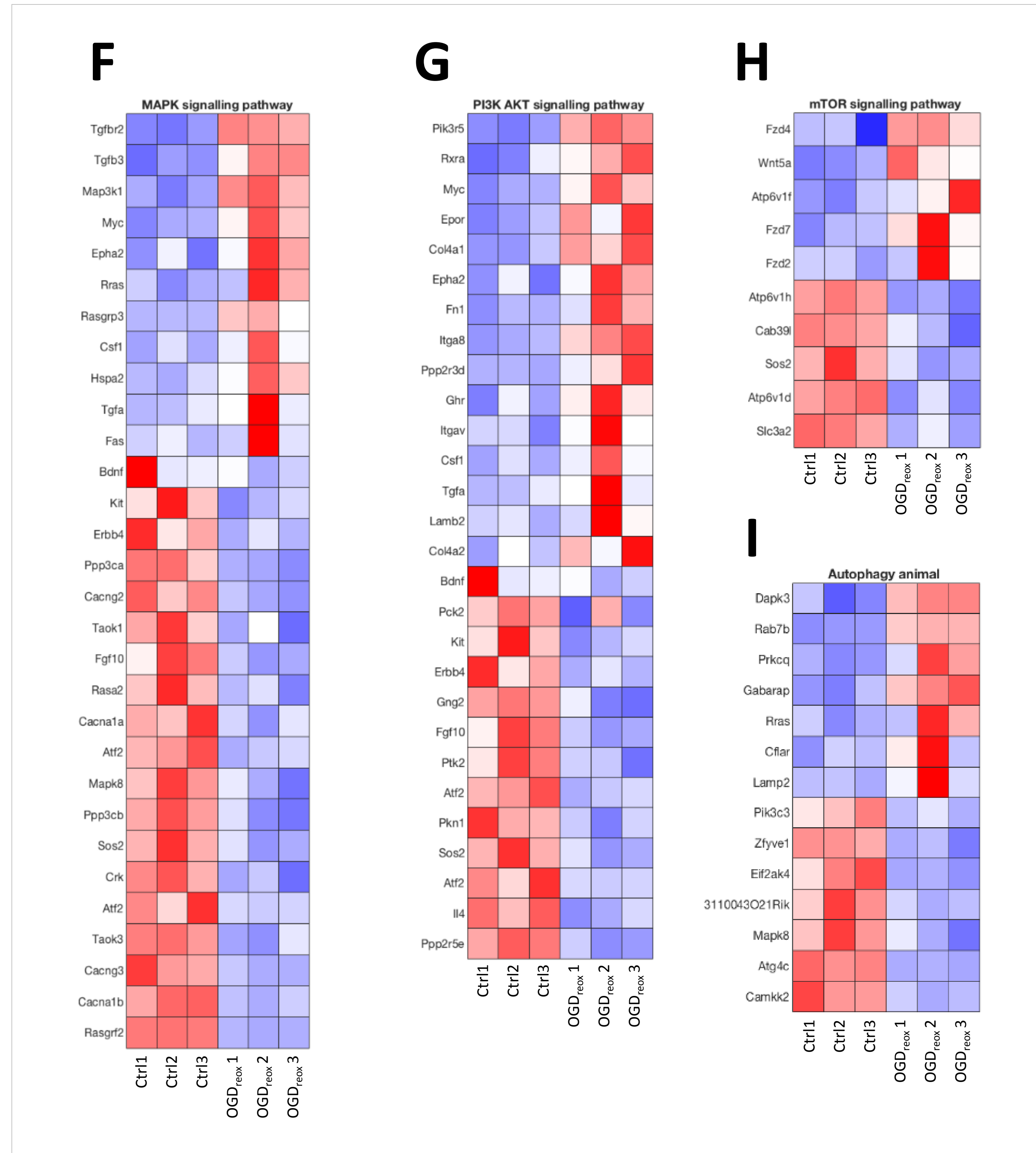
Figure 1



Gene expression significantly changed in both Ctrl versus OGD_{reox} and Ctrl versus OGD_{reox} + PLAT



Gene expression significantly changed ONLY in Ctrl versus OGD_{reox}



Gene expression significantly changed ONLY in Ctrl versus OGD_{reox} + PLAT

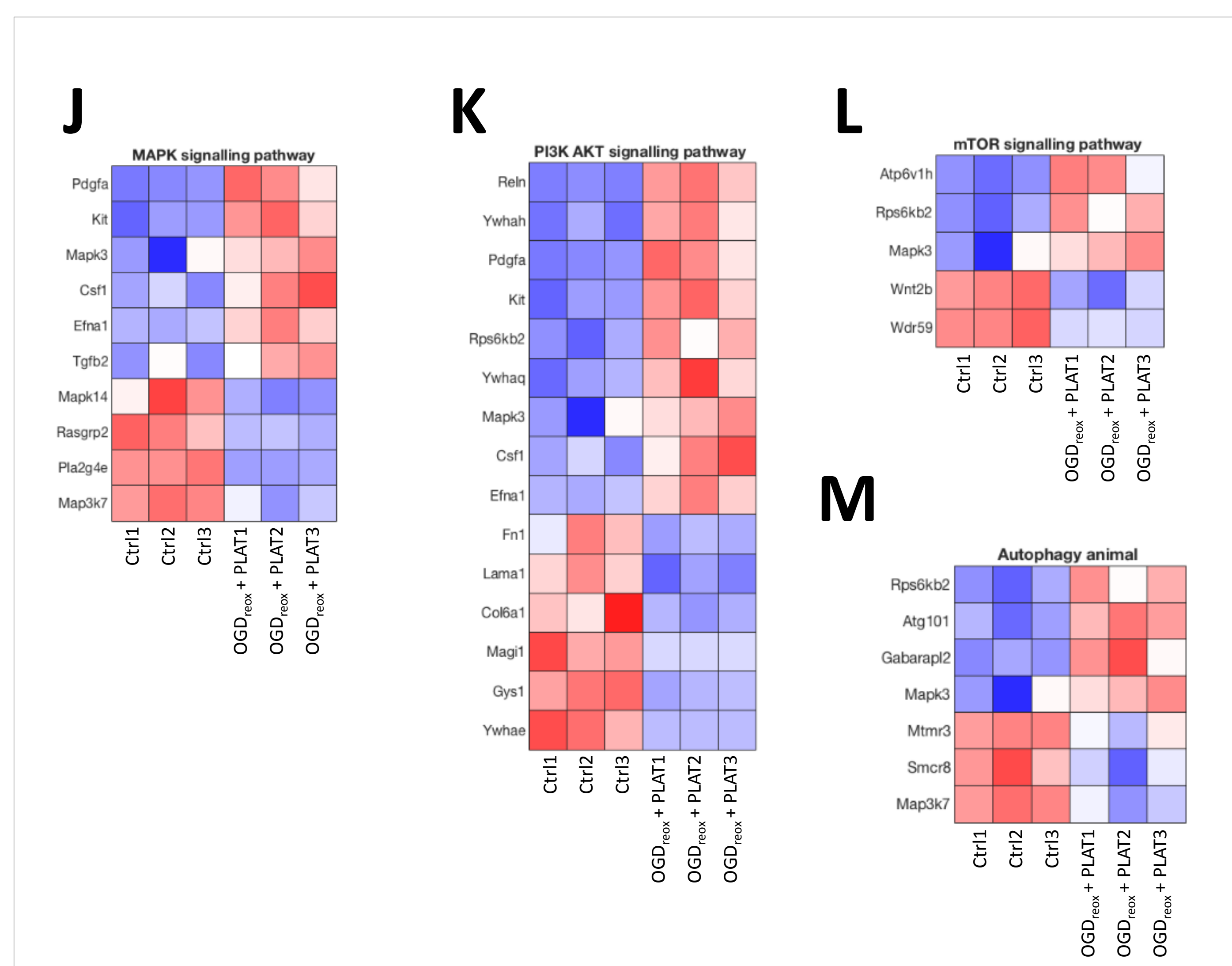
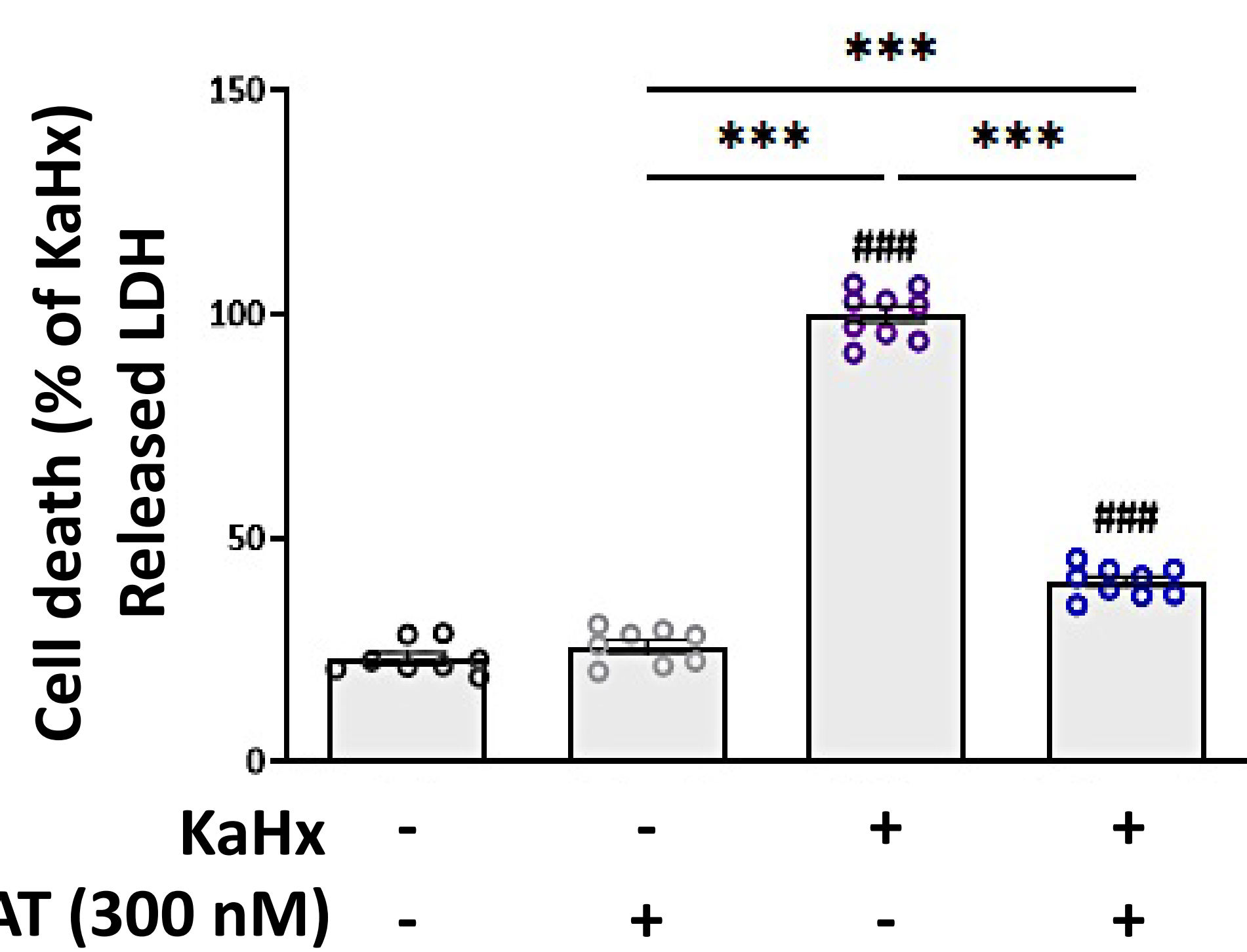
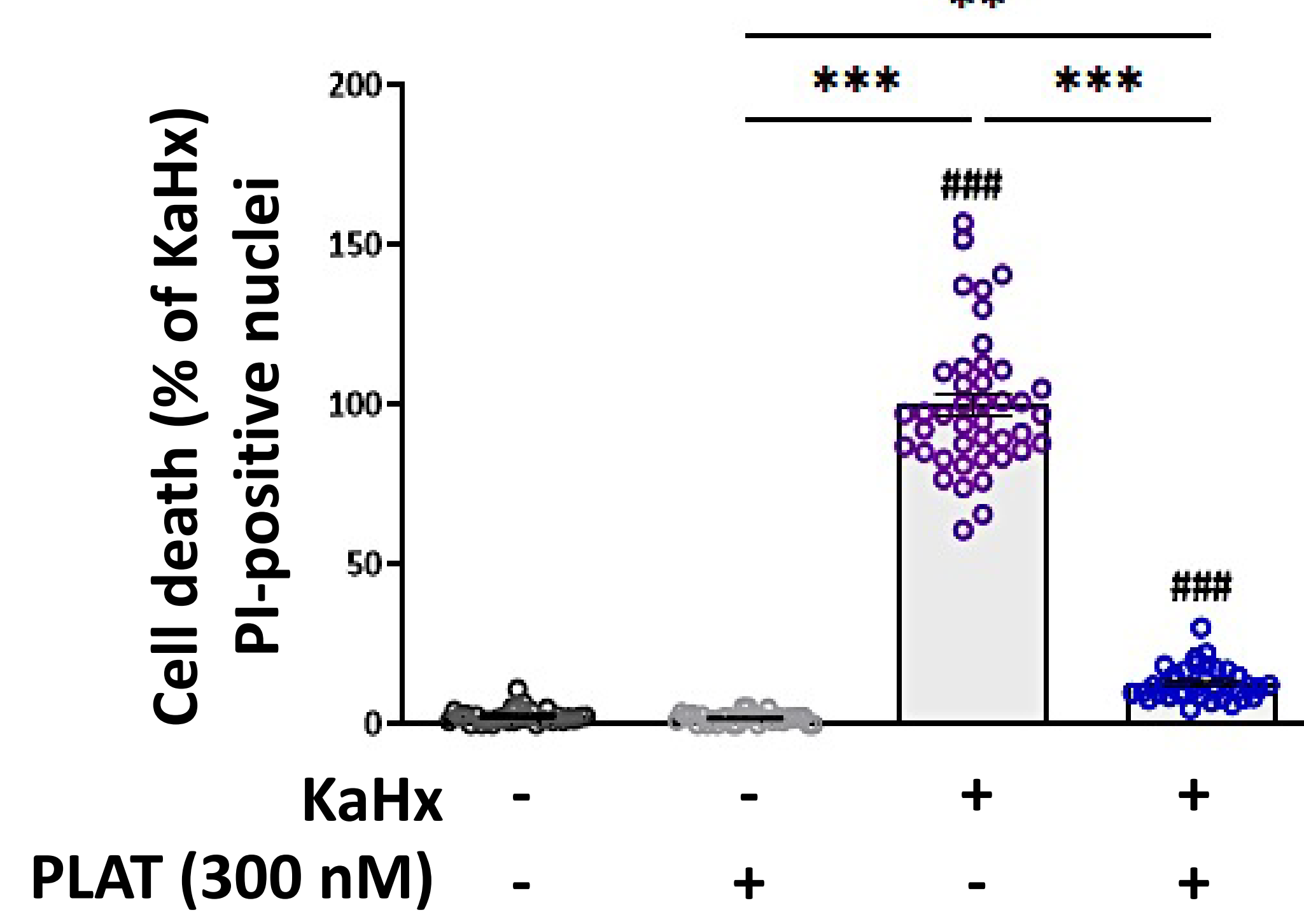


Figure 3

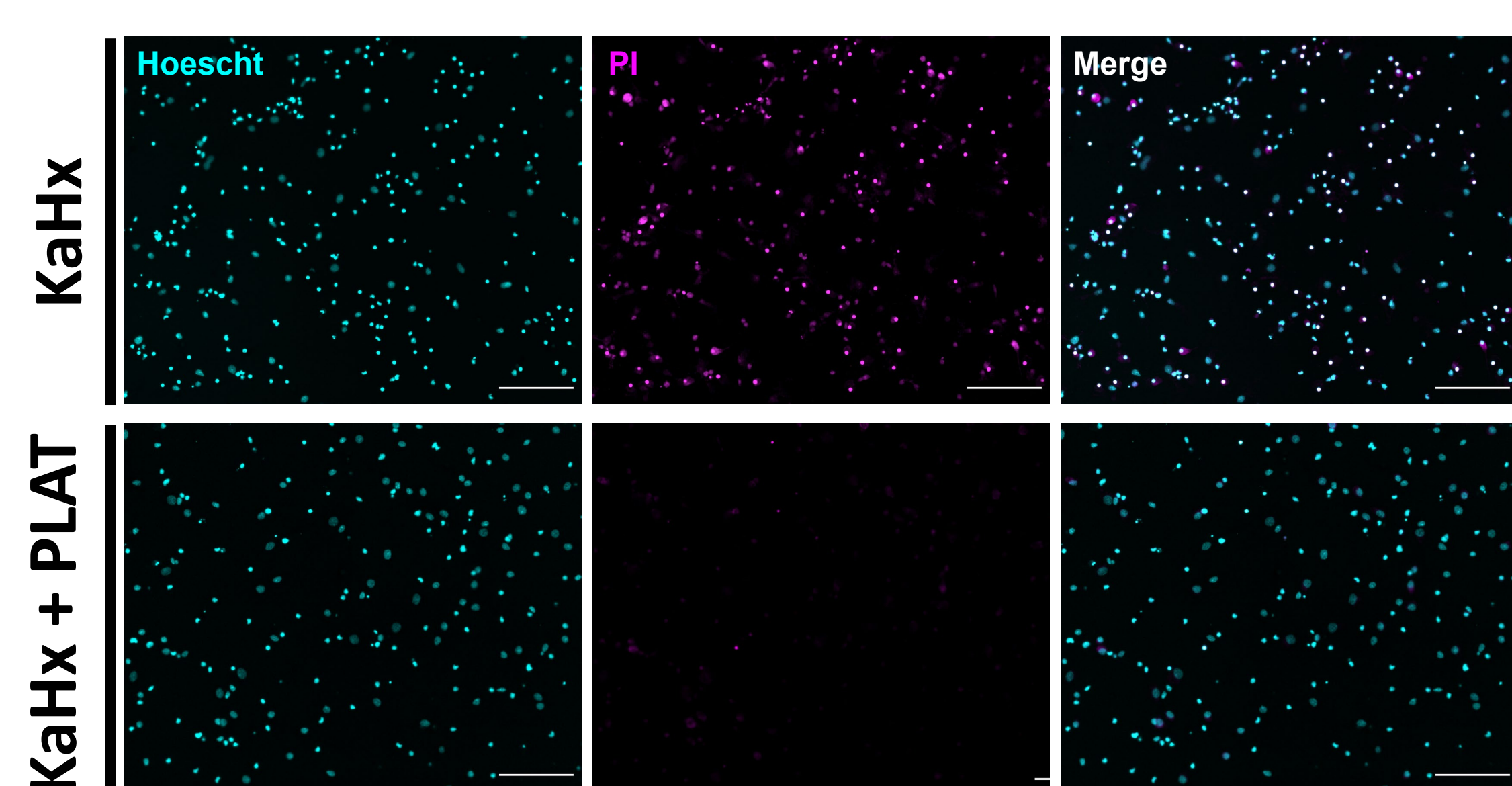
A



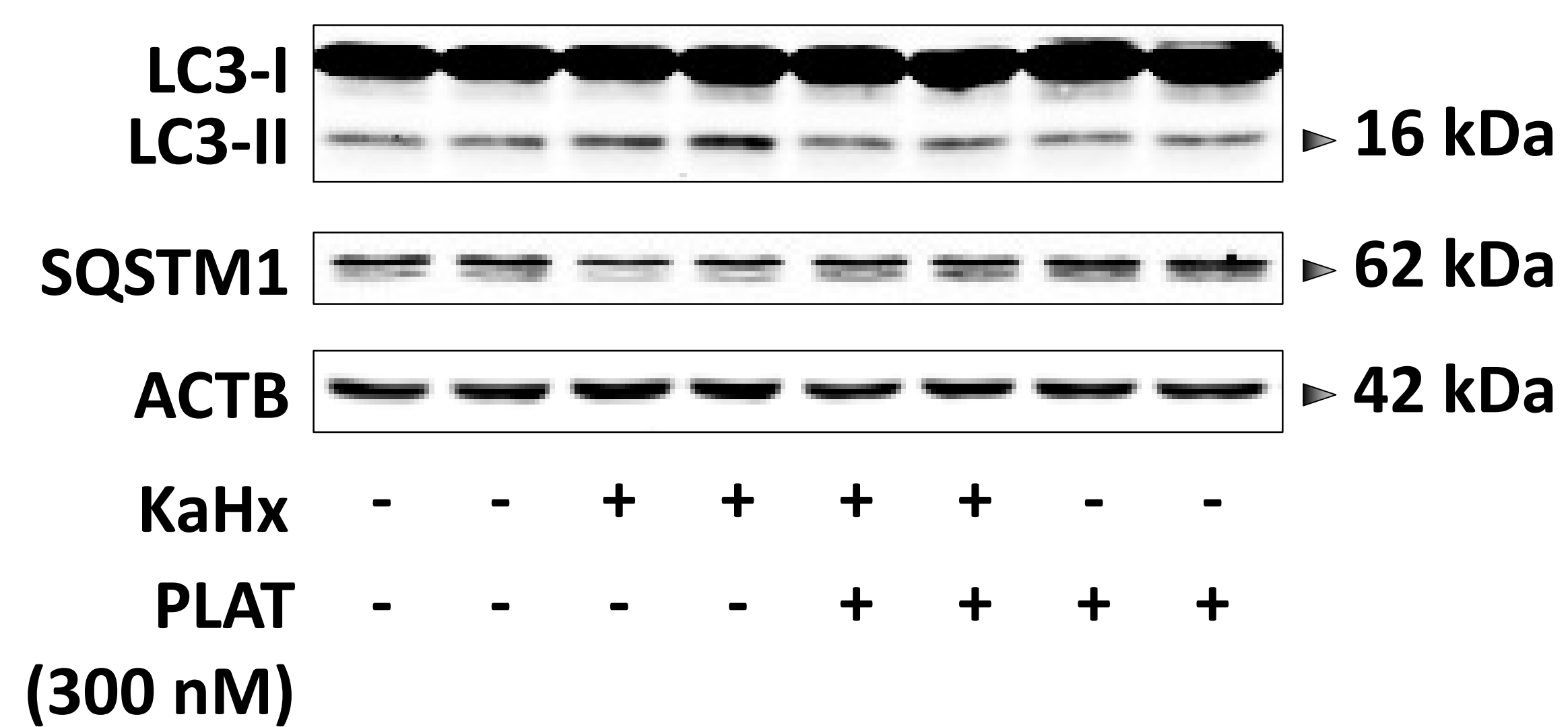
B



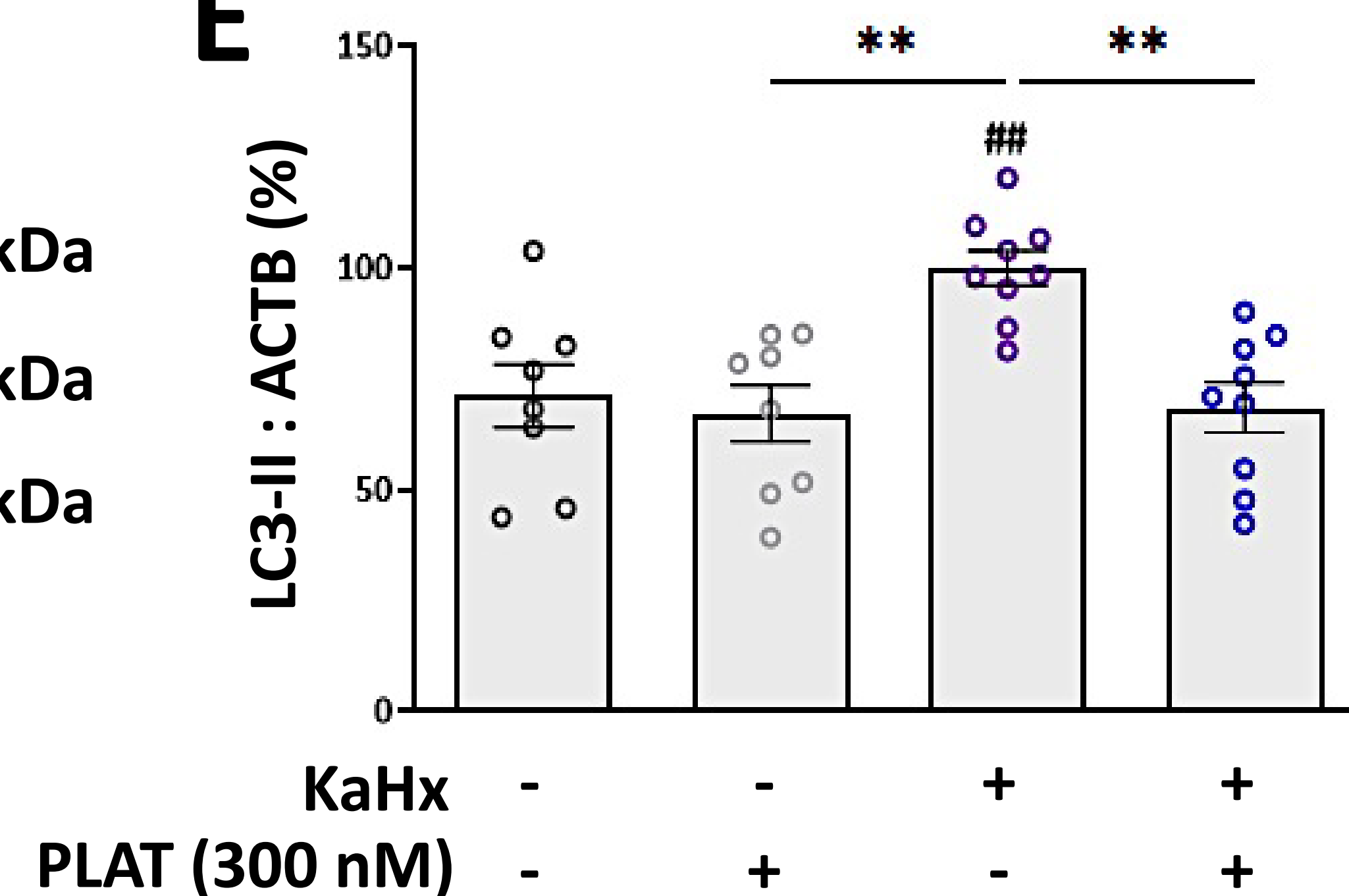
C



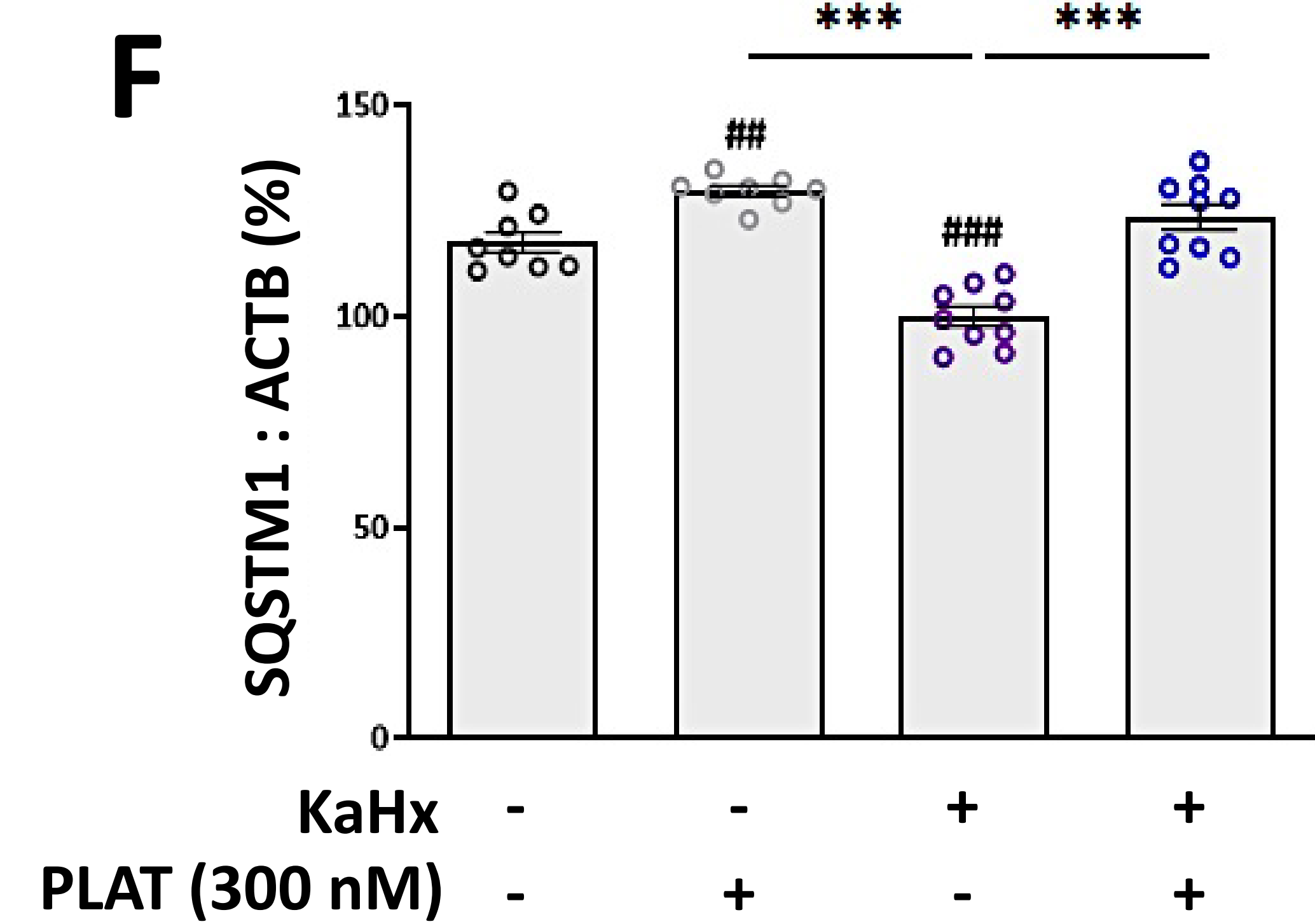
D



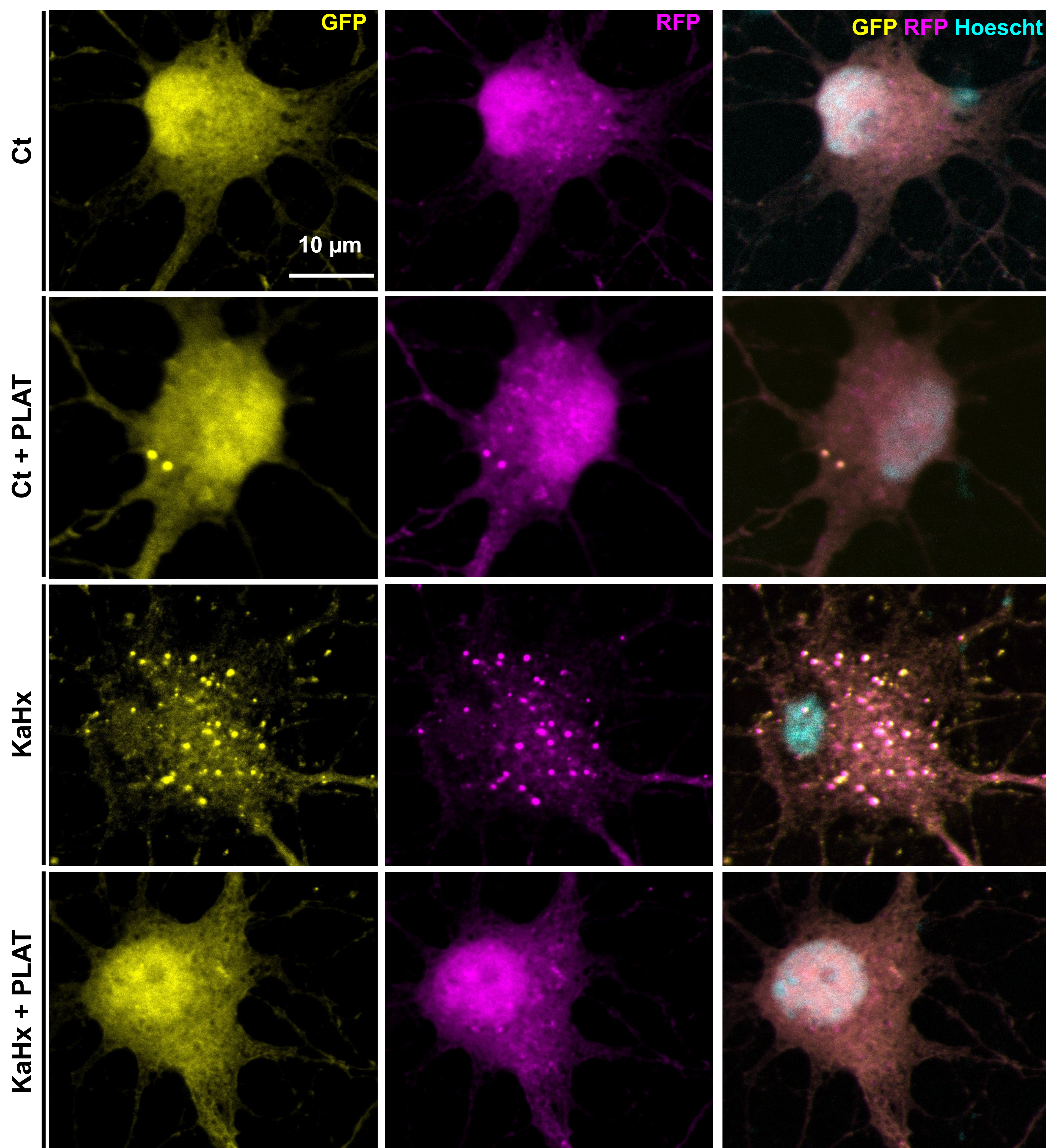
E



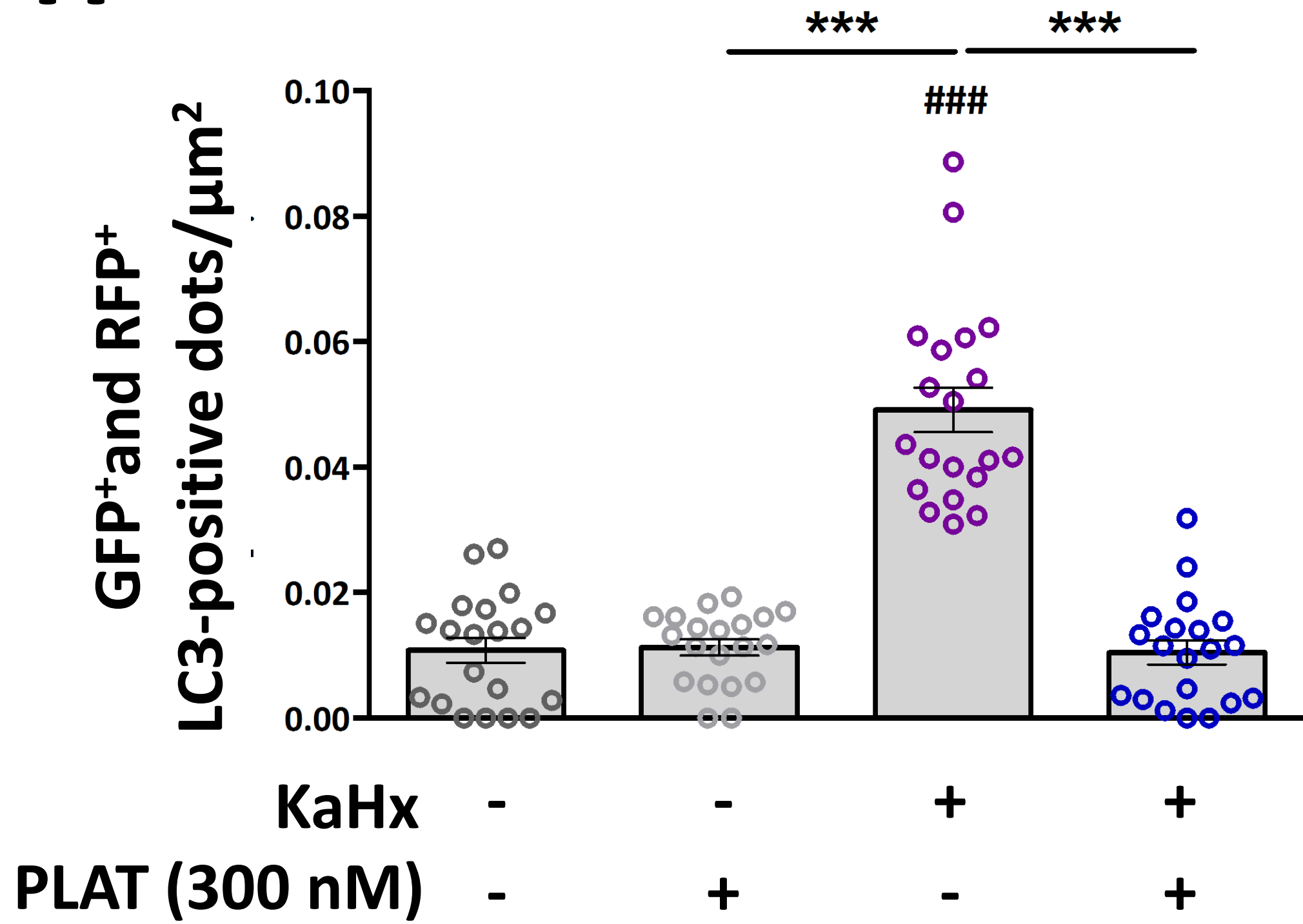
F



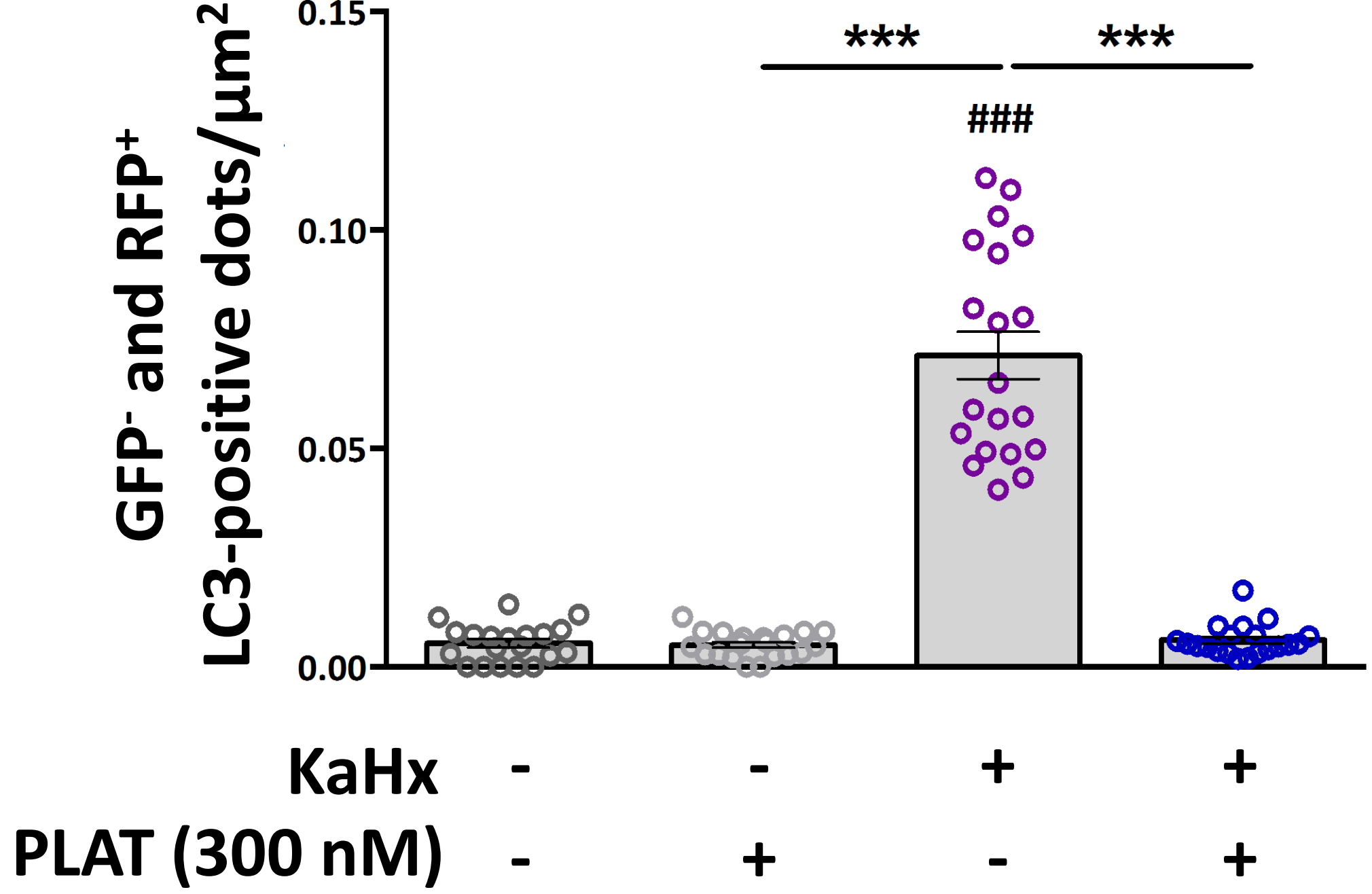
G



H



I



J

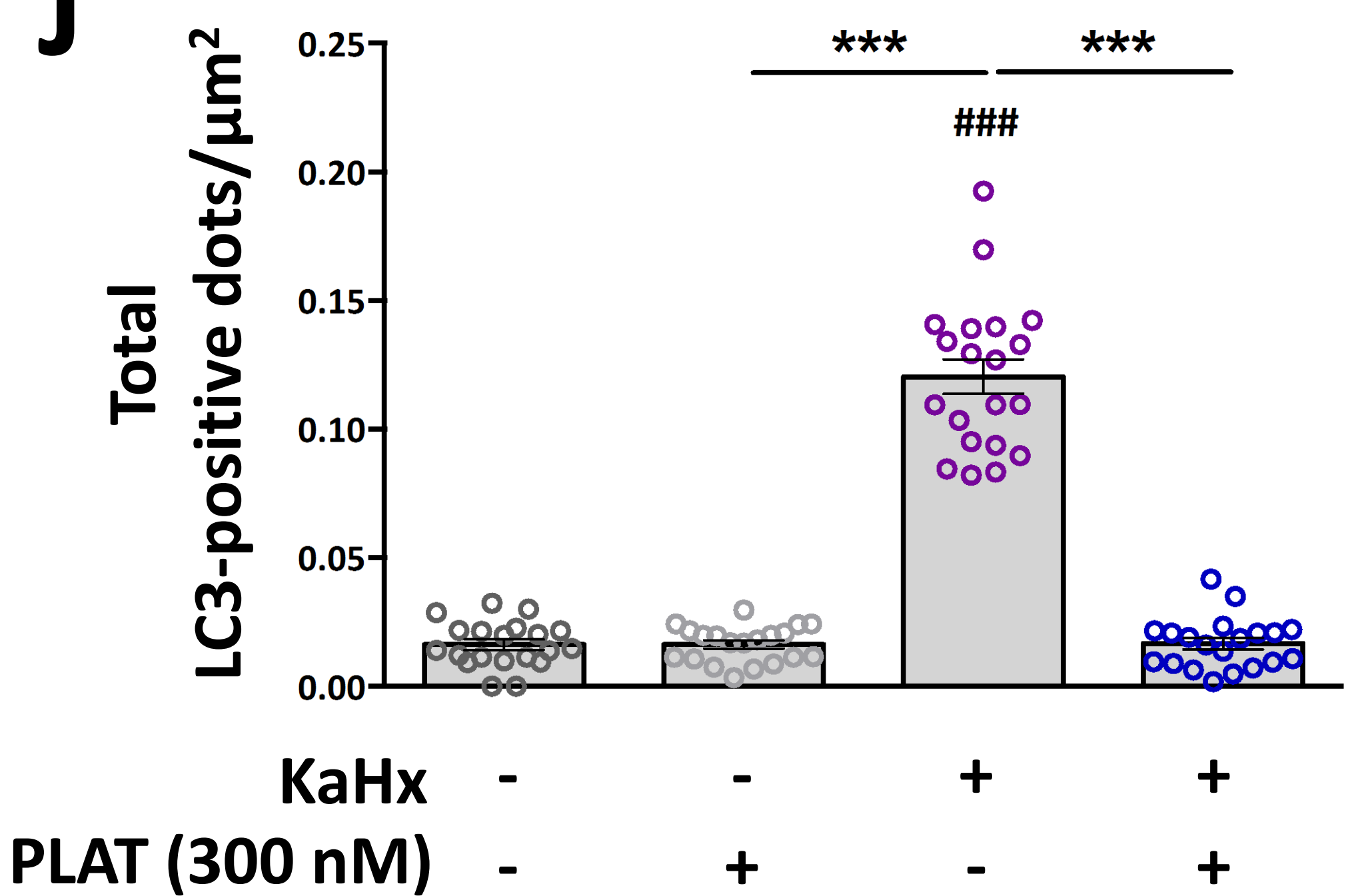


Figure 4

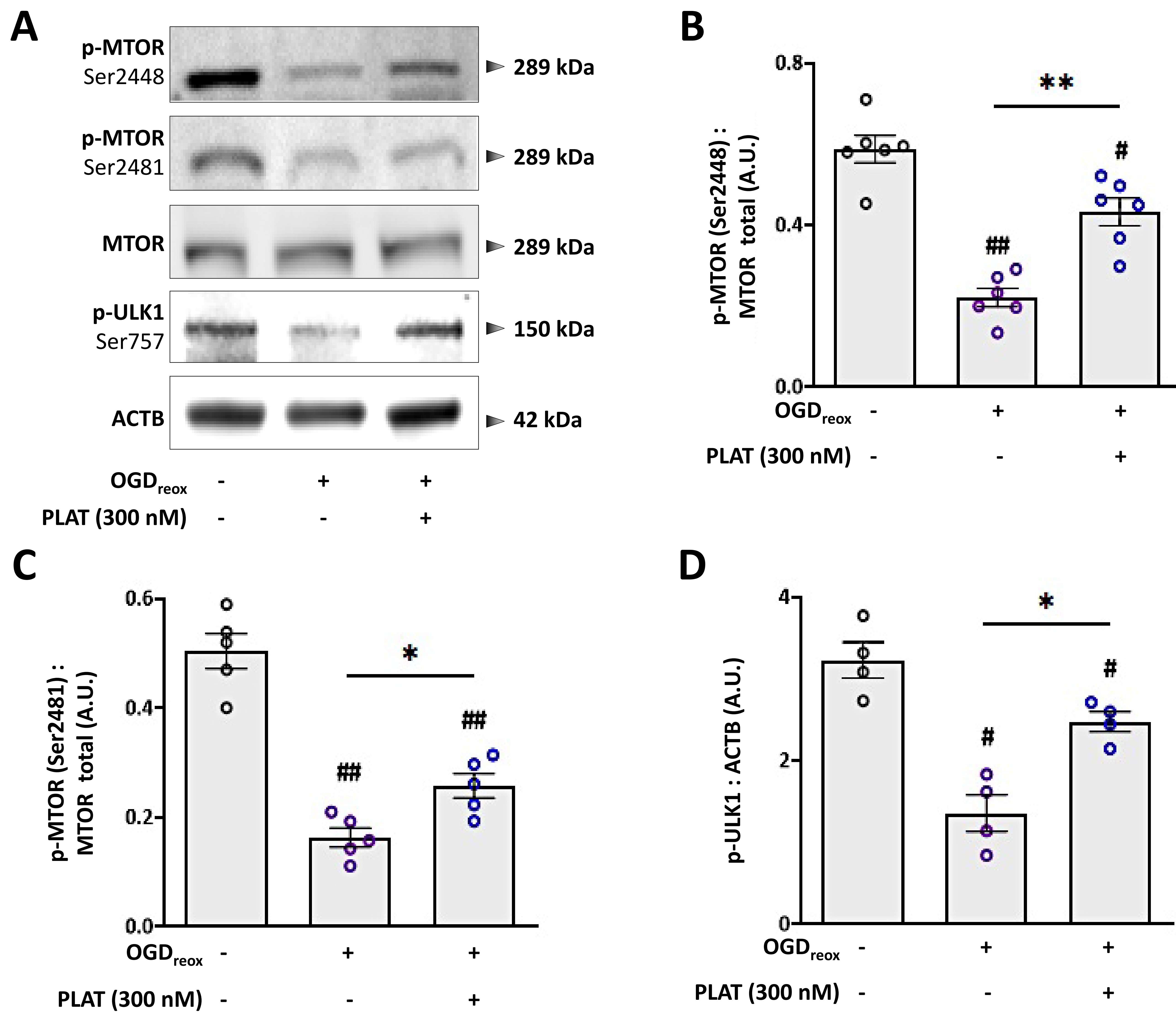


Figure 5

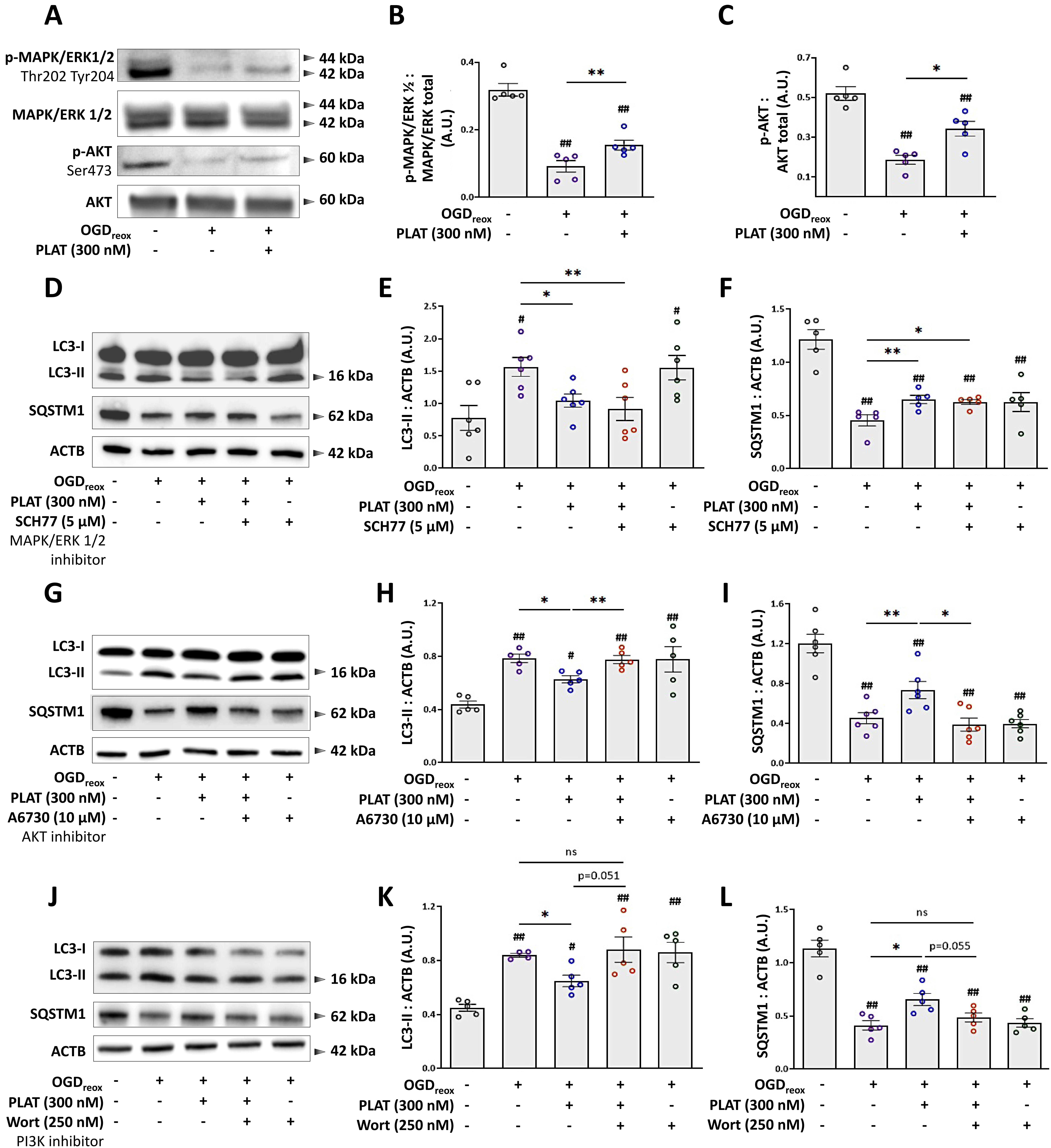


Figure 6

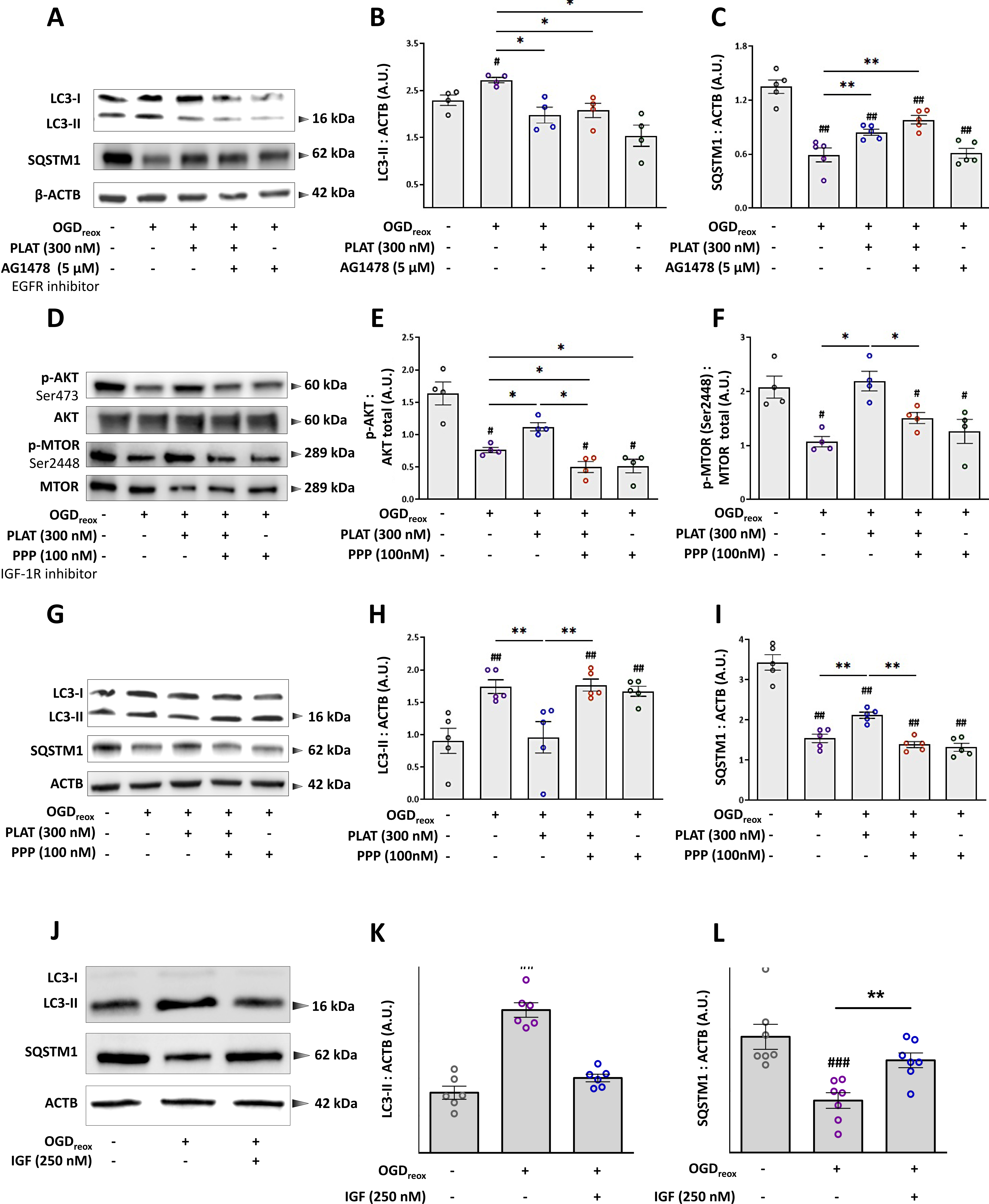


Figure 7

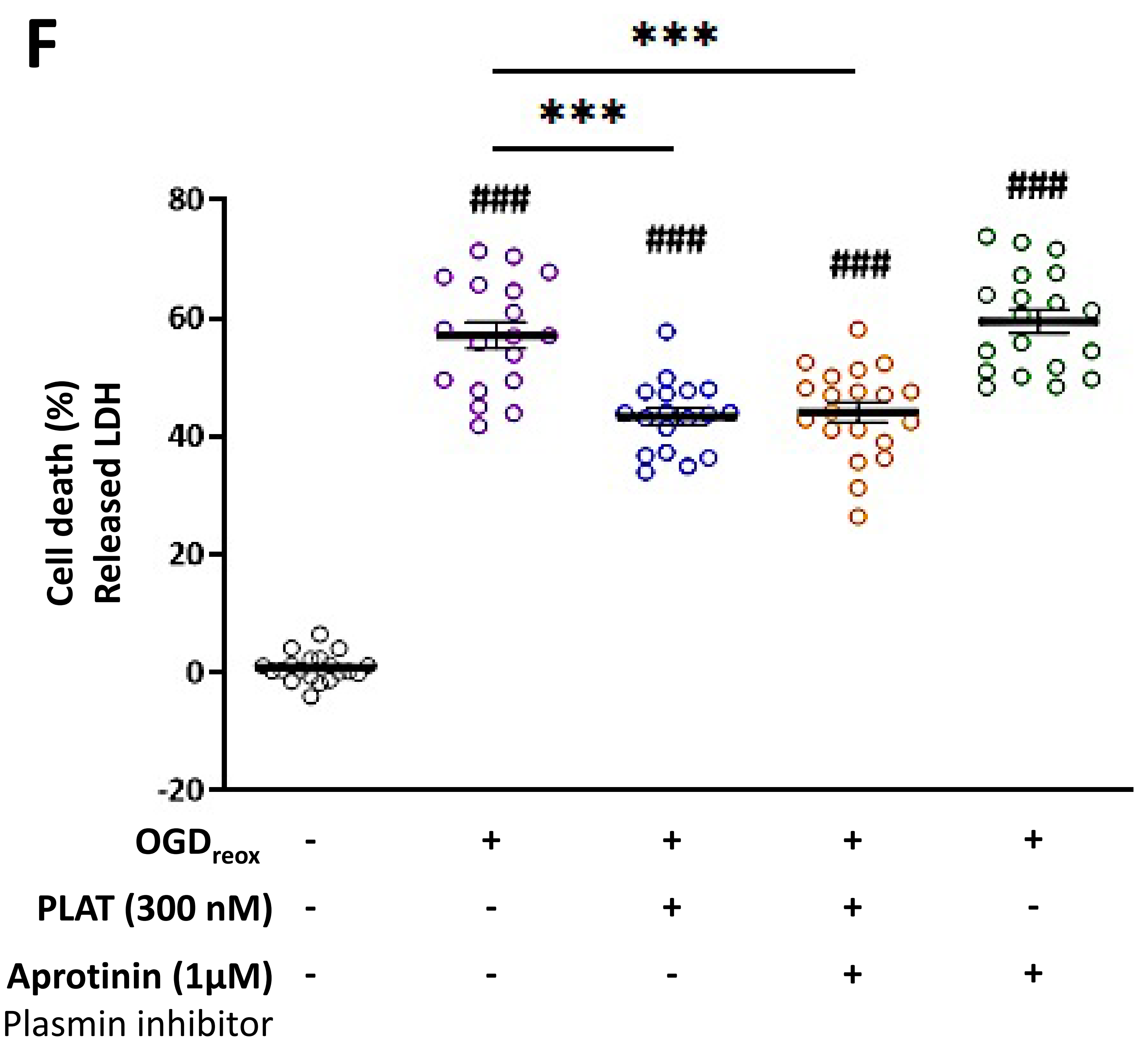
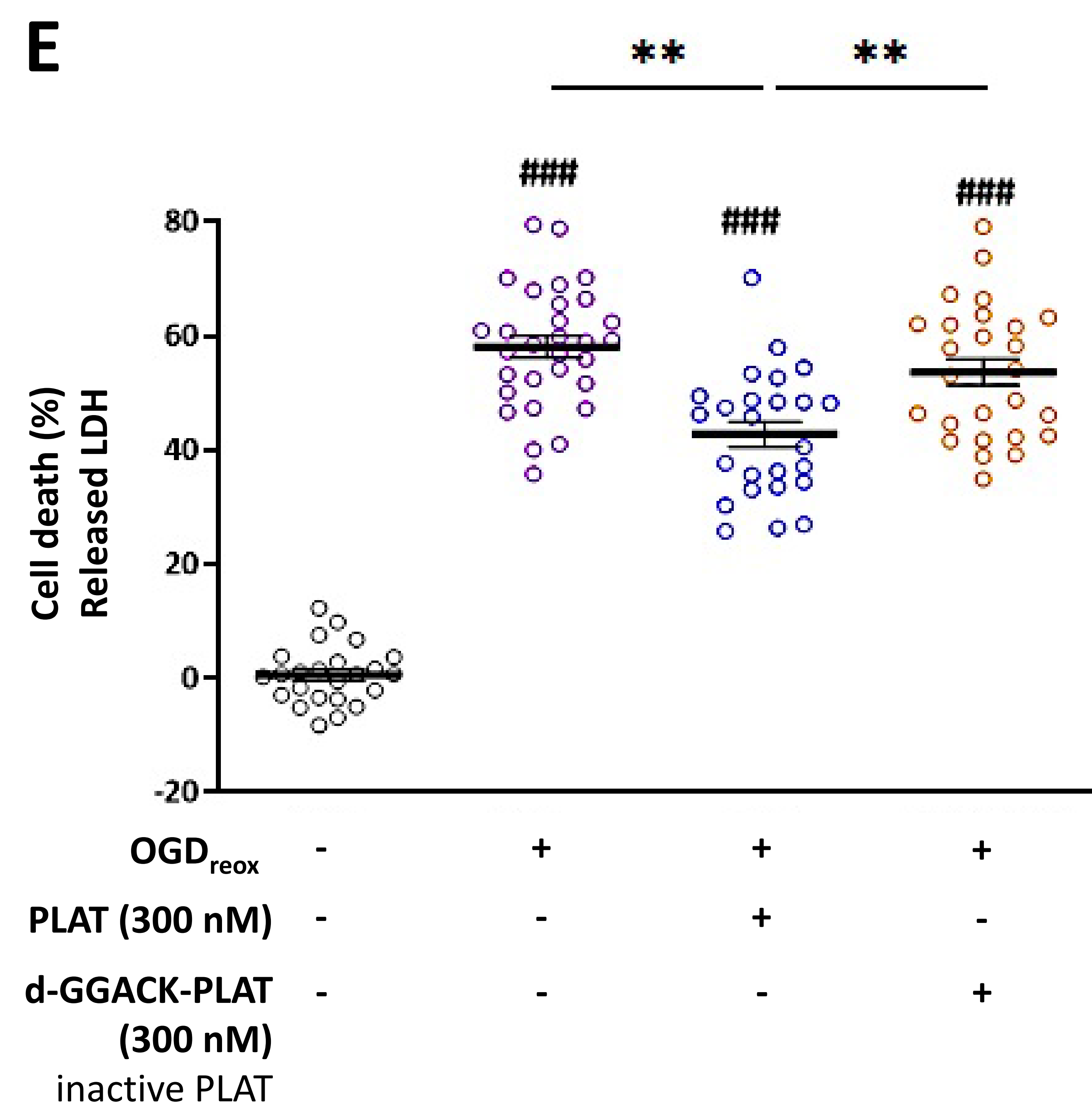
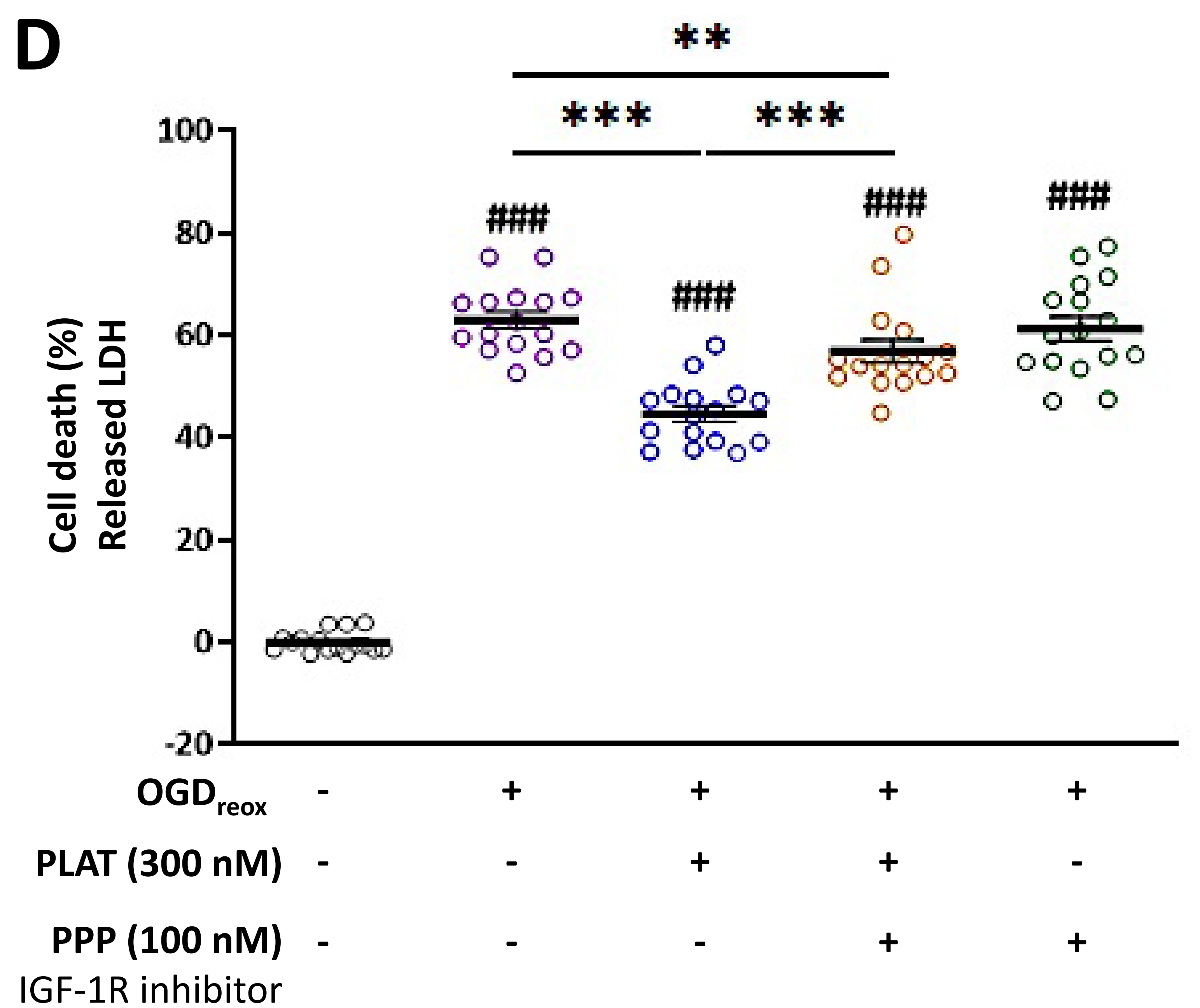
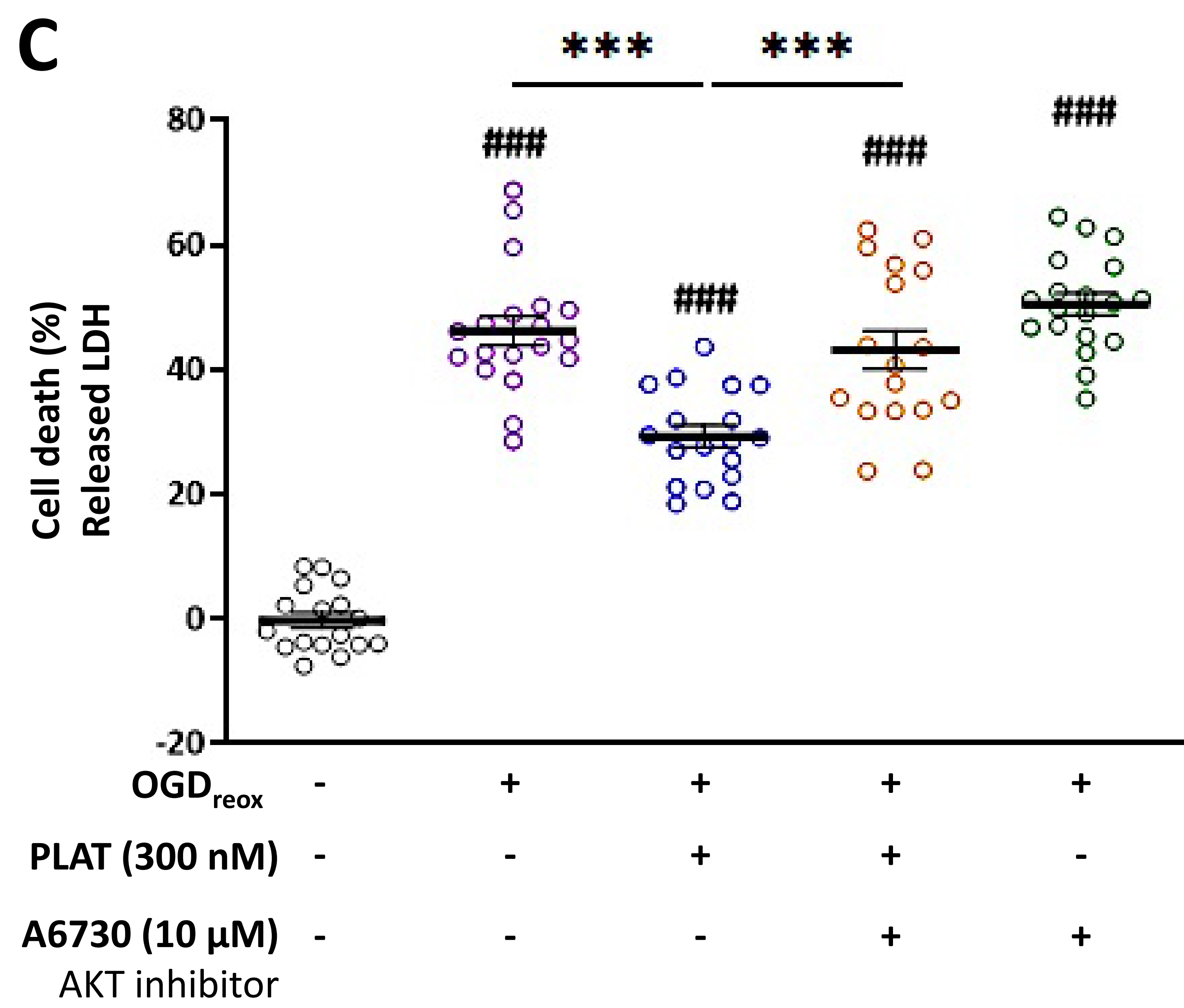
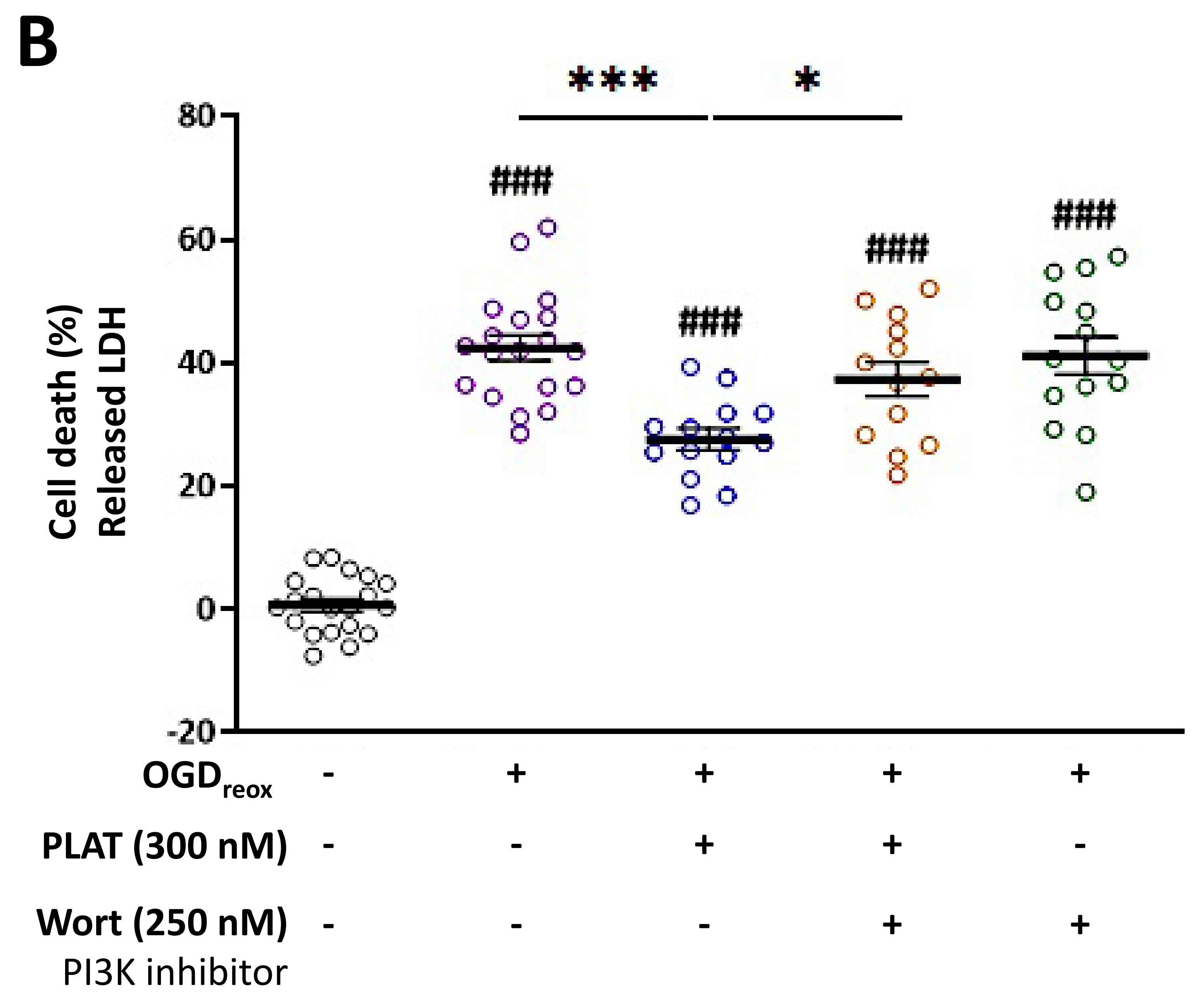
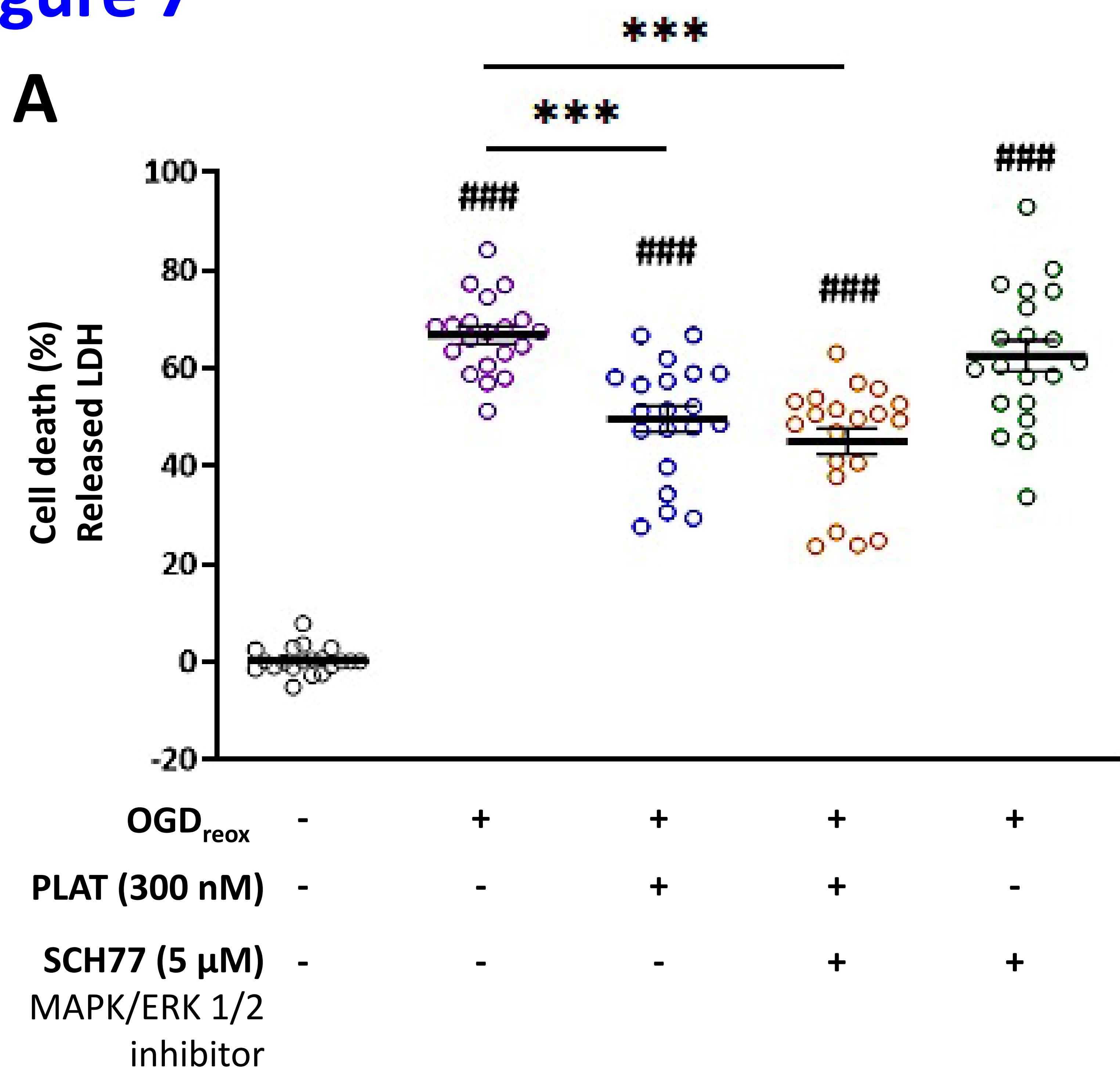


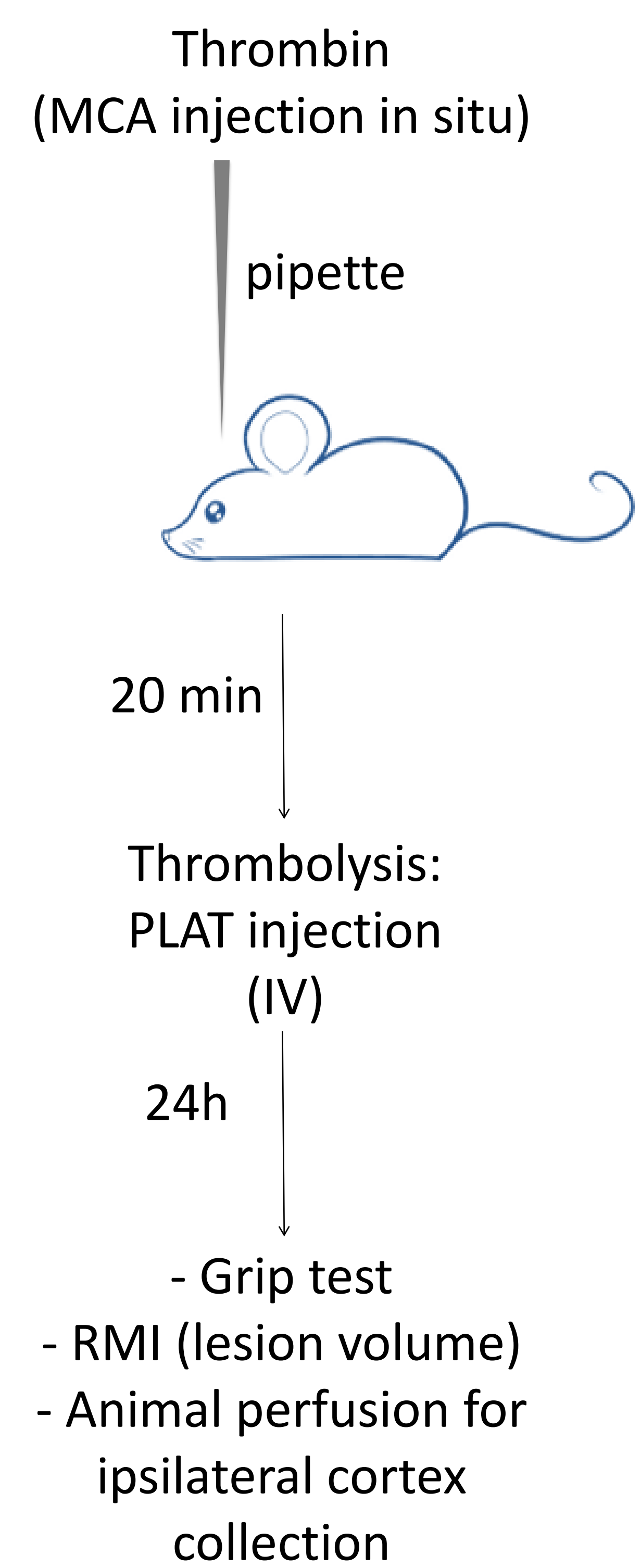
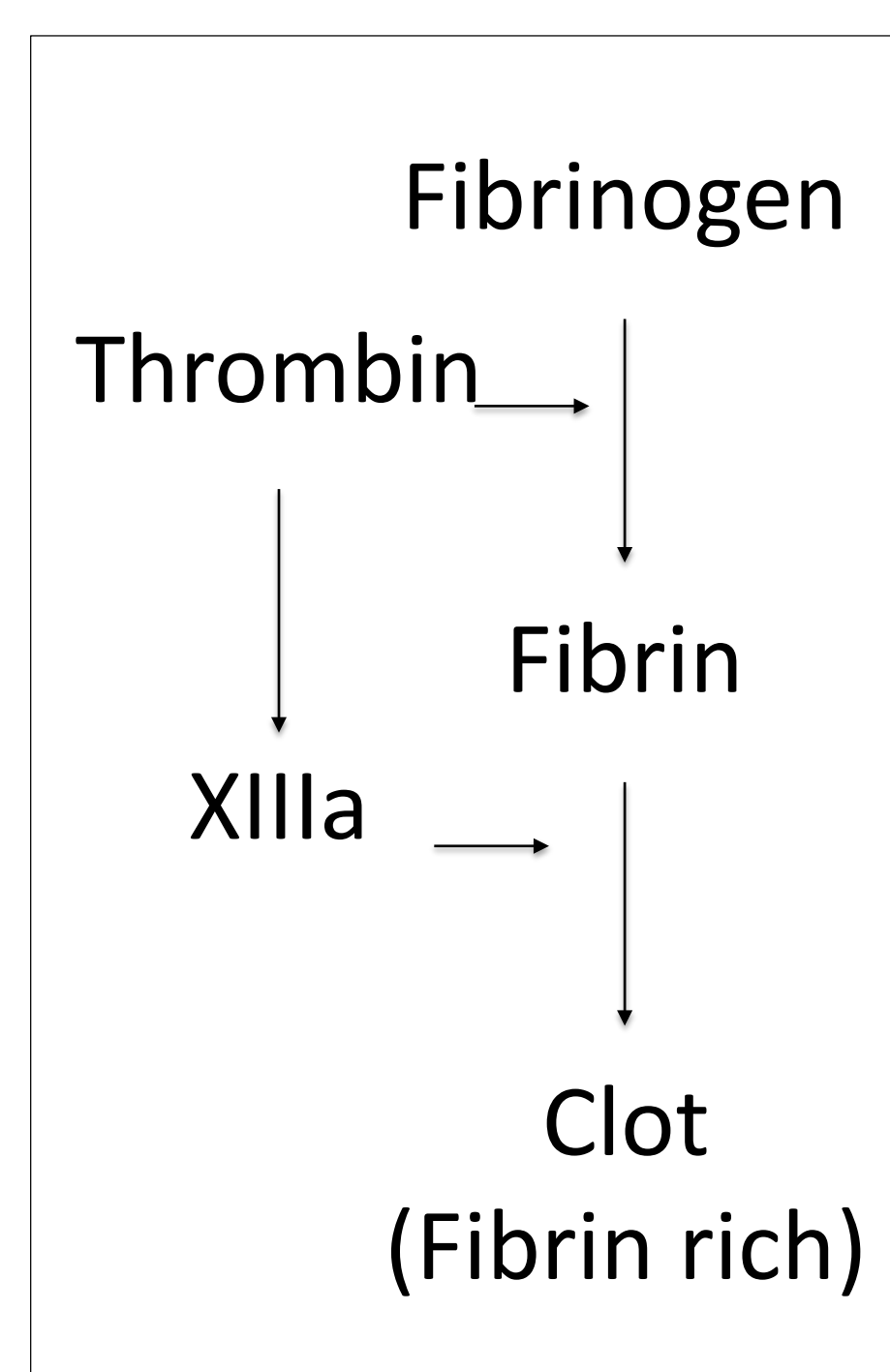
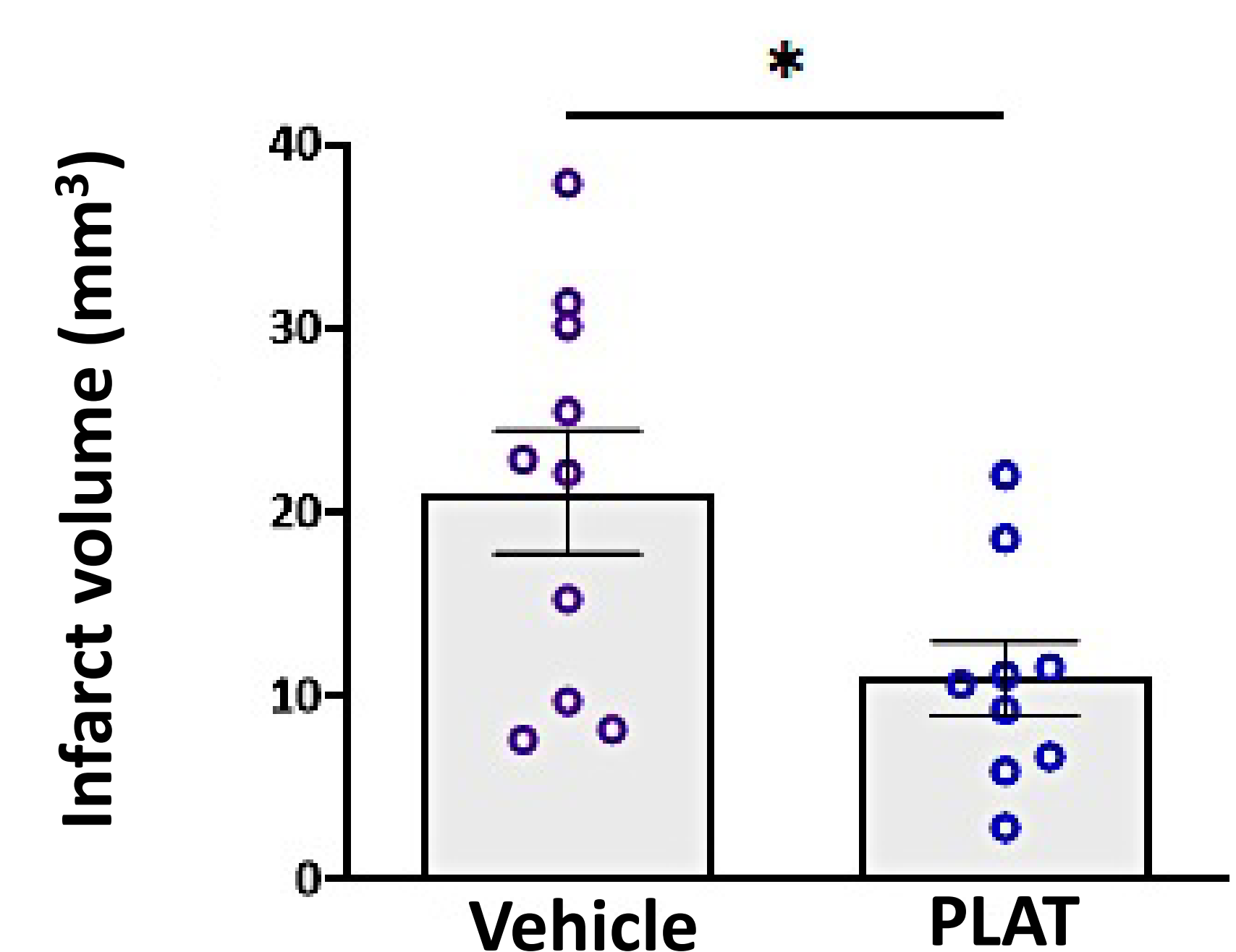
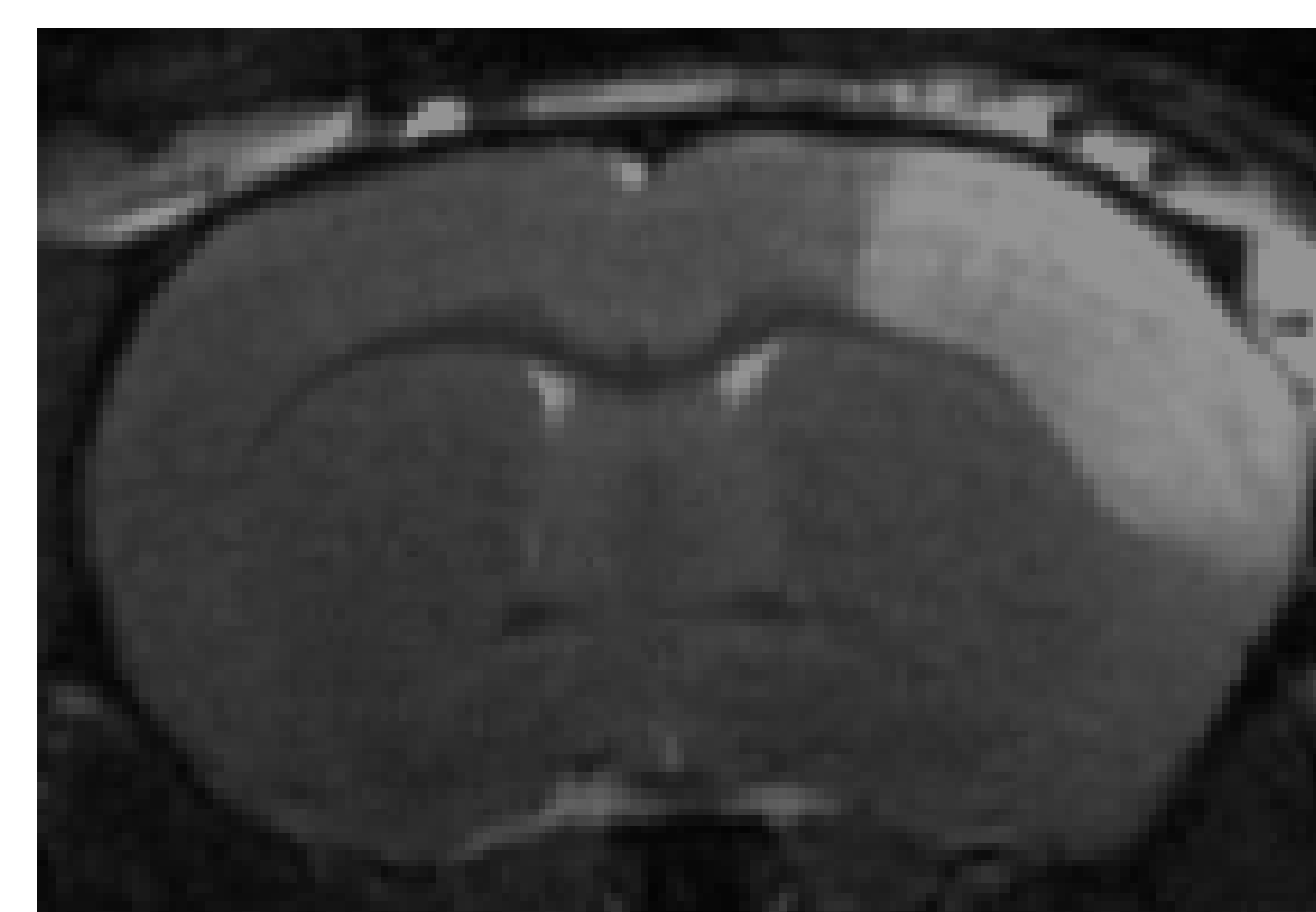
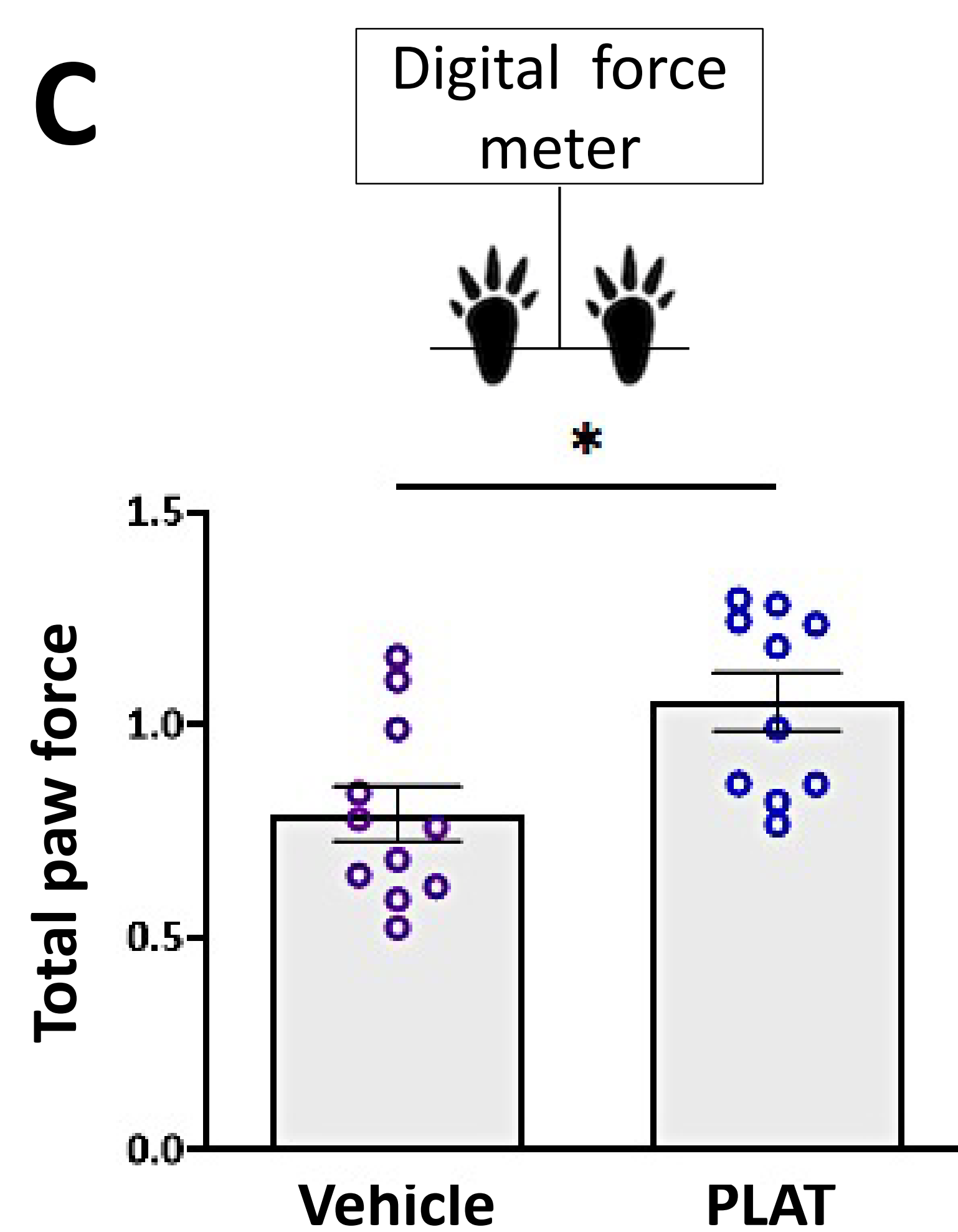
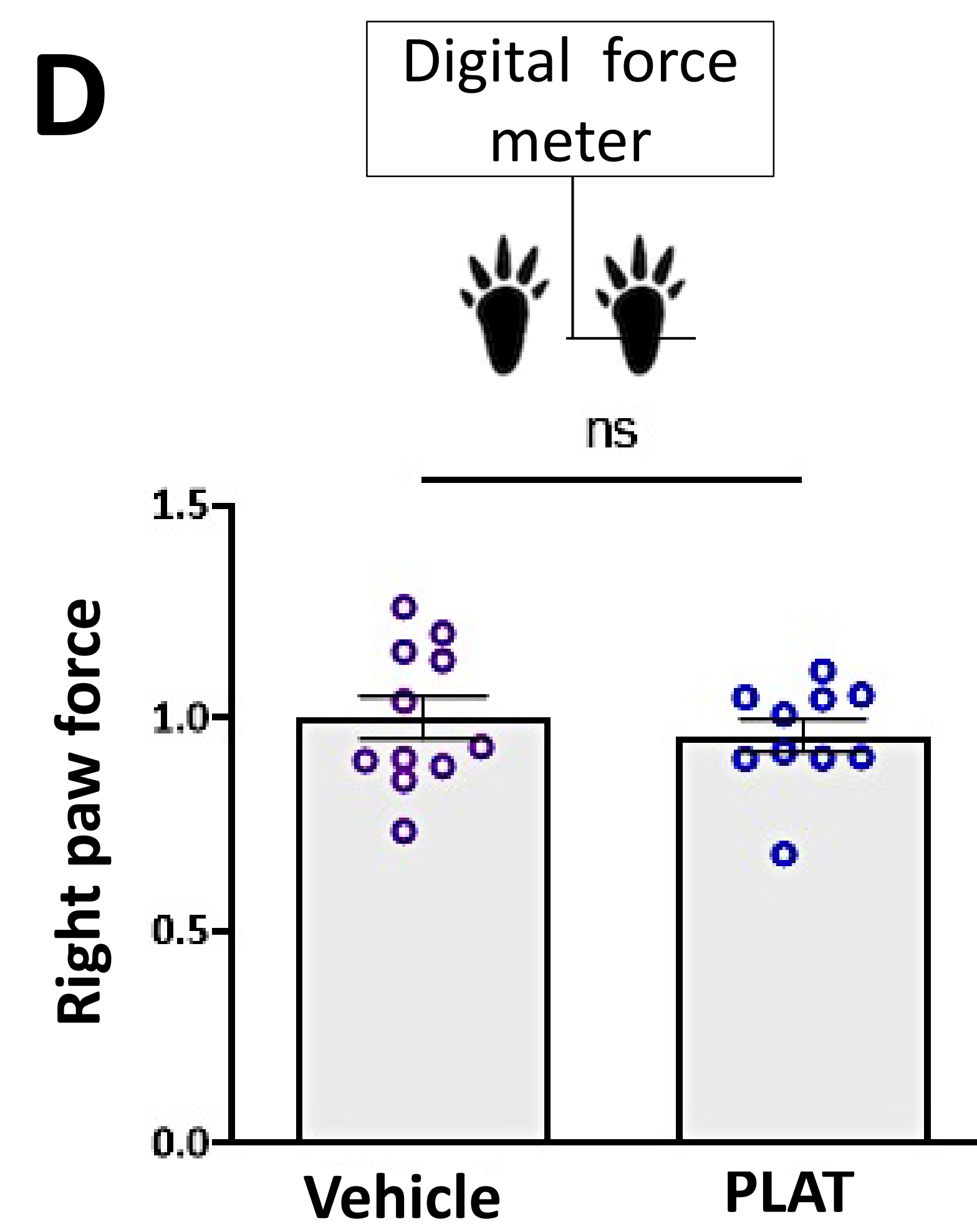
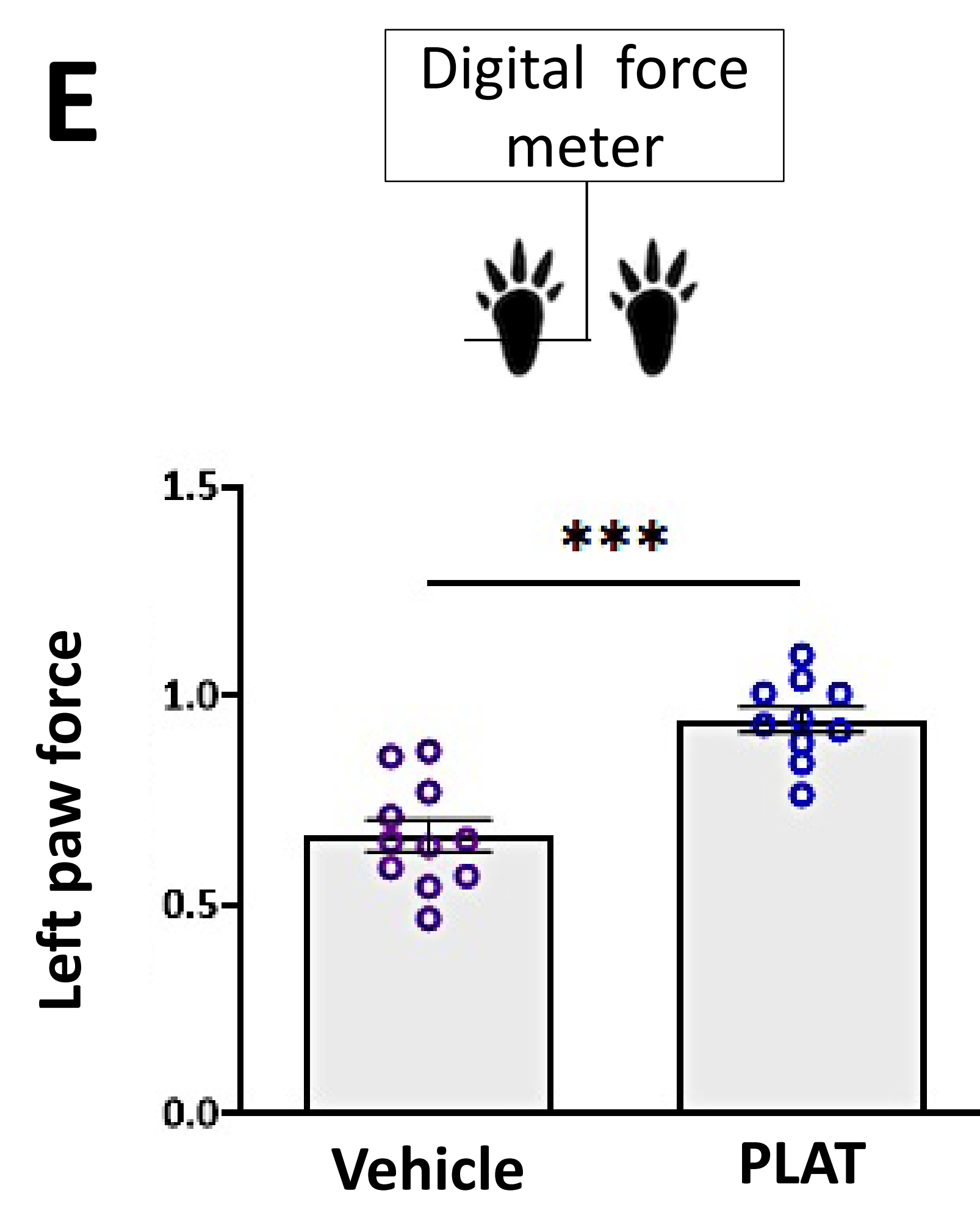
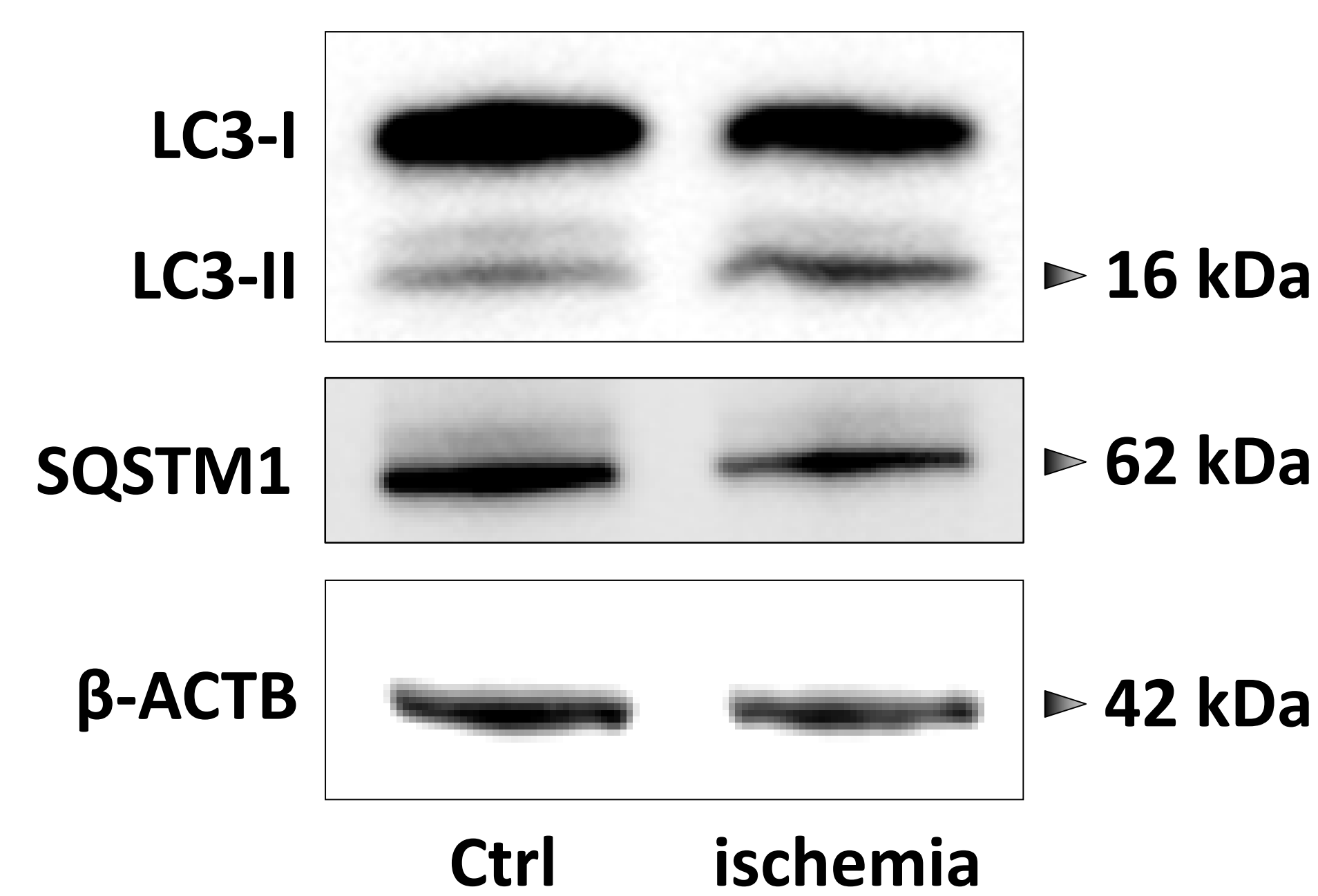
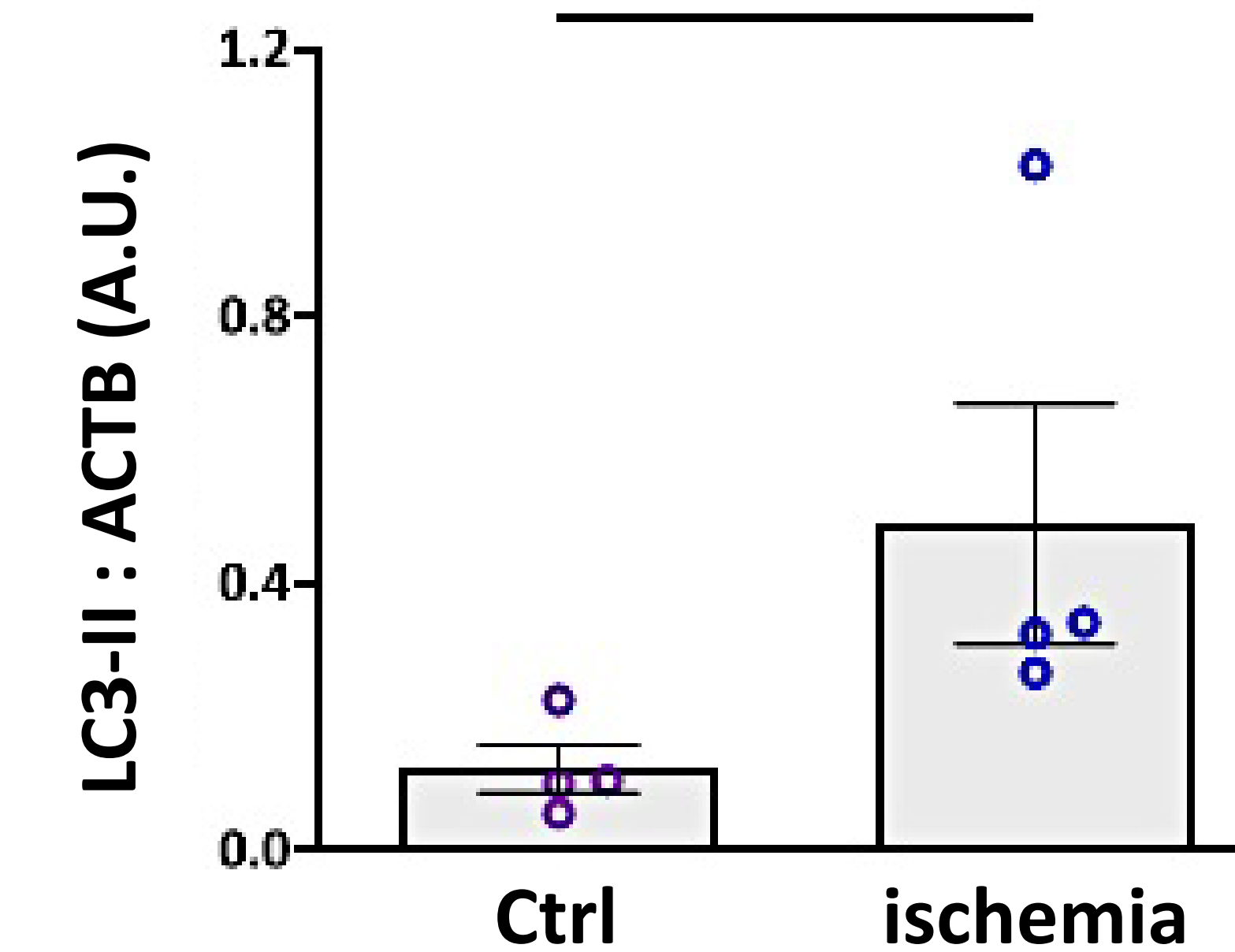
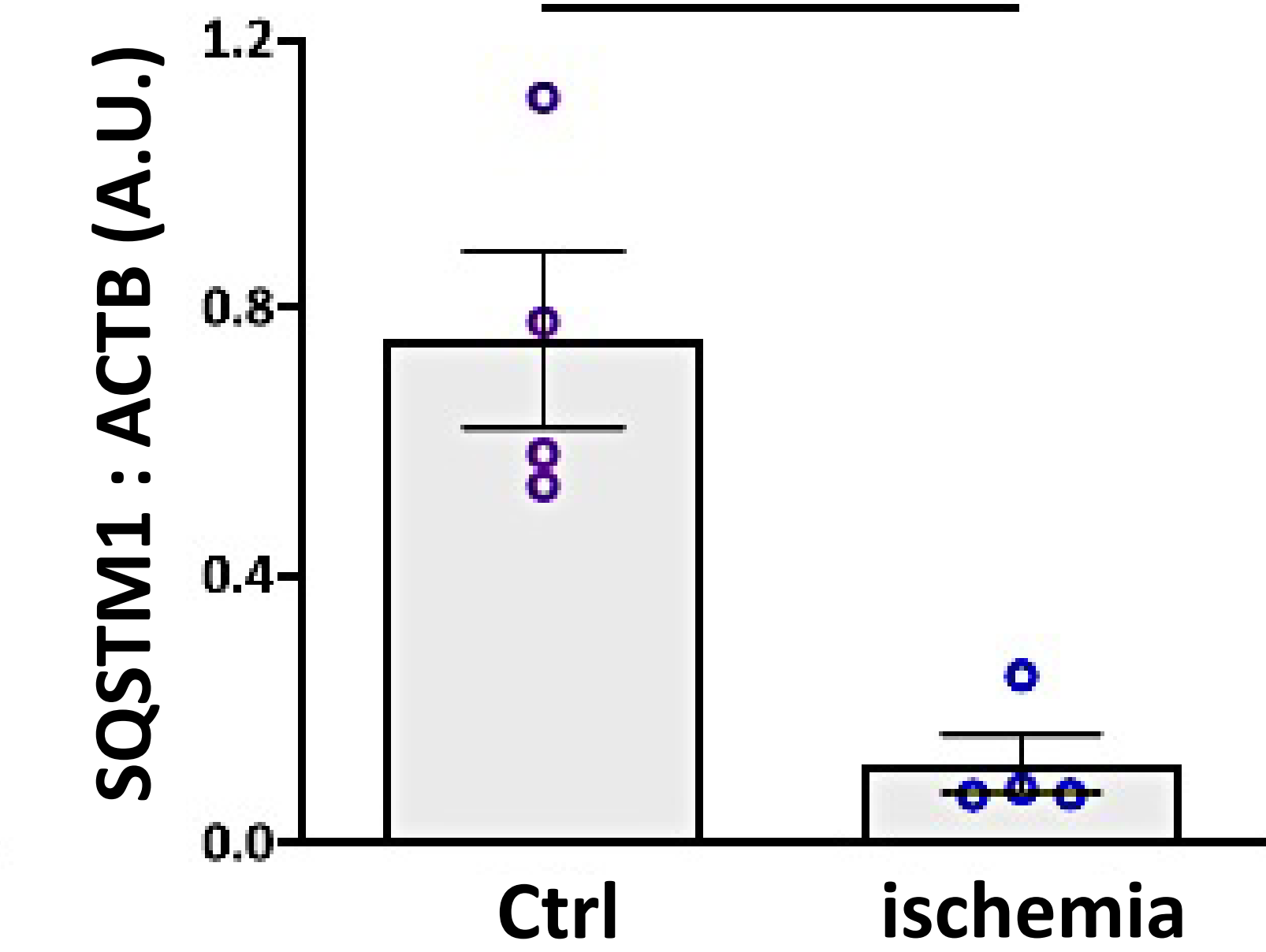
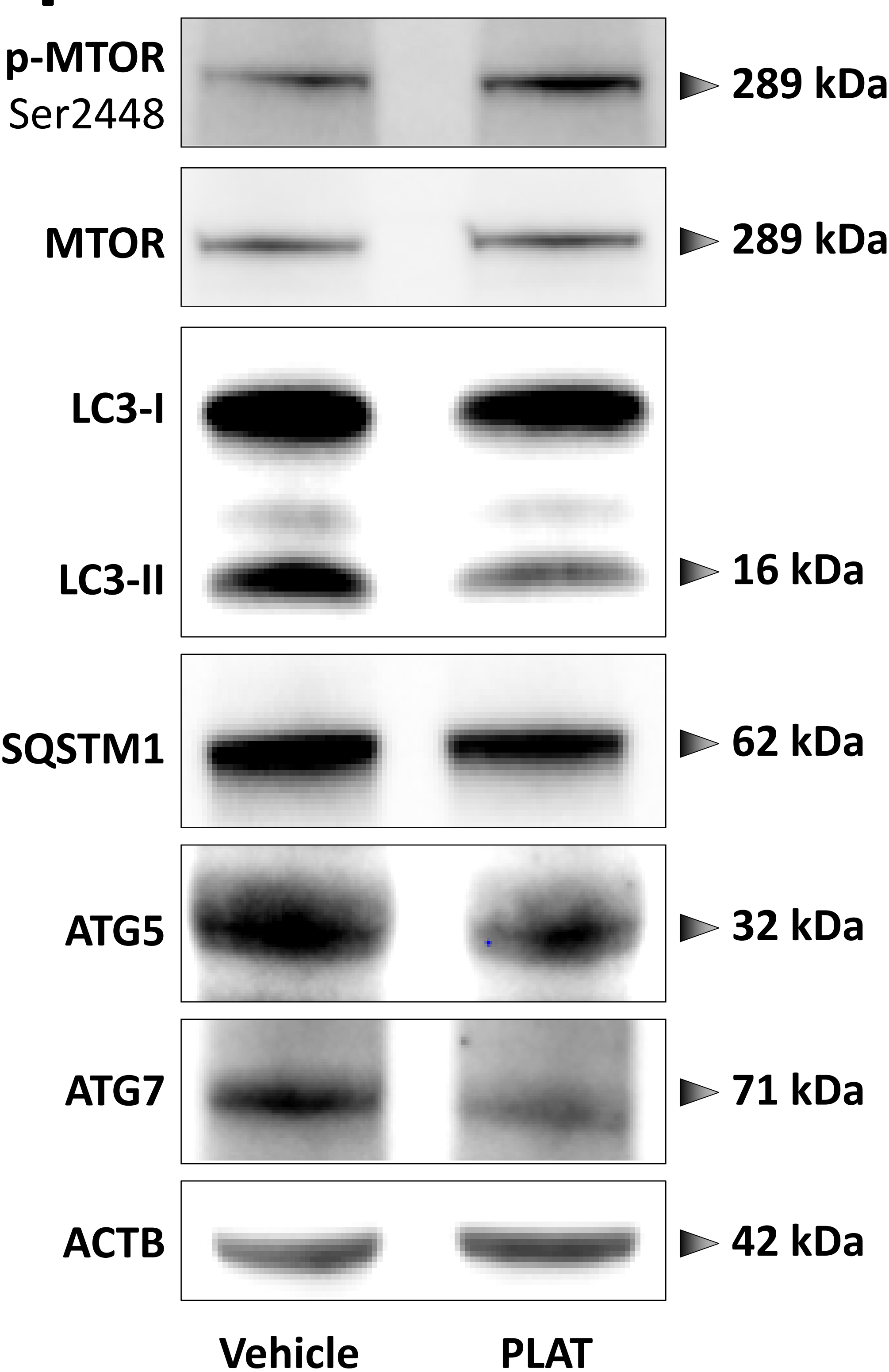
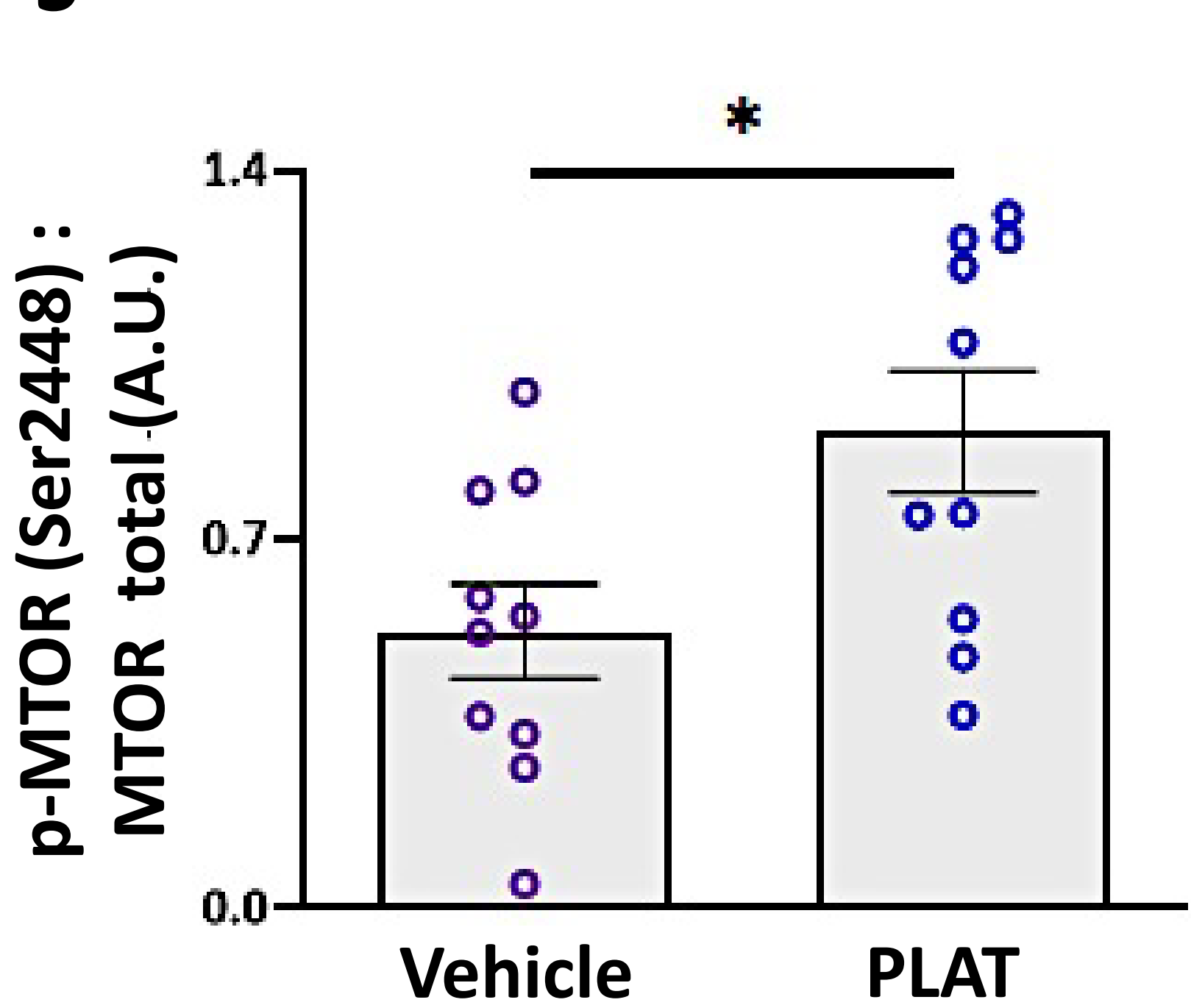
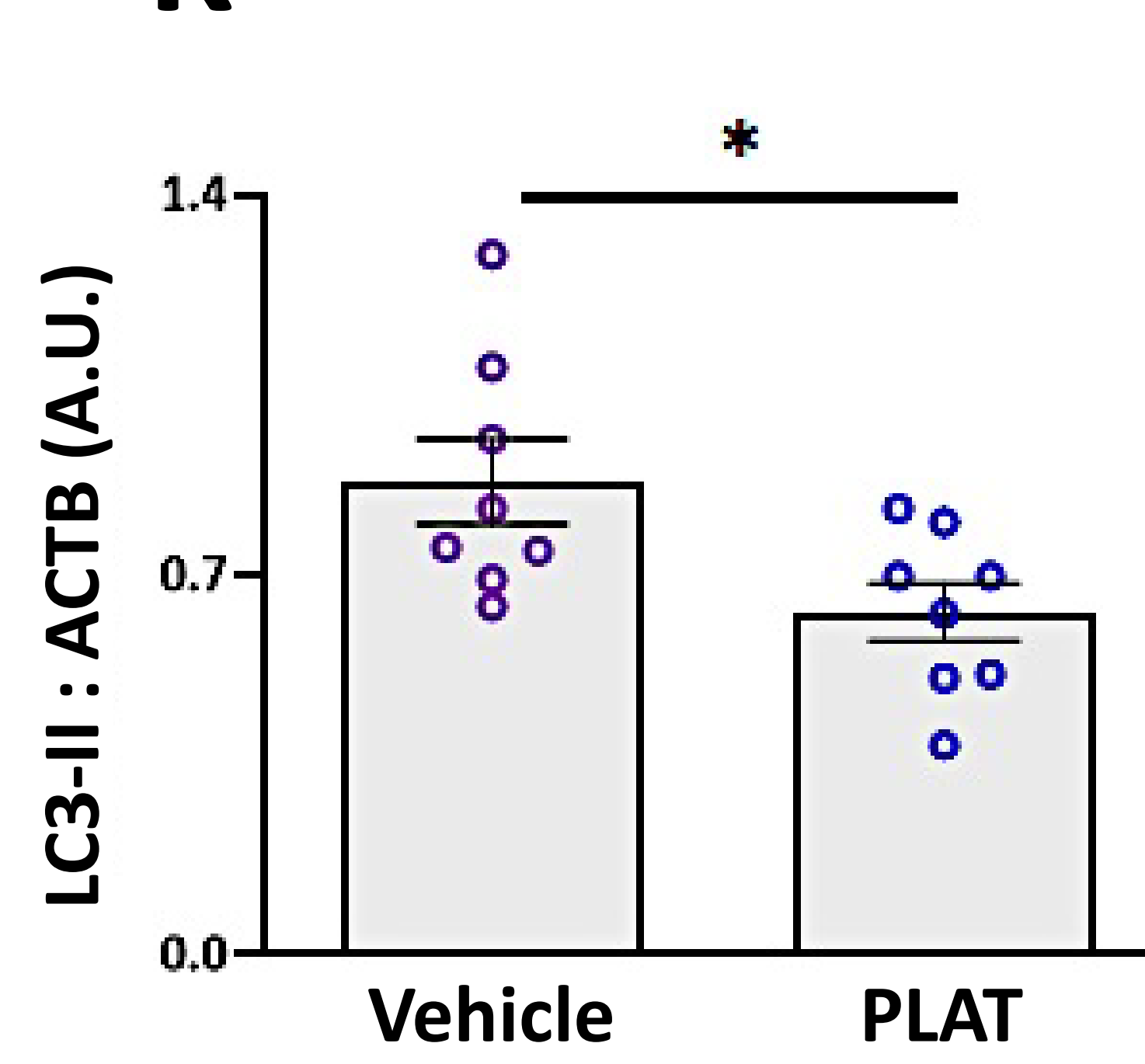
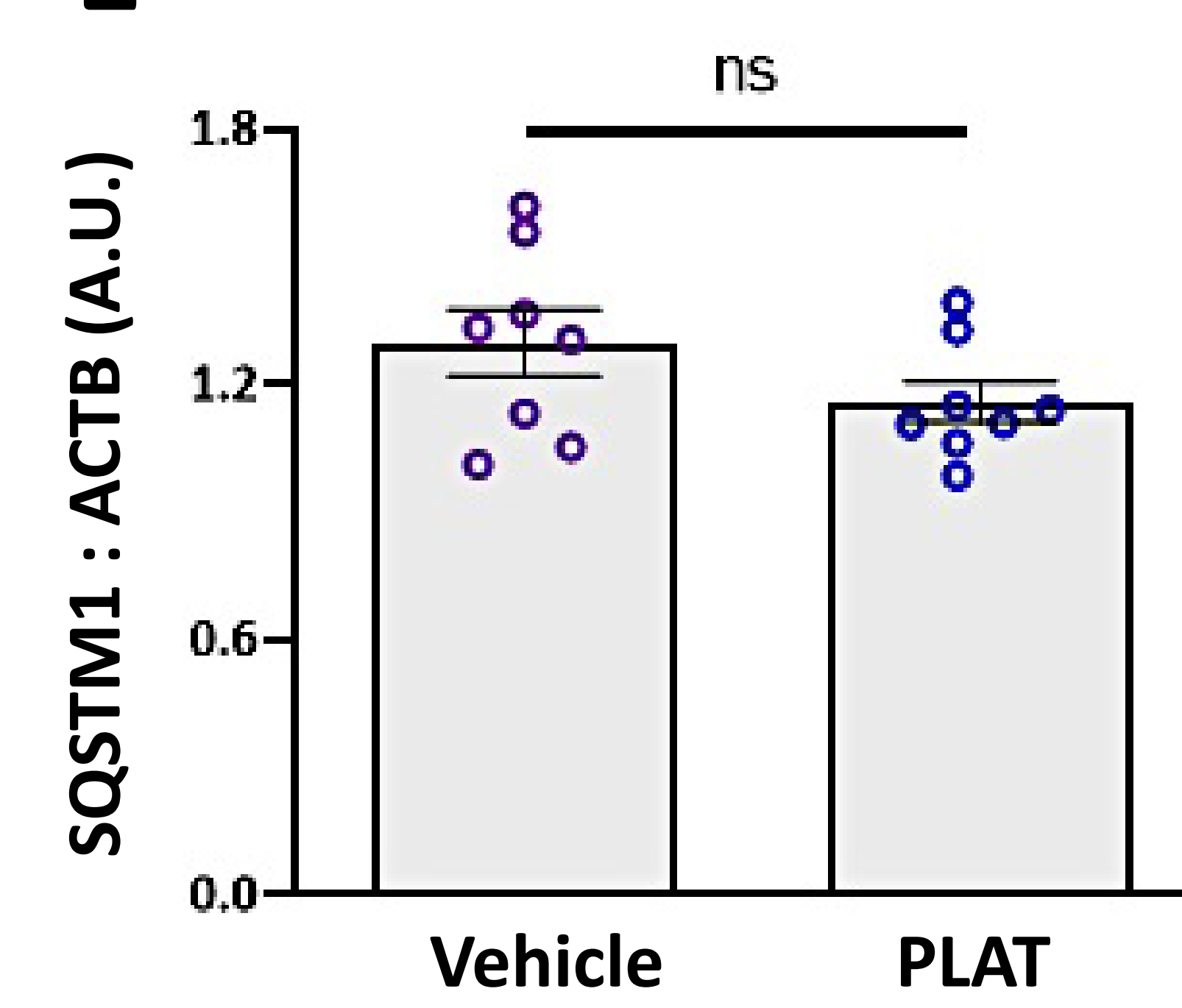
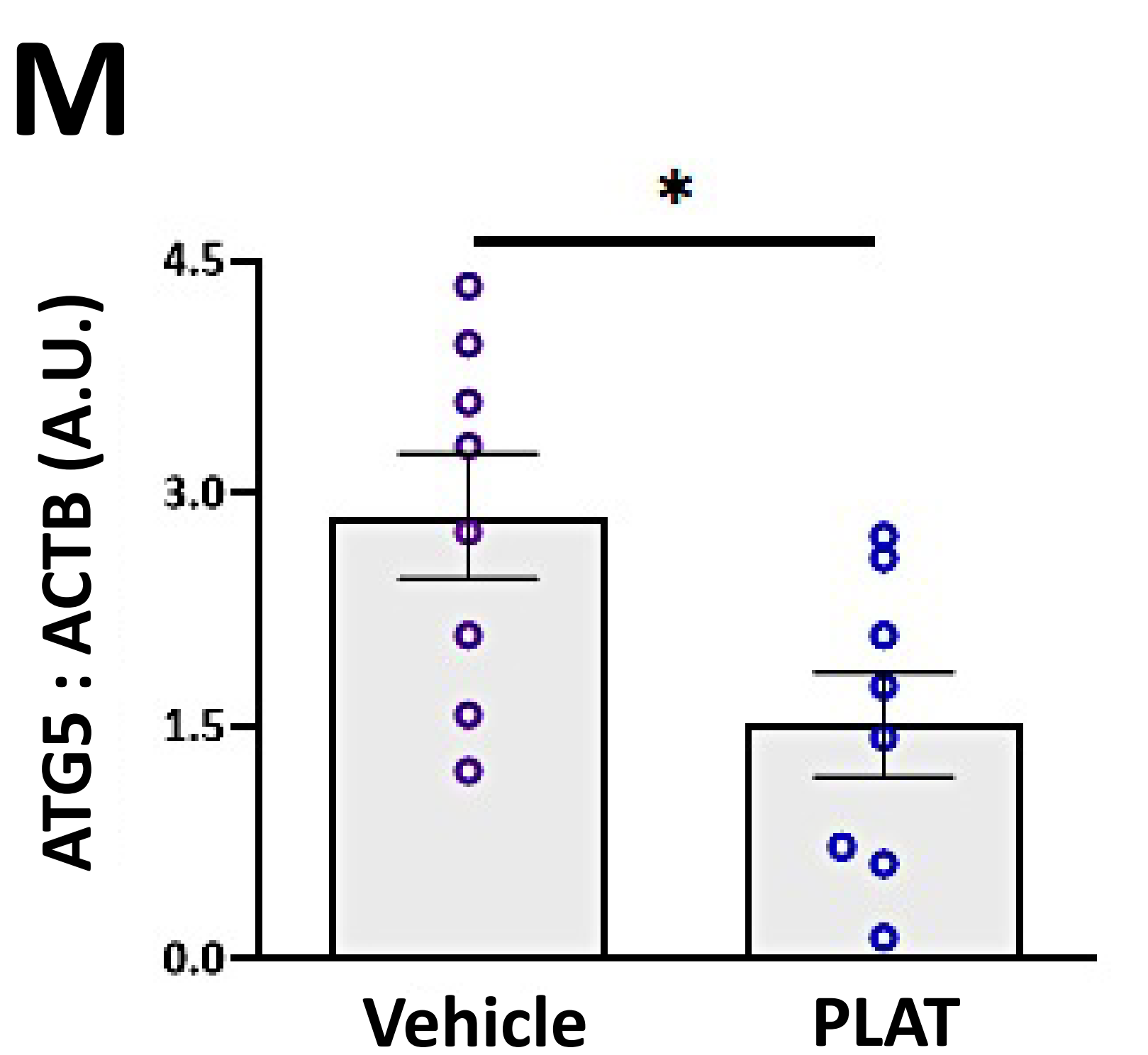
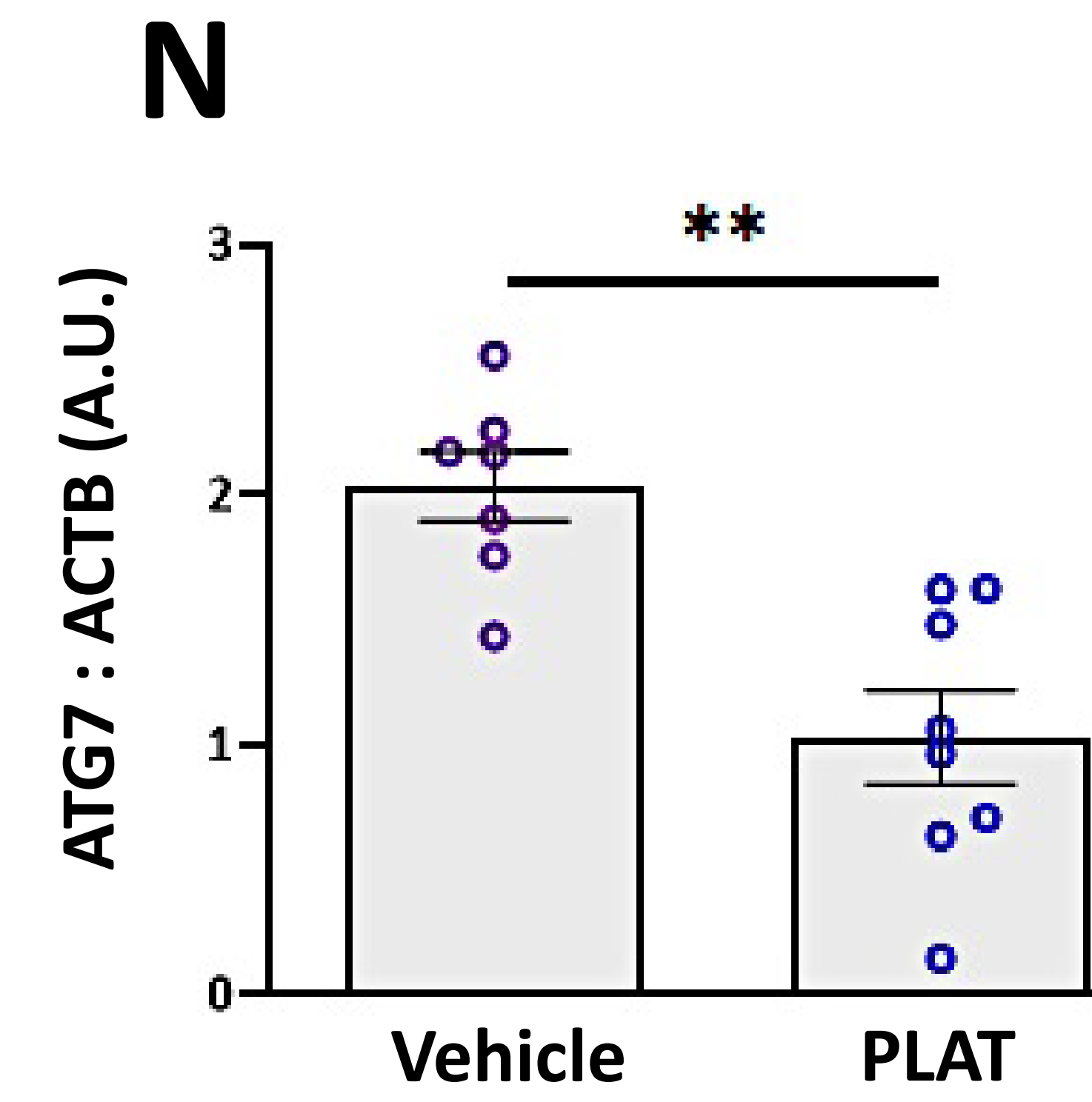
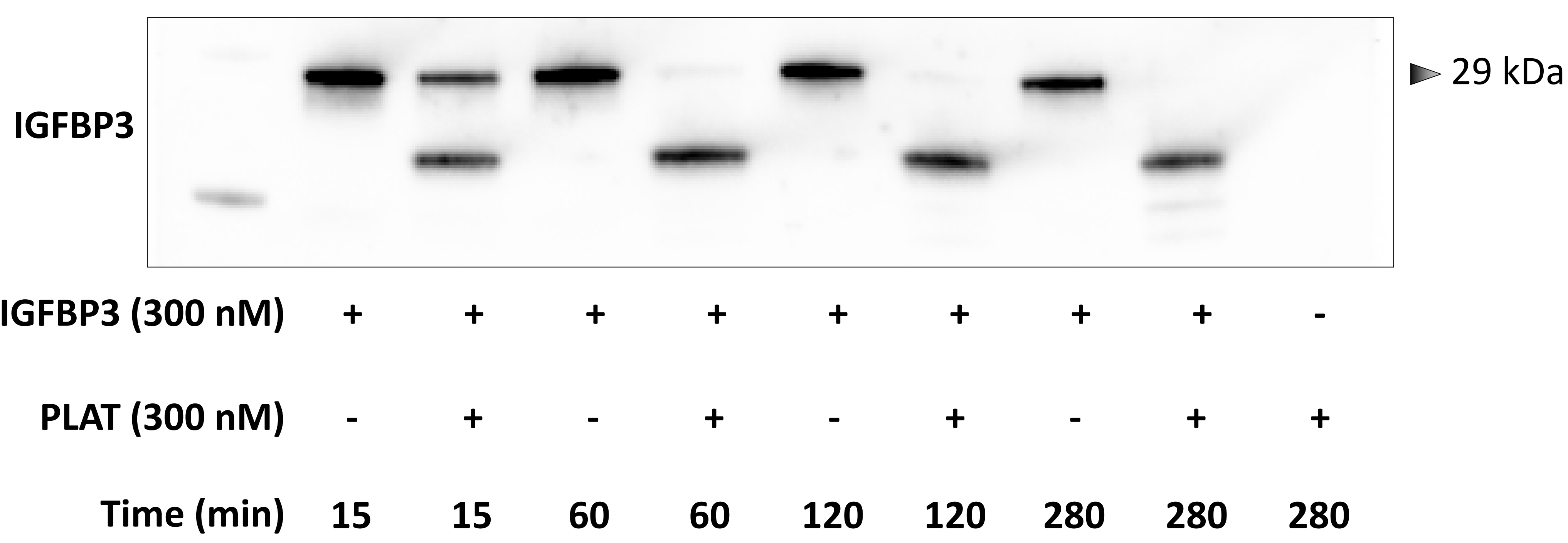
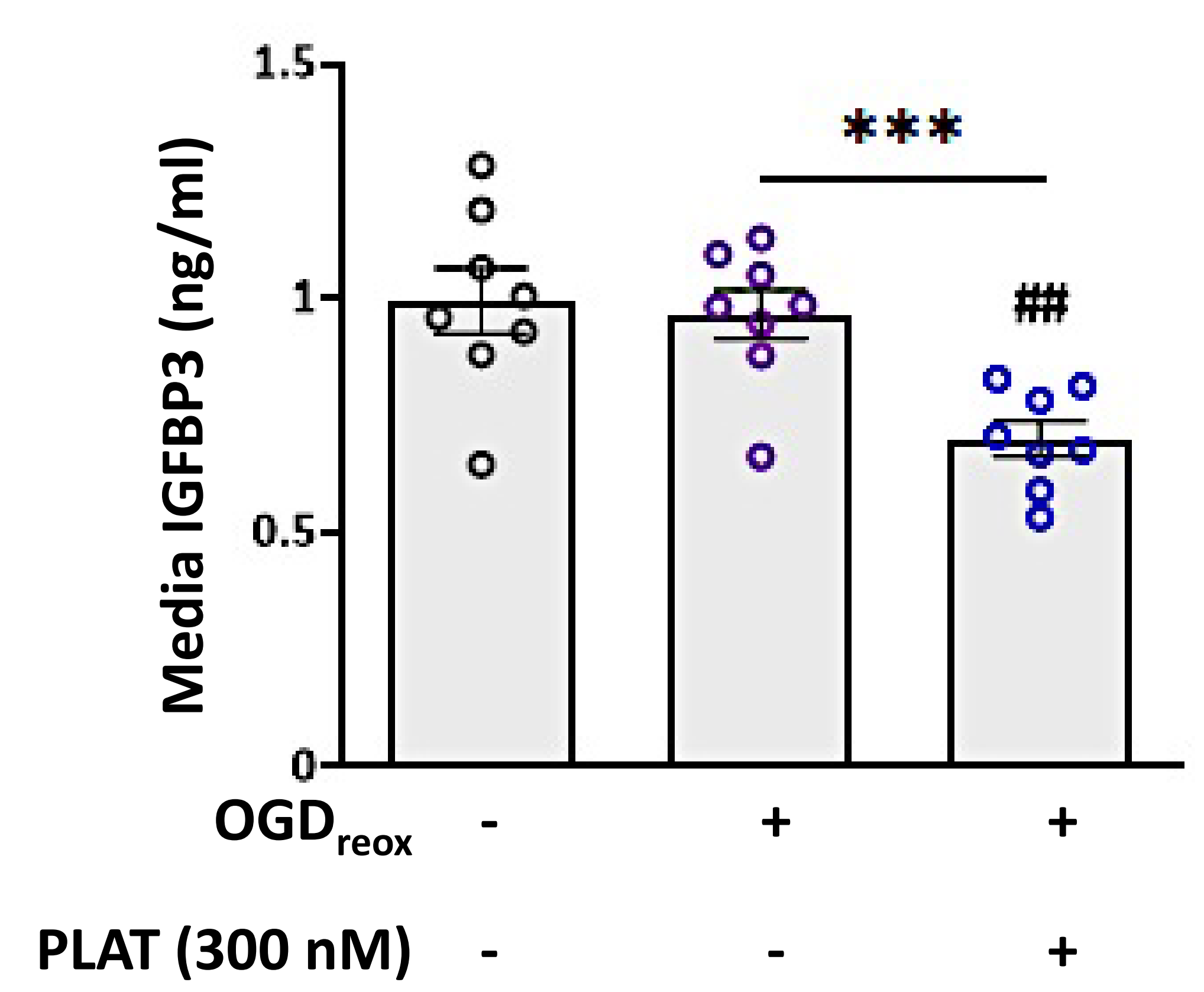
Figure 8**A****B****C****D****E****F****G****H****I****J****K****L****M****N**

Figure 9

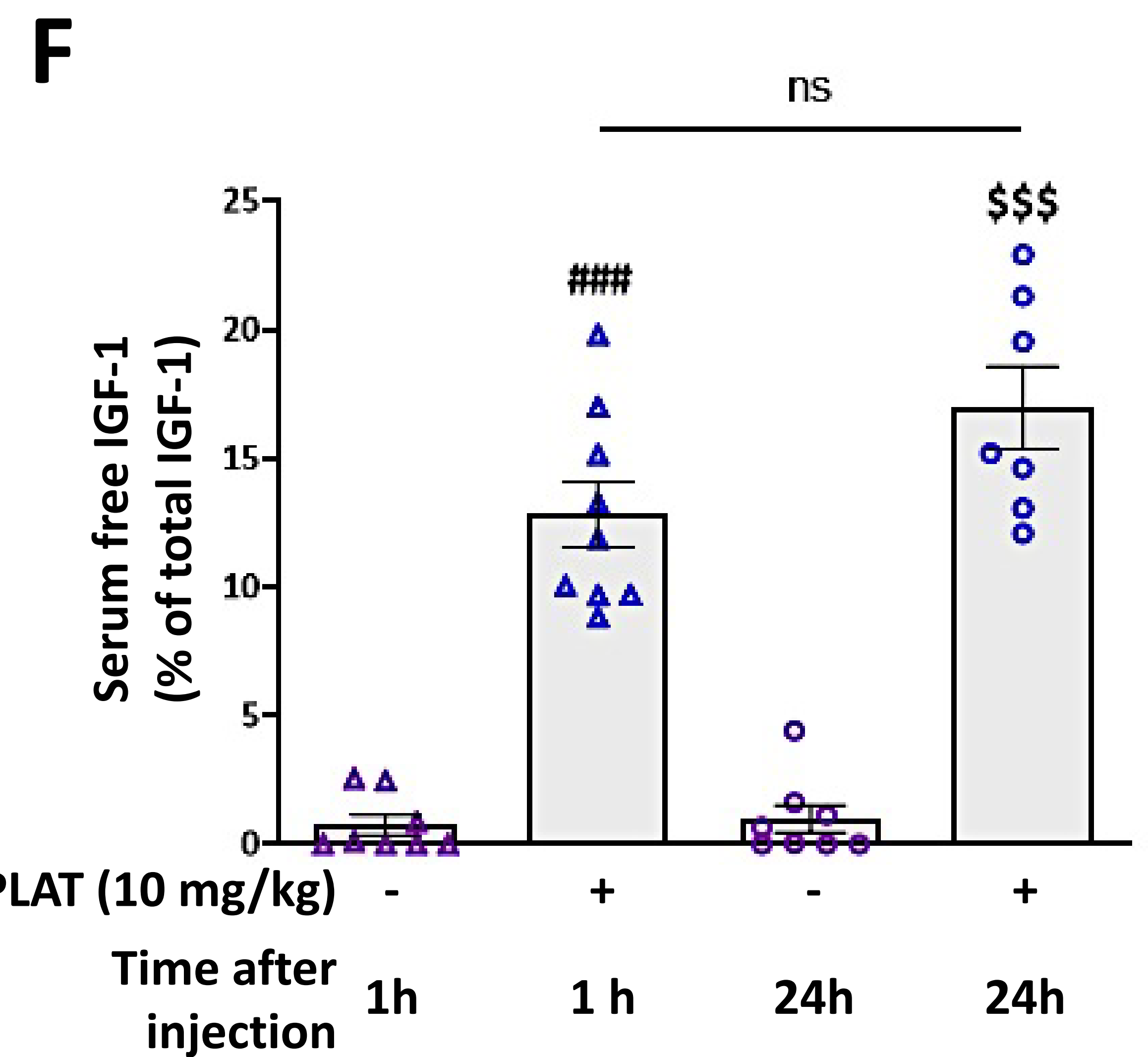
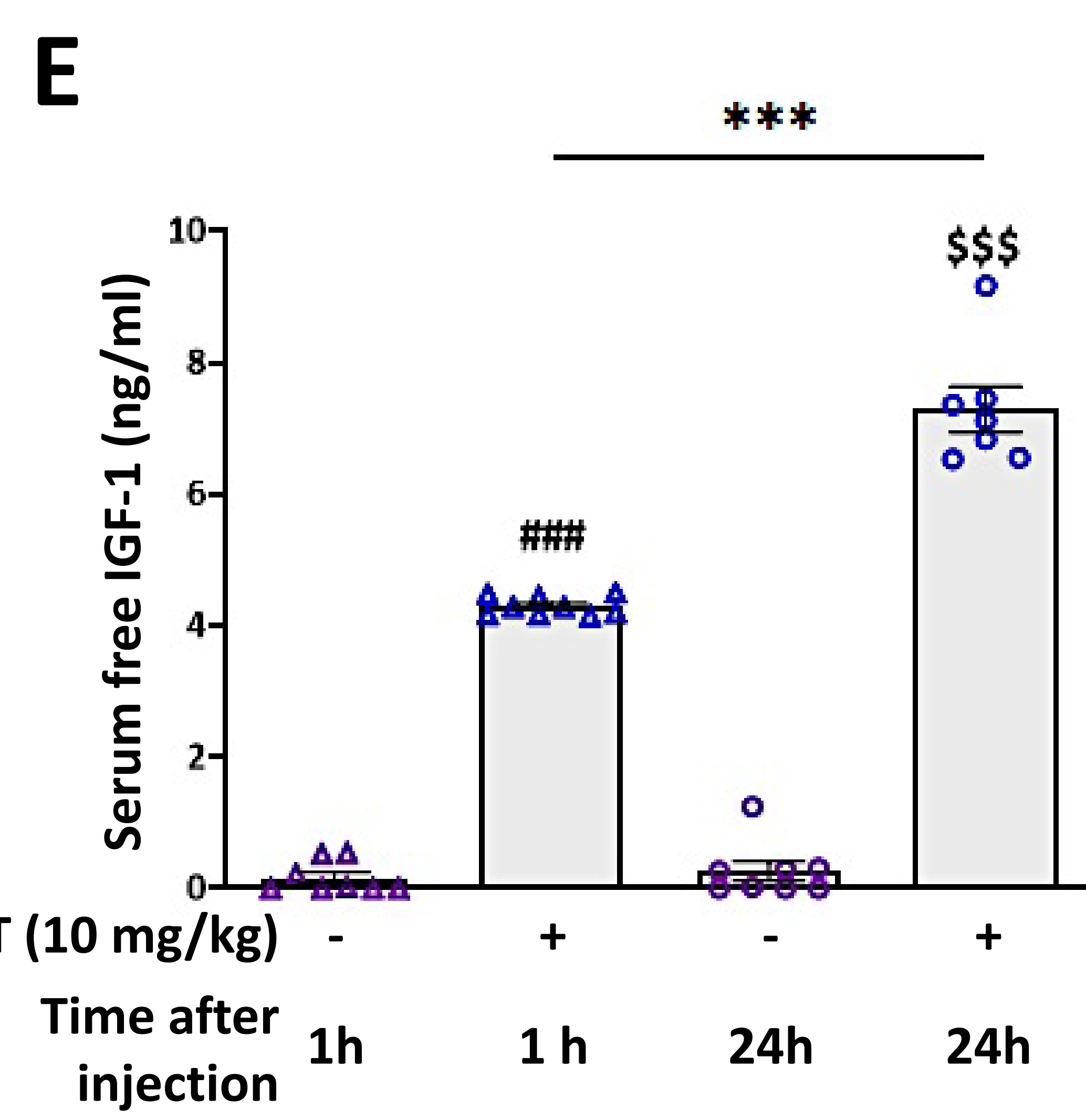
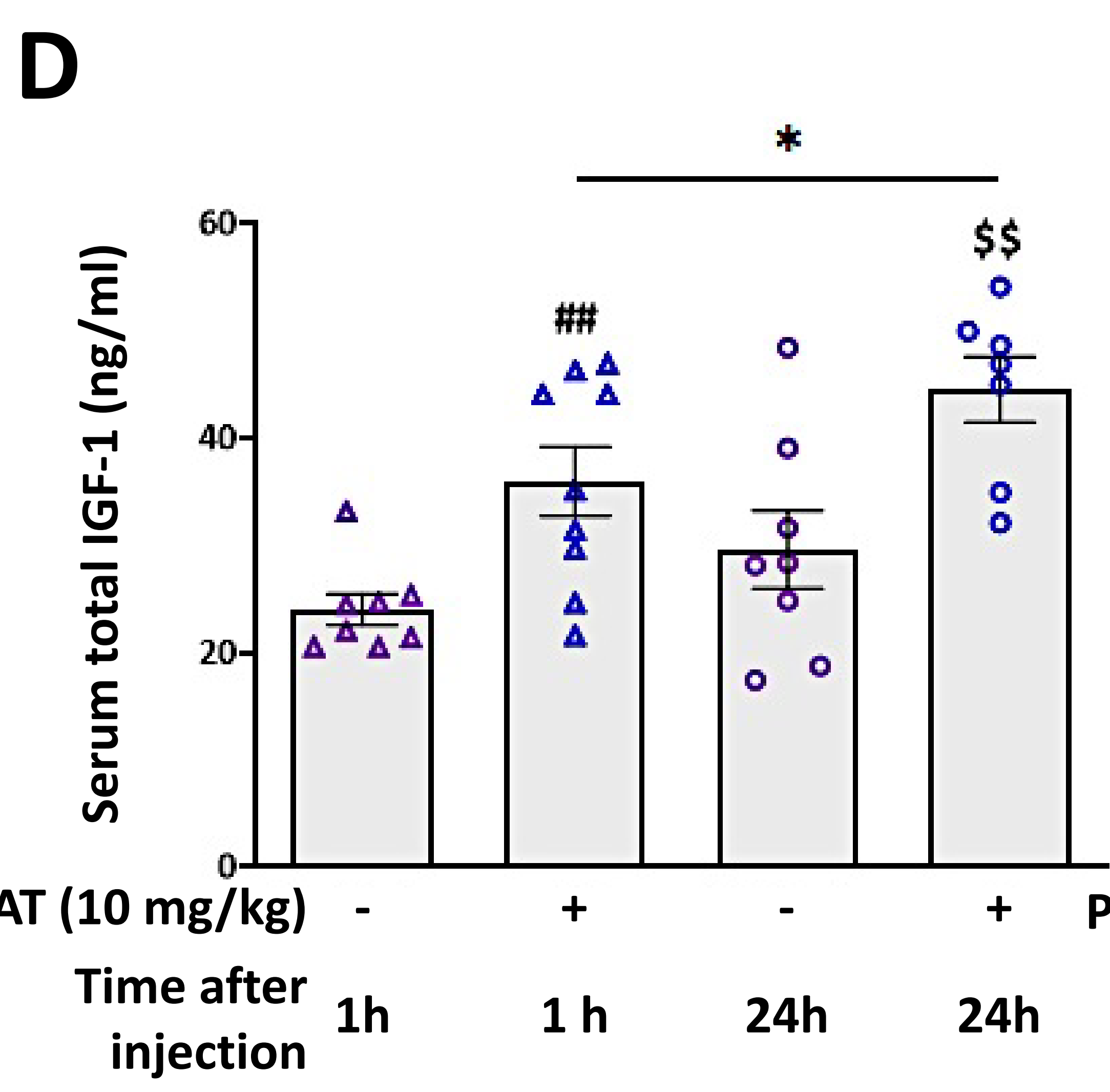
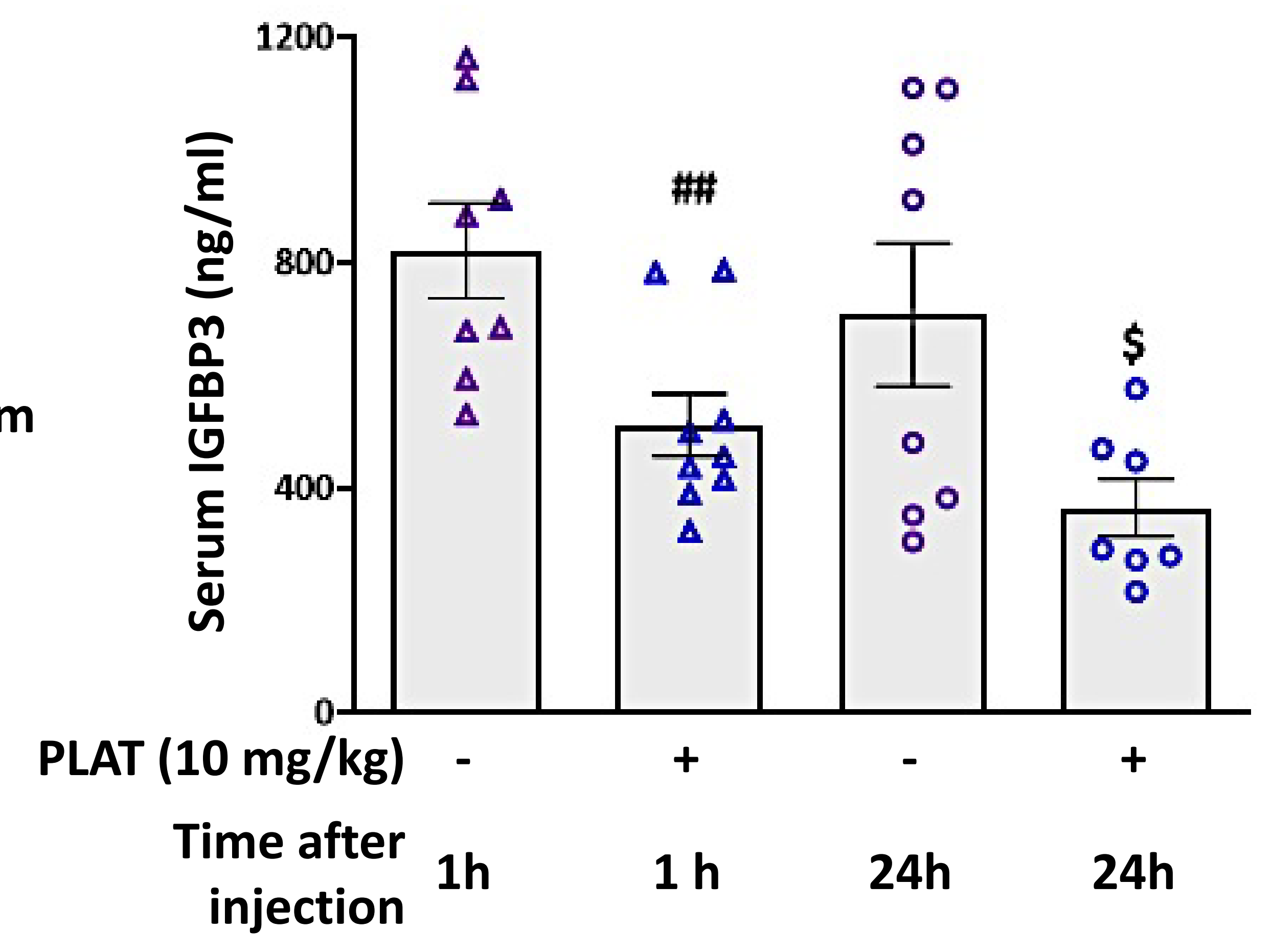
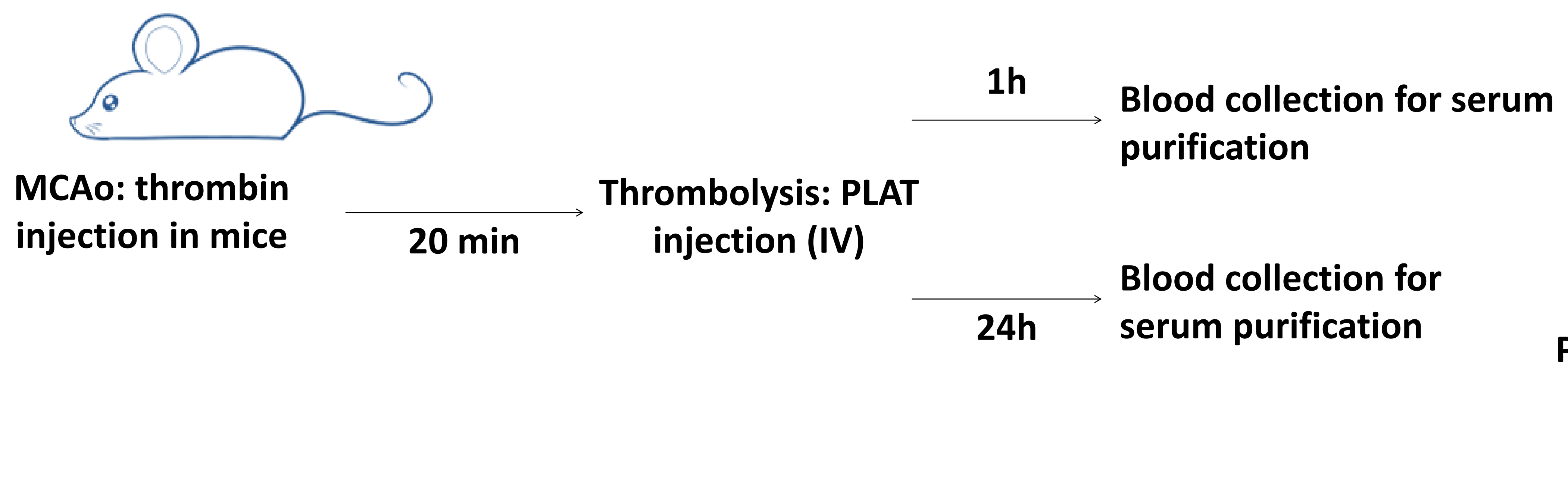
A  *in vitro*, cell-free experiment



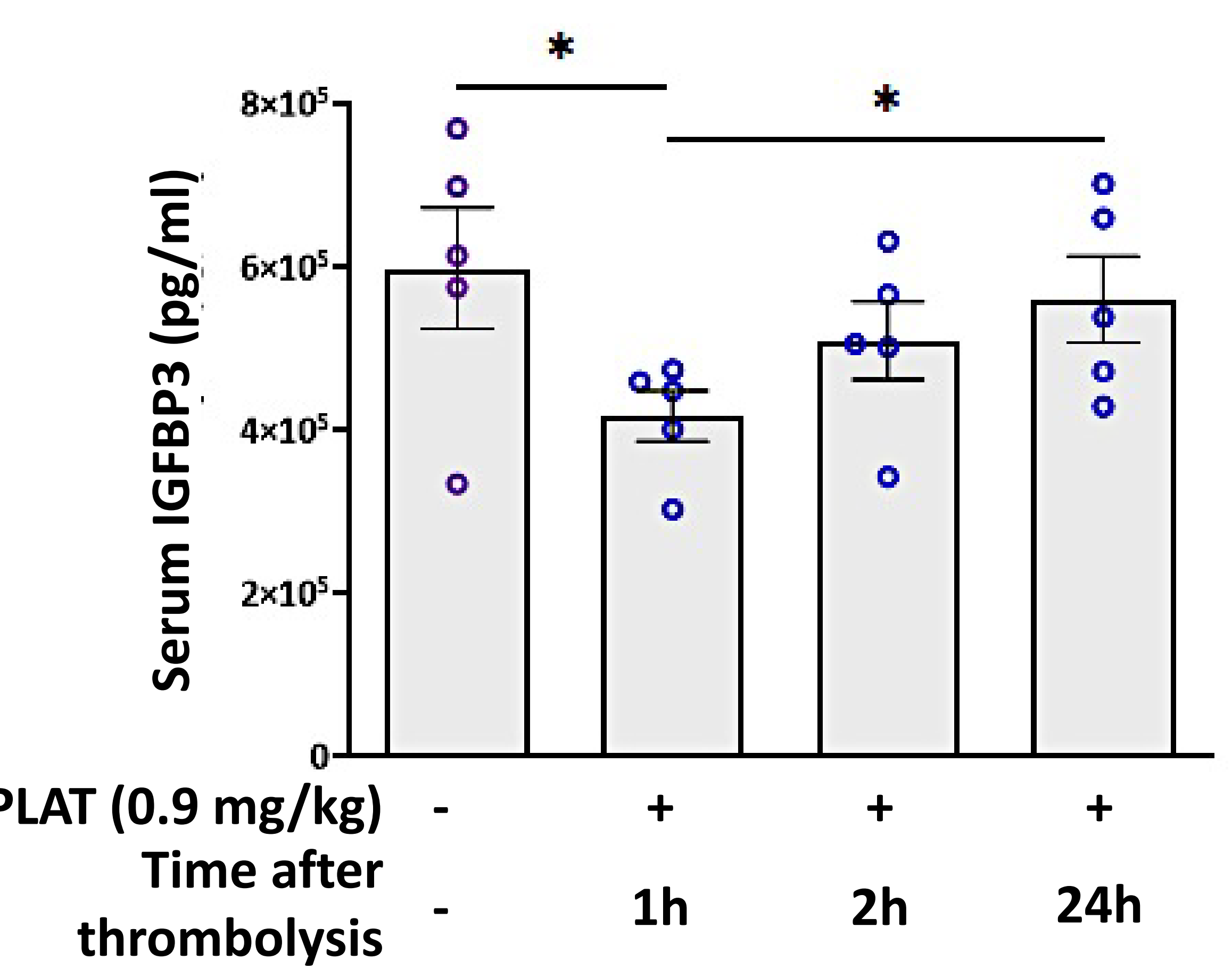
B  *in cellulo*, neuronal culture



C *in vivo*, preclinical experiment



G  *in vivo*, Clinical experiment



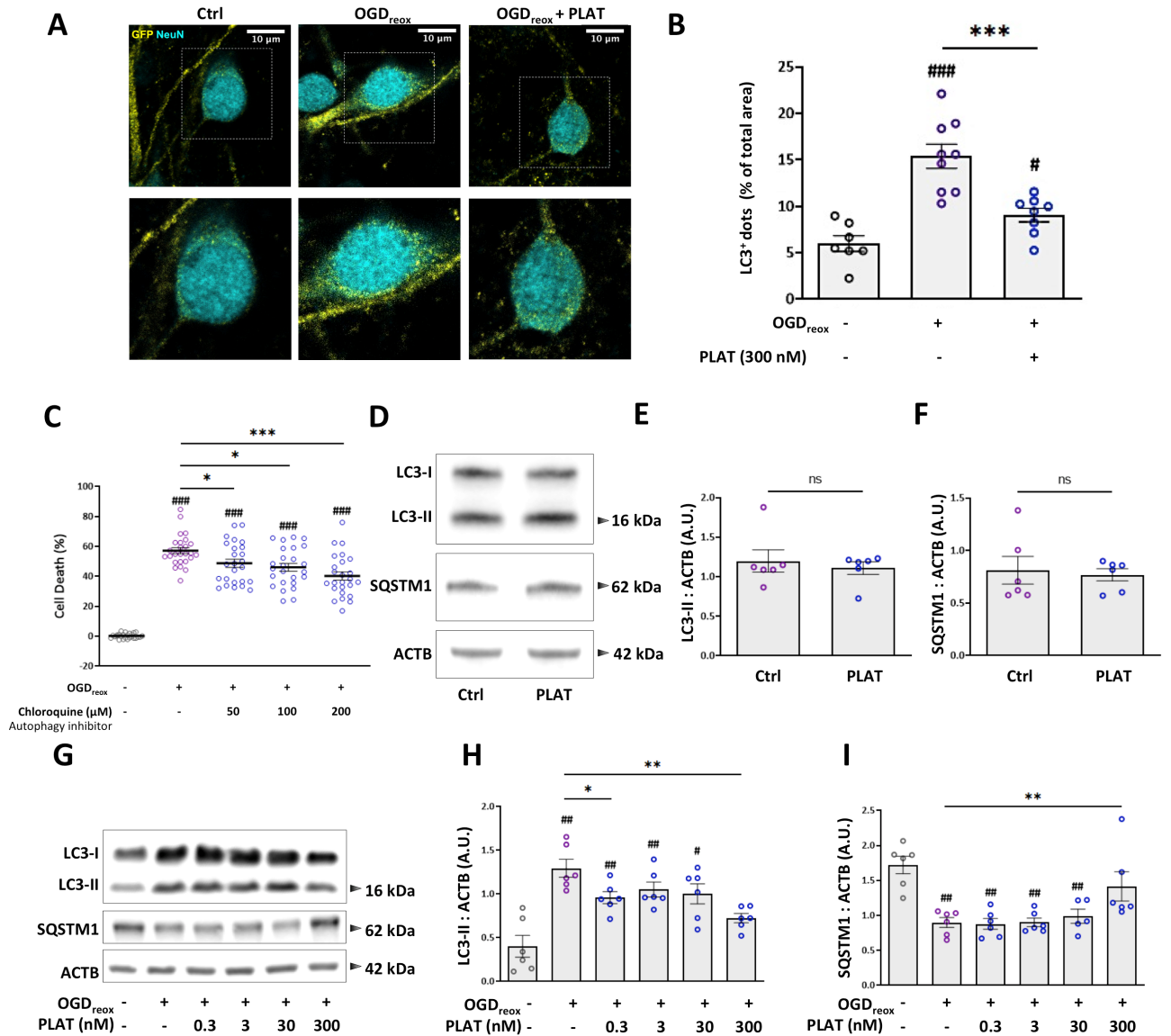


Figure S1. Effect of chloroquine during OGD_{reox} and effects of PLAT/TPA on autophagy flux under normoxic conditions and dose effects during OGD_{reox}. **(A)** Representative immunostaining of neurons transduced with GFP-LC3 lentivirus then stain with anti-GFP antibody (yellow), and subjected or not to OGD_{reox} with or without 300 nM PLAT. RBFOX3/NeuN staining appears in cyan. **(B)** Corresponding percentage of area with GFP-LC3-positive dots compared to total area of neuron (mean±S.E.M. n=7 for Ctrl; n=9 for OGD_{reox}; n=9 for OGD_{reox} + PLAT; from 4 independent experiments; ###: p<0.001 compared to Ctrl; *: p<0.05 compared to Ctrl; ns: not significant).

p<0.05 compared between OGD_{reox}; Mann–Whitney test). **(C)** Neuronal death of pure cortical neurons assessed by LDH release after OGD_{reox} in the presence or not of 50, 100 or 200 μ M of Chloroquine (mean \pm S.E.M. n=25 from 6 independent experiments; ***: p<0.001 and *: p<0.05 compared between OGD_{reox}; Mann–Whitney test; dose/response correlation, Pearson r=0.9801 and *: p<0.05). **(D)** Representative western blots of LC3-II, SQSTM1/p62 and actin in cortical neurons in the presence or not of PLAT (300 nM). Densitometric quantification of LC3-II **(E)**, or SQSTM1/p62 **(F)** normalized to actin (mean \pm S.E.M. n=6 independent experiments; ns: not significant; Mann–Whitney test). **(G)** Representative western blots of LC3-II, SQSTM1 and actin in neurons subjected or not to OGD_{reox} in the presence of PLAT 0 to 300nM. Densitometric quantification of LC3-II **(H)** and SQSTM1 **(I)** normalized to ACTB/actin (mean \pm S.E.M. n=5 independent experiments; ##: p<0.01 and #: p<0.05 compared to Ctrl; **: p<0.01 and *: p<0.05 compared between OGD_{reox}; Mann–Whitney test).

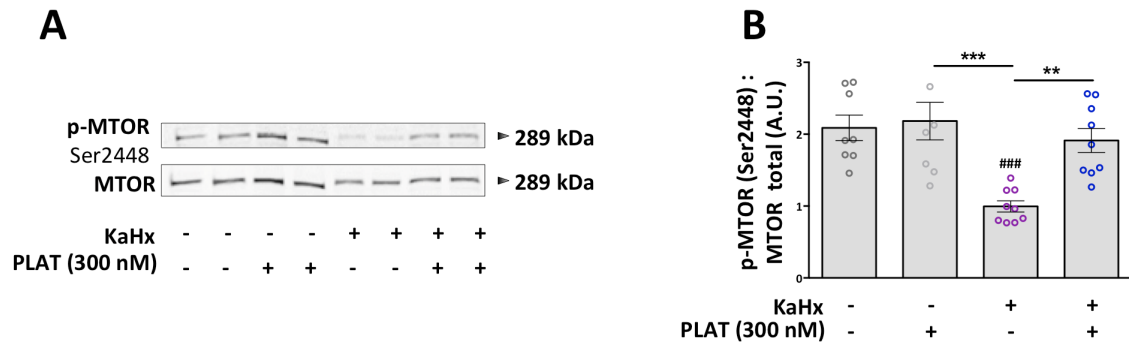


Figure S2. PLAT prevents hypoxic/excitotoxic-induced MTOR dephosphorylation. PLAT (300 nM) treatment prevents KaHx-induced decrease in MTOR phosphorylation (at Ser2448) as shown by **(A)** representative immunoblots and **(B)** the corresponding quantifications of the ratio p-MTOR:MTOR (Ct: $2.1 \pm 0.2\%$, Ct+PLAT: 2.2 ± 0.3 , KaHx: $1 \pm 0.1\%$, KaHx: $1.9 \pm 0.2\%$ PLAT (300 nM). Values are mean \pm SEM. $n = 8$ or 9 from 3 independent experiments. $### p < 0.01$ compared to untreated control neurons, $*p < 0.05$, $**p < 0.01$. Tukey's multiple comparisons tests.

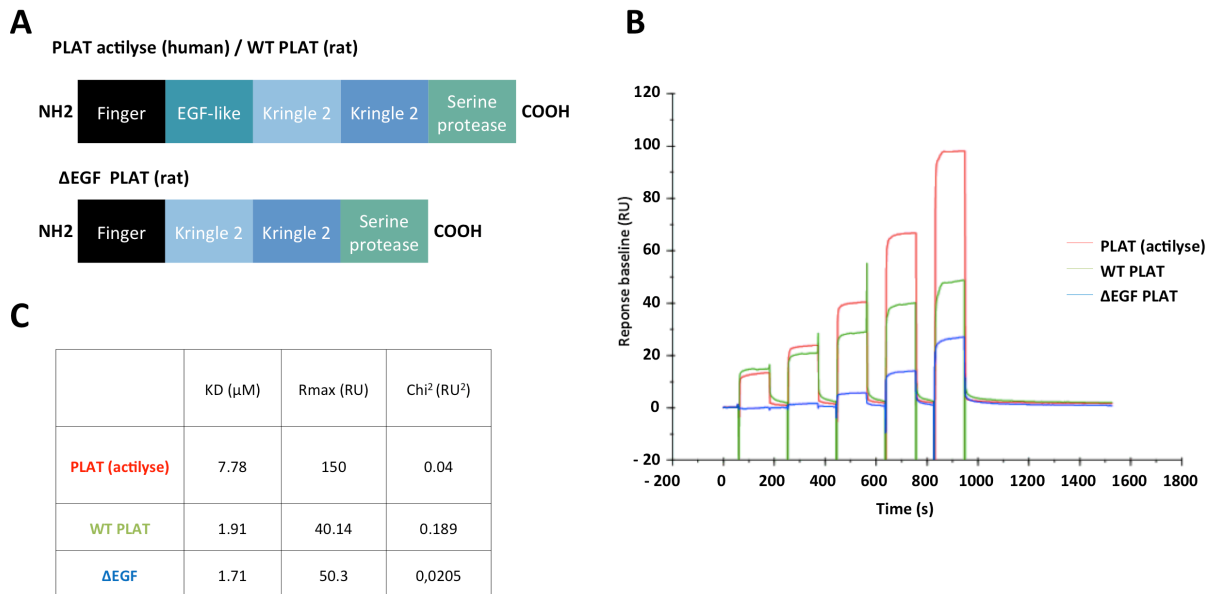


Figure S3. PLAT does not mediate a biological effect by a direct interaction to IGF1R. **(A)** Schematic representation of PLAT actilyse, wild-type PLAT (WT PLAT) and Δ EGF PLAT. PLAT (actilyse), WT PLAT and Δ EGF PLAT binding on IGF1R was measured by surface plasmon resonance (SPR) **(B)** Sensorgrams of the response (RU) versus time of the single-cycle kinetics assay performed by injecting five increasing concentrations (10, 5, 2.5, 1.25 and 0.625 μM) of PLAT (actilyse; red), PLAT WT (green) or PLAT Δ EGF (blue) on human recombinant IGF1R. **(C)** The equilibrium dissociation constant (KD), the analyte binding capacity (Rmax) and the Chi² (the sum of squared differences between the experimental data and reference data at each point values) reported in the table were obtained by fitting data with the langmuir 1:1 binding model and with the steady state model.